DESIGN OF LPI WAVEFORMS FOR MONOSTATIC RADAR

Rami Kassab

THÈSE DE DOCTORAT DE
L'UNIVERSITÉ PIERRE ET MARIE CURIE
PARIS VI

Spécialité :

Électronique
(SMAER)

Présentée par :

Rami KASSAB

Pour obtenir le grade de :

DOCTEUR DE L'UNIVERSITÉ PIERRE ET MARIE CURIE

OPTIMISATION ET CONCEPTION DE FORMES D'ONDE LPI POUR RADAR MONOSTATIQUE

Devant le jury composé de :

Pr. Hugh GRIFFITHS, Univeristy College London	Rapporteur
Pr. Philippe FORSTER, Université Paris X	Rapporteur
Pr. Aziz BENLARBI-DELAI, Université Paris VI	Examinateur
Pr. Marc LESTURGIE, Onera/ Sondra (Directeur)	Co-Directeur de thèse
Dr. Jocelyn FIORINA, Supélec	Examinateur
Pr. Walid TABBARA , Université Paris VI	Directeur de thèse

Université Pierre & Marie Curie - Paris 6
Bureau d'accueil, inscription des doctorants et base de données
Esc G, 2ème étage
15 rue de l'école de médecine
75270-PARIS CEDEX 06

Tél. Secrétariat : 01 42 34 68 35
Fax : 01 42 34 68 40
Tél. pour les étudiants de A à EL : 01 42 34 69 54
Tél. pour les étudiants de EM à ME : 01 42 34 68 41
Tél. pour les étudiants de MF à Z : 01 42 34 68 51
E-mail : scolarite.doctorat@upmc.fr

Résumé étendu

Introduction

Le progrès qu'a connu la technologie électronique a permis au radar d'intégrer de nouveaux composants, d'appliquer de nouvelles techniques de traitement de signal et d'implémenter des formes d'onde encore plus complexes ce qui a radicalement amélioré ses performances. Parallèlement, c'est cette même technologie qui a doté les mesures de support électronique (MSE) et les détecteurs radars de leurs performances actuelles, menaçant l'efficacité et le fonctionnement du radar.

L'art de concevoir des équipements radars qui puissent « voir » sans être « vus » a commencé à la fin de la deuxième guerre mondiale et a évolué vers l'un des plus importants traits du radar moderne : la faible probabilité d'interception (Low Probability of Interception : LPI).

Un coup d'œil sur l'équation radar suffit pour comprendre le défi que doit relever un radar LPI. Selon cette équation, le radar est condamné à recevoir un signal beaucoup plus atténué après une propagation aller-retour, que le signal reçu par un détecteur radar. Le radar qualifié « LPI » doit ainsi adopter une stratégie lui permettant de bouleverser cet avantage tactique dont dispose le détecteur.

Cette stratégie peut être résumée par l'étalement de l'énergie transmise dans toutes les dimensions possibles, que ce soit en espace, temps, fréquence ou polarisation. En étalant la transmission dans le temps, le radar réduit ainsi sa puissance crête, dont dépend la performance du détecteur radar, pour se cacher sous le niveau du bruit de ce récepteur. Cependant, ceci ne doit pas affecter sa propre performance puisqu'il peut toujours recourir à une intégration cohérente assez longue afin de pouvoir restituer le niveau du rapport signal à bruit (SNR) désiré. Les formes d'ondes continues sont dans ce contexte les plus convenables, fournissant le meilleur rapport puissance moyenne à puissance crête. Toutefois, pour un radar monostatique utilisant une isolation temporelle efficace entre les voies d'émission et de réception, il s'agit plutôt d'utiliser des formes d'onde quasi-continues avec un bon rapport cyclique, 0.5 étant le plus grand rapport cyclique raisonnable pouvant être utilisé.

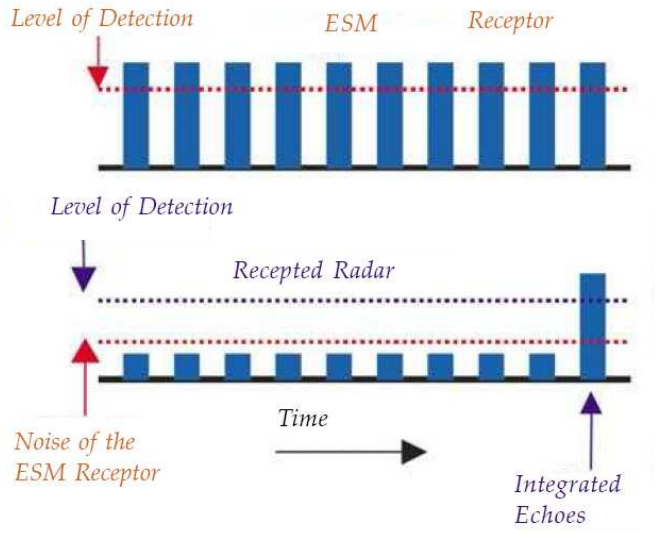

Fig. 1 Le niveau de transmission réduit du radar est caché dans le bruit de la MSE mais les échos dépassent quand-même le seuil de détection après intégration cohérente.

Cependant, avec toute augmentation du rapport cyclique, surgit le problème de perte par éclipse, cette perte de partie ou même de la totalité du signal reçu due à la coupure du canal de réception durant le temps d'émission. Les cases distance affectées par cette perte, témoignent d'une dégradation des performances radar en détection et en localisation.

En outre, l'étalement de l'énergie transmise en fréquence pose un problème pour le détecteur radar qui, d'une part a besoin d'une bande assez étroite afin de distinguer les différents signaux proches en fréquence, et d'autre part voit sa sensibilité de détection réduite à cause de l'augmentation du niveau du bruit proportionnel à la largeur de la bande de réception. De plus, l'augmentation de la bande radar permet d'accroître ses performances, notamment son pouvoir de séparation en distance. Toutefois, la bande disponible pour le radar est limitée, contrainte par des restrictions, et parfois partagée avec d'autres applications. Souvent la bande est discontinue et interrompue par des canaux interdits où de forts émetteurs risquent d'interférer, ou bien des applications critiques risquent d'être perturbées.

Pour toutes ces raisons, nous proposons d'optimiser dans un premier temps la stratégie d'émission/réception afin de réduire les effets d'éclipse en fonction de la distance. Dans un deuxième temps, il s'agit de trouver le code de phase correspondant à l'enveloppe trouvée qui permet de répondre à des contraintes d'occupation spectrales. En même temps, le code résultant doit garder de bonnes performances en termes de résolution et niveau de lobes secondaires de la fonction d'ambigüité (FA) utilisée habituellement pour l'évaluation de la réponse distance –Doppler du filtre adapté correspondant.

Gestion du temps

Ce chapitre traite l'aspect de gestion des temps d'émission et de réception afin de permettre un usage de forme d'onde à fort rapport cyclique avec un minimum de dégradations dues aux pertes d'éclipses.

Origine de la stratégie LPI

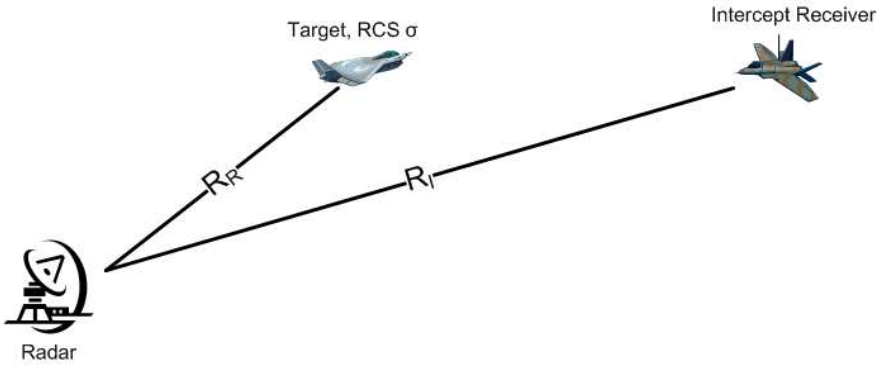

Fig. 2 Le radar contre le récepteur d'interception.

Considérons le scenario de la Fig. 2, où un radar capable de détecter une cible de section efficace radar (SER) σ distante jusqu'à R_R est en présence d'un détecteur radar dont la distance d'interception vis-à-vis du radar en question est R_I. En supposant que le détecteur présente aussi une SER σ, on peut déduire que si $R_I > R_R$ alors le radar est détecté par le récepteur d'interception qui reste invisible au radar. Sinon, c'est le radar qui le détecte sans être intercepté. C'est ce genre de situation qu'on vise réaliser, et le radar en question sera qualifié LPI.

Afin d'évaluer la performance de la faible probabilité d'interception, le facteur de portée est introduit comme suit :

$$\alpha = \frac{R_I}{R_R}$$

avec

$$R_R = \left[\frac{G_T \frac{E_T}{\tau} \sigma G_R \frac{\lambda^2}{L_R}}{(4\pi)^3 K T_R B_R S_R} \right]^{\frac{1}{4}}$$

où G_T et G_R sont les gains des antennes émettrice et réceptrice du radar respectivement, E_T est l'énergie transmise par le radar, τ est la durée de l'impulsion, λ est la longueur d'onde utilisée, L_R est le facteur de perte pour le radar, K est la constante de Boltzmann, T_R est la température du bruit du radar, B_R est la bande passante et S_R est le rapport signal à bruit nécessaire à l'entrée du radar pour assurer des probabilités de détection et de fausse alarme données,

$$R_I = \left[\frac{G_{TI} \frac{E_T}{\tau} G_I \frac{\lambda^2}{L_I}}{(4\pi)^2 K T_I B_I S_I} \right]^{\frac{1}{2}}$$

où G_{TI} est le gain de l'antenne émettrice du radar en direction du récepteur d'interception, G_I est le gain du récepteur d'interception, L_I est son facteur de perte, T_I est sa température de bruit, B_I est sa bande effective et S_I est le rapport signal à bruit nécessaire à l'entrée du récepteur d'interception afin d'assurer les mêmes probabilités de détection et de fausse alarme que le radar.

Ainsi

$$\alpha = \left[\frac{1}{4\pi} \frac{{G_{TI}}^2}{G_T} \frac{{G_I}^2}{G_R} \frac{\lambda^2}{\sigma} \frac{S_R}{{S_I}^2} \frac{L_R}{{L_I}^2} \frac{E_T K T_R}{K^2 {T_I}^2} \frac{B_R/\tau}{{B_I}^2} \right]^{\frac{1}{4}} = R_R \left[\frac{4\pi}{\sigma} \frac{T_R}{T_I} \frac{B_R}{B_I} \frac{L_R}{L_I} \frac{G_{TI} G_I}{G_T G_R} \frac{S_R}{S_I} \right]^{\frac{1}{2}}$$

Le rapport suivant peut être reformulé :

$$\frac{S_R}{S_I} = \frac{S_{oR}/\mathrm{G_{PR}}}{S_{oI}/\mathrm{G_{PI}}} = \frac{\mathrm{G_{PI}}}{\mathrm{G_{PR}}}$$

avec $S_{oR} = S_{oI}$ les rapports signal à bruit à la sortie nécessaires pour assurer les probabilités de détection et fausse alarme.

D'après le rapport $\frac{G_{TI}}{G_T G_R}$ qu'on trouve dans l'expression du facteur de portée, on déduit la nécessité d'étaler l'énergie transmise par le radar en espace. Autrement, l'antenne émettrice doit avoir un faisceau large afin de cacher ses émissions du radar d'interception. D'autre part, le radar doit réaliser un faisceau le plus étroit possible en réception et sans lobes secondaires afin de réduire ce facteur de portée.

D'après le rapport $\frac{G_{PI}}{G_{PR}}$, et si le radar utilise une intégration cohérente sur une durée T_c son gain d'intégration sera de $B_R T_c$. Maintenant, si le récepteur d'interception arrive à s'adapter à la bande du radar, son gain incohérent lui fournit un gain pour la même durée d'intégration de $(B_R T_C)^{\gamma}$ avec γ variant entre 0.7 et 0.8. Ceci laisse au radar un avantage de $(B_R T_C)^{1-\gamma}$, d'où l'intérêt de l'étalement en temps et fréquence.

Les pertes d'éclipse

Les pertes d'éclipse sont les pertes qui se produisent alors que le récepteur est bloqué durant l'émission.

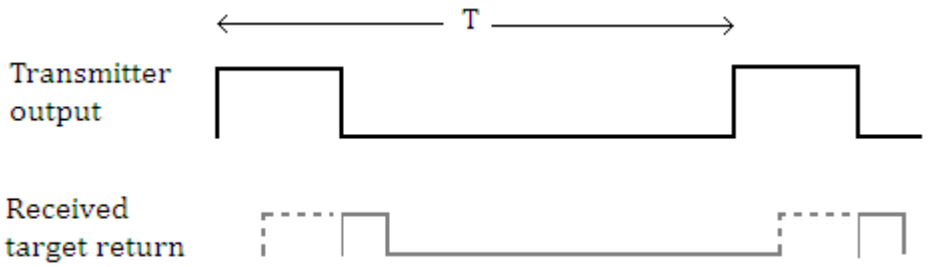

Fig. 3 Exemple de perte partielle de la forme d'onde pendant la durée d'émission.

A ces pertes sont associées en même temps une dégradation de performance au niveau du SNR et une dégradation de la résolution et au niveau des lobes secondaires de la FA comme présenté dans Fig. 4, R_z étant la largeur de la zone d'éclipse liée à la largeur de l'impulsion de la forme d'onde conventionnelle.

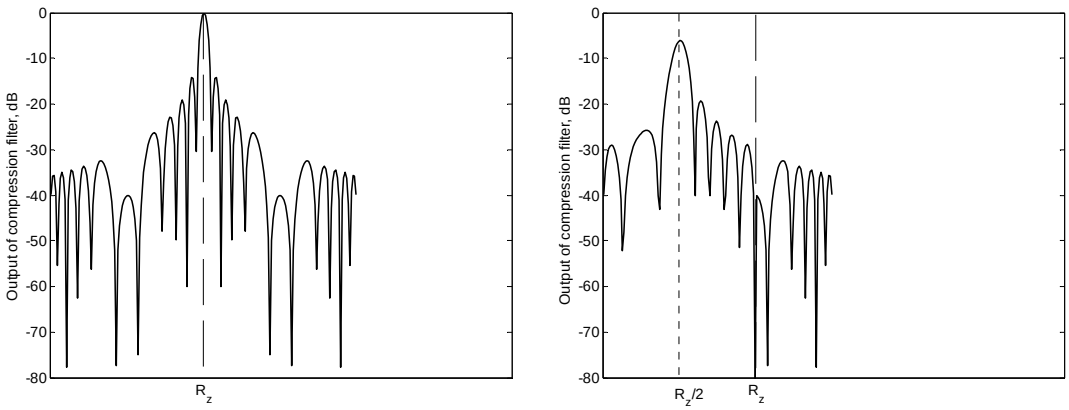

Fig. 4 La sortie du filtre adapté à la frontière R_z de la zone d'éclipse (gauche) et au milieu de la zone d'éclipse (droite).

Maintenant, soit $a(t)$ un signal dont l'amplitude prend les valeurs 0 et K pour les états bloqué et saturé de l'émetteur, souvent limité en puissance crête. L'interruption de la voie de réception fait qu'elle opère de façon inverse donc selon$1 - |a(t)/K|$. Pour une énergie transmise A durant un temps d'intégration T, on peut calculer la fonction de perte d'éclipse pour un retard τ correspondant à une distance d par :

$$l(\tau) = \frac{1}{A}\int_0^T |a(t-\tau)|^2 \, |a(t)/K| \, dt, \tau = \frac{2d}{c}$$

Désignons par $\theta_0 = (d_0, v_0)$ le décalage en temps et en fréquence dû à une distance d_0 et une vitesse $v_0$de la cible. Le signal reçu en provenance de cette dernière est atténué par un facteur complexe α_0 puis interrompu par $1 - |a(t)/K|$:

$$s(t, \theta_0) = \alpha_0 a(t, \theta_0)[1 - |a(t)|/K]$$

Pour la suite et sans perte de généralité on peut considérer $K = 1$.

La sortie du filtre adapté en présence d'un bruit additif blanc gaussien $b(t)$ de densité spectrale de puissance N_0 sera :

$$Q(\theta, \theta_0) = (1/Pr(\theta)) \left| \int [\alpha_0 \, a(t, \theta_0) + b(t)][1 - |a(t)|] a^*(t, \theta) dt \right|^2$$

avec $Pr(\theta)$ le profil d'énergie en fonction de la distance :

$$Pr(\theta) = \int |a(t, \theta)|^2 [1 - |a(t)|] \, dt$$

Soit

$$\chi(\theta, \theta_0) = \int a(t, \theta_0) a^* \, (t, \theta)[1 - |a(t)|] dt$$

et

$$X(\theta) = (1/|\alpha_0|) \int b(t) a^* \, (t, \theta)[1 - |a(t)|] dt$$

ainsi

$$Q(\theta, \theta_0) = (|\alpha_0|^2 / Pr(\theta)) |\chi(\theta, \theta_0) + X(\theta)|^2$$

$\chi(\theta, \theta_0)$ étant connue sous le nom de fonction d'ambigüité.

Optimisation de la forme d'onde en présence de bruit

L'objectif de cette optimisation est d'accroître le rapport cyclique jusqu'à la limite supérieure de 0.5. L'idée principale sera de prendre en compte des pertes de propagation en espace libre qui sont une fonction en d^{-4} de la distance. Ces pertes sont telles qu'on puisse moins tolérer, du point de vue SNR, les pertes d'éclipse pour les distances lointaines fortement affectées par les pertes de propagation, que pour les distances proches dont les échos sont relativement forts. En outre, l'idéal sera que la distance maximale du radar puisse bénéficier de la totalité de la forme d'onde transmise. Ceci pourra définir la valeur idéale du SNR minimal qu'on pourrait avoir le long de la portée du radar.

Ainsi, une première fonction de coût est proposée. Cette fonction permet de pénaliser toute chute du SNR en dessous de cette valeur minimale du SNR qu'on désire avoir le long de la portée du radar. En considérant un code périodique a_p

de longueur N et en supposant que la portée du radar correspond à un retard de la moitié du code, cette fonction de coût s'écrit :

$$F_1(a_p) = \left| 10 \log \left(\min_{i=1..N/2} Q(i) / (N/2) \right) \right|$$

avec

$$Q(i) = (2i/N)^{-4} Pr(i)$$

L'une des solutions possible qui annule cette fonction de coût, est une impulsion carrée dont le rapport cyclique est de 50%. La résolution de cette forme d'onde se dégrade dramatiquement en s'approchant du radar, alors que d'autres solutions qui contiennent des impulsions plus courtes souffrent moins de ce problème. Pour cette raison, une autre fonction pénalisant les longues impulsions dans le code est agrégée à la première à l'aide d'une simple pondération :

$$F_2(a_p) = \left| 10 \log \left(\min_{i=1..N/2} Q(i) / (N/2) \right) \right| + \delta \left| \max_{i=1..N/2} \left(CS(i) \right) \right|$$

avec CS (Somme Cumulative) définie comme :

$$CS(i) = \left| \sum_{k=1}^{k=i} \left(2a_p(k) - 1 \right) \right|$$

Un algorithme génétique a été utilisé pour minimiser cette nouvelle fonction de coût, puisqu'il permettait de bénéficier de la nature binaire des codes qu'on cherche à optimiser. Fig. 5 montre le code solution et son spectre en comparaison avec l'impulsion classique ayant le même rapport cyclique et codé également avec une rampe linéaire en fréquence ayant un facteur 20 de compression. Deux autres mesures sont aussi présentées : la résolution distance et la largeur effective vis-à-vis du fouillis définie comme :

$$\tau_c(d) = \frac{\int |\chi(d,r)|^2 dr}{|\chi(d,d)|^2}$$

Le code montré obtenu avec δ=0.03 a atteint un rapport cyclique de 47% et a une dynamique totale à la sortie du filtre adapté $[\max_i Q(i)]/[\min_i Q(i)]$=58.14 dB alors que la perte en propagation libre entre la 1ere et la 50ème case distance crée une dynamique de 68 dB. Quant à la résolution, elle demeure quasiment inaltérée le long de la portée du radar sans subir de dégradation.

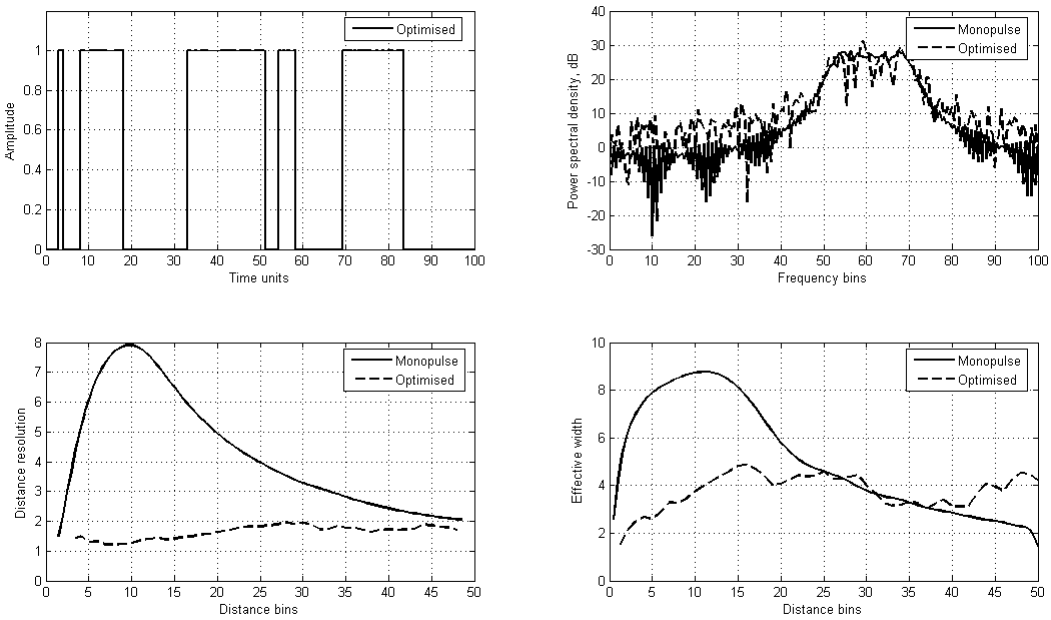

Fig. 5 Spectre et performances de la forme d'onde optimisée en comparaison avec la forme d'onde conventionnelle ayant le même facteur de compression de 20 (rampe linéaire en fréquence).

Optimisation de la forme d'onde en présence de fouillis

Dans cette partie, le cas du radar onde de surface (HFSWR) a été traité en prenant en considération les propriétés du fouillis de mer. La densité de puissance utilisée pour ce fouillis a été dérivée à partir du modèle de Bremmer [1] [2] pour la propagation de l'onde de surface avec les corrections de Barrick [3] pour la rugosité de la mer. Une deuxième propriété concerne la géométrie du patch de mer entourant la cible à une case distance donnée. La surface de ce patch croît linéairement en fonction de la distance comme le montre la Fig. 6.

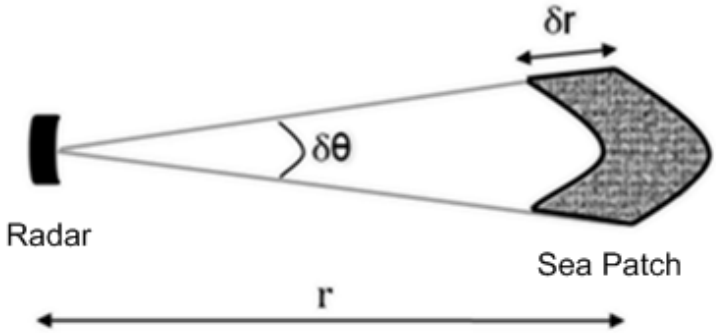

Fig. 6 La géométrie du patch de mer dont la surface croît linéairement en fonction de la distance.

La SER de ce patch de mer pourra ainsi être exprimée par :

$$\sigma_{sea}(r) = \sigma_{00}\, r\, \delta r\, \delta\theta$$

L'idée consiste à trouver le code d'interruption permettant de limiter la contribution des échos de mer dont l'effet s'intensifie avec l'augmentation du rapport cycle de la forme d'onde, du faite de l'intégration de fouillis additionnel à la réponse de la cible. Le rapport signal à fouillis, nommé aussi taux de contraste, permet ainsi d'évaluer la performance radar.

Pour ce faire, le code transmis est défini par une série périodique de bits $x[k]$ représentant les états saturé et bloqué de l'émetteur. Et si on désigne par T_c la durée de la sous impulsion, le signal transmis pourra s'exprimer par :

$$x(t) = \sum_k x[k]\, rect_{T_c}(t - kT_c)$$

avec

$$rect_{T_c}(t) = \begin{cases} 1 & Si\ 0 \le t \le T_c \\ 0 & partout\ ailleurs \end{cases}$$

Les performances de l'ambigüité Doppler de la forme d'onde sont gouvernées par les propriétés du code périodique (donnant une fonction « Sinc » dans le domaine fréquence Doppler) : plus long est le temps d'intégration et plus bas sont les lobes secondaires et plus étroite est la résolution. Par conséquent, on se limitera à l'étude et la conception du code sur une période de répétition et ses propriétés en distance évaluées par la fonction de corrélation croisée, définie pour les distances D et r comme suit :

$$A_x(D, r) = \int_0^T x\left(t - \tfrac{2D}{c}\right)\, x\left(t - \tfrac{2r}{c}\right)\, \left(1 - x(t)\right) dt$$

avec T la période de répétition qu'on considère multiple de $\frac{2D_{max}}{c}$ où D_{max} est la portée du radar en question.

Une estimation du taux de contraste sera :

$$CR_x(D) = \frac{\sigma}{\sigma_{00}\, \delta\theta} \frac{A_x^2\,(D, D) P(D)}{\int_0^{D_{max}} A_x^2\,(D, r) P(r)\, r\, dr} = \frac{\sigma}{\sigma_{00}\, \delta\theta}\, \frac{1}{K_x(D)}$$

où σ est la SER de la cible, $P(D)$ est la perte de propagation aller-retour due à la propagation de l'onde de surface et finalement $K_x(D)$ est la contribution dépendant de la forme d'onde.

Les deux fonctions de coût qui ont été minimisées, sont deux fonctions conflictuelles. La première sert à maximiser le rapport cyclique de la forme d'onde et la deuxième évalue la perte maximale de taux de contraste le long de la portée su radar. Or, cette dernière a une tendance à augmenter avec l'augmentation du rapport cyclique d'où la nature conflictuelle des deux fonctions.

$$f_1(x) = \max_{0 \le D \le D_{max}} \left(10\ log\left(K_x(D)\right)\right)$$

$$f_2(x) = 100\ \left(1 - \frac{1}{T}\int_0^T x(t)\ dt\right)$$

En appliquant un algorithme d'optimisation multi-objectif, le NSGA-II, qui a prouvé sa supériorité dans la littérature pour les problèmes bi-objectifs tel notre cas, le front de Pareto qui existe entre ces deux fonctions a été approximé.

Les fronts ont été calculés pour des durées de code faisant 2 et 5 fois $\frac{2D_{max}}{c}$. Ces fronts approximés ont permis d'obtenir des gains moyens de 0.7 et 4 dB en moyenne par rapport à la forme d'onde conventionnelle.

Gestion du spectre

Ce chapitre étudie le problème de l'occupation spectrale du radar et propose des techniques afin d'adapter rapidement la forme d'onde transmise du radar à son environnement spectral. Le fait d'avoir une bande discontinue en fréquence et une alternance entre canaux autorisés et d'autres interdits ou occupés par de fortes interférences, pose un problème pour l'utilisation des formes d'ondes classiques tels les codes de phase ou de fréquence traités dans la littérature.

Technique du gradient

Cette technique proposée par [4] consiste à concevoir dans un premier temps une forme d'onde à émettre qui respecte les contraintes spectrales ainsi qu'une contrainte au niveau de la déviation de la puissance instantanée. Cette dernière permet de garantir un bon rapport puissance crête-puissance moyenne. La première fonction de coût, une intégration pondérée de l'énergie transmise dans les bandes interdites est agrégée par une simple somme pondérée à la déviation de la puissance crête de l'unité. Cette somme sera ensuite minimisée par la technique du gradient déterministe itérée :

$$J_T = \alpha J_{T1} + (1-\alpha) J_{T2}\ , 0< \alpha < 1$$

avec

$$J_{T1} = \sum_{k=1}^{N_b} w_k \int_{f_{k1}}^{f_{k2}} \left|\hat{h}(f)\right|^2 df$$

et

$$J_{T2} = \sum_{k=1}^{N_t} (|h_n|^2 - 1)^2$$

h_n étant les échantillons du signal temporel et $\hat{h}(f)$ sa transformée de Fourier.

Dans un deuxième temps, une forme d'onde de réception est conçue (filtre désadapté) afin de filtrer le signal reçu en provenance des bandes interdites et réduire en même temps les lobes secondaires de la fonction d'ambigüité résultante. La fonction de coût correspondante sera :

$$J_R = \beta J_{R1} + (1-\beta) J_{R2}, 0< \beta < 1$$

avec J_{R1} similaire à J_{T1} et $J_{R2} = g^{\dagger} H^{\dagger} H g$ tel que :

$$\boldsymbol{H} = \begin{pmatrix} h_1 & 0 & \dots & 0 \\ h_2 & h_1 & \dots & 0 \\ \vdots & \vdots & \vdots & \vdots \\ h_{N_t} & h_{N_t-1} & \dots & h_1 \\ \vdots & \vdots & \vdots & \vdots \\ 0 & 0 & \dots & h_{N_t} \end{pmatrix}$$

$\boldsymbol{g}$ étant le vecteur de la forme d'onde de réception.

Codage par l'algorithme génétique

Une autre alternative de la technique du gradient sera d'utiliser un algorithme génétique pour concevoir le code à émettre. Une des méthodes proposées dans [5], est de diviser les impulsions émises de la forme d'onde en sous-impulsions dans lesquelles de rampes de fréquence sont insérées correspondant aux canaux disponibles. Le rôle de l'algorithme génétique sera de déterminer le séquençage des rampes qui permet de réduire l'intégrale des lobes secondaires de la fonction d'ambigüité.

Dans un exemple tiré du rapport technique canadien concernant le spectre disponible en bande HF en été 1999 (Tableau 1), et après application de l'algorithme génétique par [5], le niveau du lobe secondaire maximale passe -9 dB à -13 dB approximativement (Fig. 8). Par contre ce résultat a été obtenu après avoir subdivisé chacune des 10 impulsions de la forme d'onde (Fig. 7) en 10 sous-impulsions d'où le débordement de puissance dans les bandes interdites (Fig. 9).

Tableau 1 Ensemble de 10 canaux disponibles en HF.

Canal	*Fréquences*
1	5.11~5.14 (MHz)
2	5.26~5.27 (MHz)
3	5.29~5.31 (MHz)
4	5.37~5.39 (MHz)
5	5.46~5.48 (MHz)
6	5.51~5.52 (MHz)
7	5.54~5.59 (MHz)
8	5.64~5.66 (MHz)
9	5.72~5.73 (MHz)
10	5.77~5.80 (MHz)

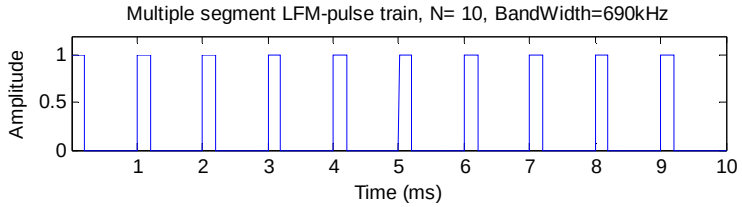

Fig. 7 Forme d'onde transmise de 10 impulsions et un rapport cyclique de 20%.

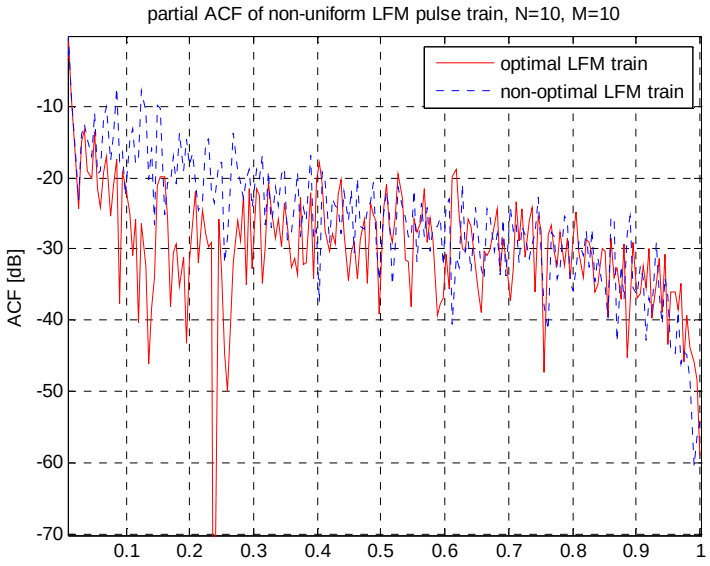

Fig. 8 Après optimisation du codage de chaque impulsion avec 10 rampes en fréquences, le niveau maximal de lobes secondaires est réduit à -13 dB.

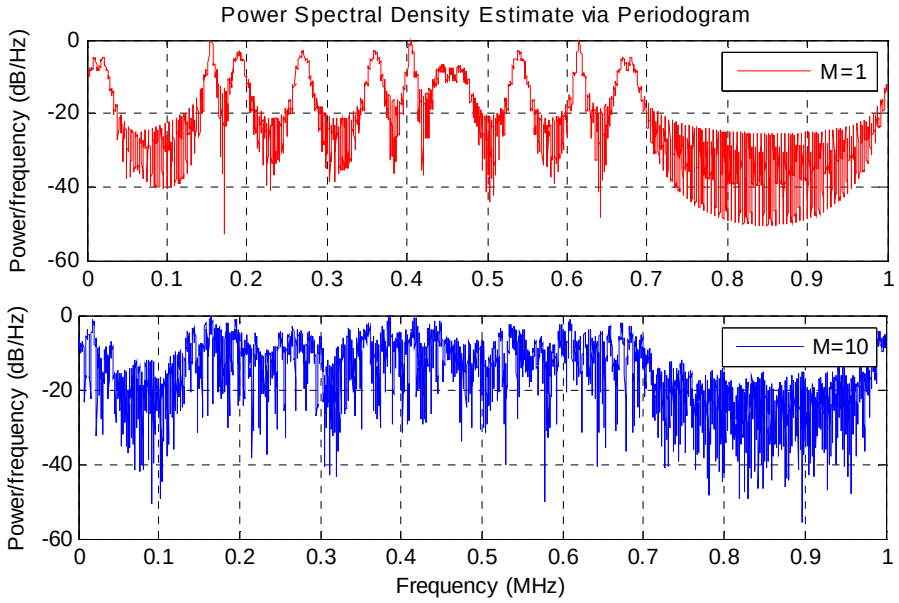

Fig. 9 La réduction du niveau maximal des lobes secondaire a été en dépit d'un étalement du spectre émis débordant dans les bandes interdites.

Approximation de la phase stationnaire

La méthode de la phase stationnaire a été proposée par Lord Kelvin au début du 19ème siècle afin d'approximer le calcul des intégrales qu'il a rencontrées en hydrodynamique. Cette méthode repose sur le faite que la majeure contribution de l'intégrale d'une fonction oscillant rapidement provient du voisinage des points où la phase est stationnaire.

$$I(\lambda) = \int_a^b f(t)\, e^{i\lambda\, g(t)} dt \sim f(c) e^{i\lambda\, g(c)} \sqrt{\frac{2\pi}{\lambda |g''(c)|}}\; e^{\frac{\pi i \mu}{4}}, \lambda \to \infty$$

avec $c \in [a,b] / \; g'(c) = 0, g''(c) \neq 0 \; et \; f(c) \neq 0$

Cette méthode trouve ainsi son application pour déterminer le code de phase qui permet de doter une enveloppe donnée dans le temps d'un spectre défini par son amplitude. Autrement, il s'agit de trouver $\varphi(t)$ qui vérifie $\left| \mathcal{F}\left(a(t) e^{j\varphi(t)}\right)\right| = A(f)$ avec des amplitudes $a(t)$ et $A(f)$ bien définies, $\mathcal{F}$ étant l'opérateur de la transformée de Fourier :

$$\mathcal{F}\left(a(t) e^{j\varphi(t)}\right) = \int_{-\infty}^{+\infty} a(t)\, e^{j[-2\pi f t + \varphi(t)]} dt = A(f) e^{j\phi(f)}$$

En appliquant la méthode de phase stationnaire à cette dernière intégrale :

$$A(f_k) \approx a(t_k) \sqrt{\frac{2\pi}{\varphi''(t_k)}}, f_k = \frac{1}{2\pi} \varphi'(t_k)$$

En posant :

$$\psi = \frac{\varphi'}{2\pi}$$

On peut écrire sous la condition de $\psi = f$

$$\frac{d\psi}{dt} = \frac{a^2(t)}{A^2(f)}$$

L'intégration de cette dernière égalité donne :

$$\int_{-\infty}^{\lambda} a^2(t)dt = \int_{-\infty}^{\psi(\lambda)} A^2(f)df$$

Ainsi, en évaluant l'aire de la surface sous la fonction $a^2(t)$ puis de celle sous $A^2(f)$, ont peut évaluer $\psi(\lambda)$ et remonter ainsi par simple intégration à φ.

En reprenant l'exemple du spectre disponible du rapport technique canadien, Fig. 10 montre le spectre résultant du signal occupant les canaux disponibles. Toutefois, le niveau du lobe secondaire maximal demeure élevé à -8.7 dB sans moyen de le contrôler (Fig. 11).

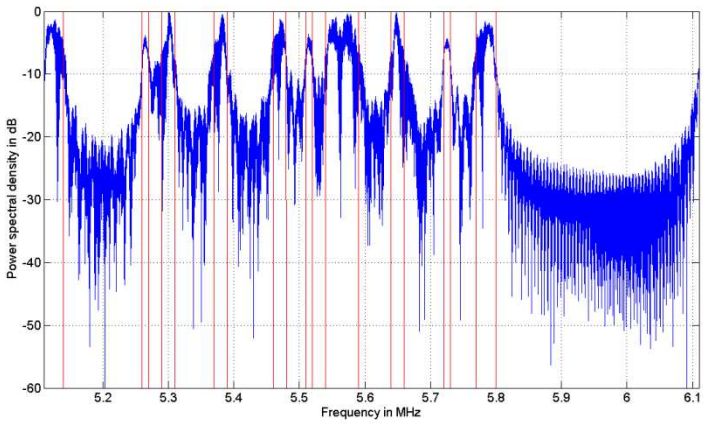

Fig. 10 Un cas pratique de spectre disponible occupé en utilisant la méthode de la phase stationnaire.

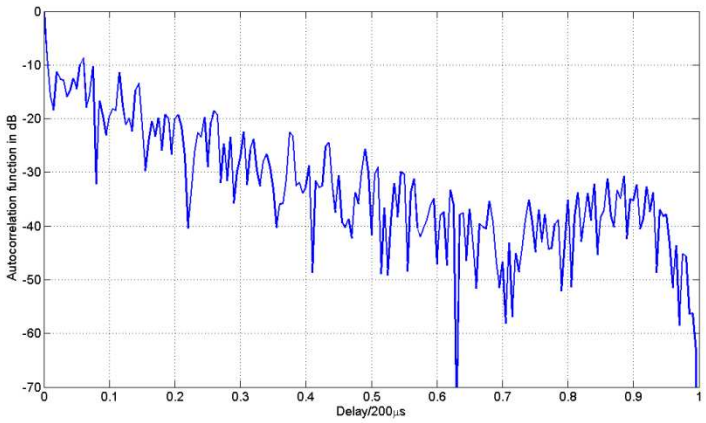

Fig. 11 La fonction d'autocorrélation du signal dont le spectre est montré dans la figure précédente.

La technique des projections alternées (PA)

Dans le cadre de ce travail, nous avons proposé une nouvelle technique de codage des formes d'onde radar, une technique basée sur des projections alternées et de corrections dans les domaines du temps, fréquence et de l'autocorrélation. Le passage entre ces domaines étant assuré par des transformées de Fourier, la technique proposée marie à la fois la simplicité de l'implémentation à une complexité quasi-linéaire de calcul (celle de la Transformée de Fourier Discrète ou TFD).

Le schéma suivant montre le principe de cette technique :

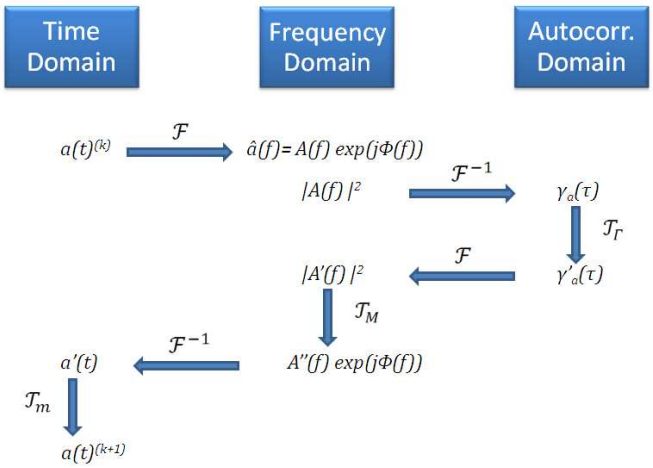

Fig. 12 de la technique des projections alternées pour le codage radar.

Le problème revient mathématiquement à trouver l'intersection de trois ensembles définis comme suit :

$$S_1 = \{a \in \mathcal{L} | (\forall\, t \in \mathbb{R})\ \ m_L(t) \leq |a(t)| \leq m_U(t)\}$$

$$S_2 = \{a \in \mathcal{L} | (\forall\, f \in \mathbb{R})\ M_L(f) \leq |\hat{a}(f)| \leq M_U(f)\}$$

$$S_3 = \{a \in \mathcal{L} | (\forall\, \tau \in \mathbb{R})\ \ |\gamma_a(\tau)| \leq \Gamma_U(\tau)\}$$

Avec $\hat{a}(f)$ et $\gamma_a(\tau)$ la transformée de Fourier et la fonction d'autocorrélation de $a(t)$ respectivement.

En partant d'une solution arbitraire de S_1, il s'agit de passer dans un premier temps au domaine fréquentiel en calculant le spectre du signal en question. A partir de l'amplitude du spectre la fonction d'autocorrélation est calculée. Cette dernière est corrigée en écrêtant les valeurs dépassant le seuil prédéfini. Le spectre correspondant à la nouvelle fonction d'autocorrélation est ensuite calculé puis corrigé selon le même principe avec les bornes supérieures et inférieures cette fois du spectre, agissant uniquement sur l'amplitude et gardant la phase. Un retour au domaine temporel et une dernière correction de l'amplitude et le signal est de nouveau prêt pour une prochaine itération.

Cette technique a été testée sous plusieurs configurations : avec contrainte spectrale uniquement, avec contrainte d'autocorrélation uniquement, et finalement avec les deux contraintes.

Dans le premier cas, le même scenario de bande HF a été repris pour comparer les performances, et le niveau de rejection de la bande interdite est passé de -6.22 dB dans le cas de la phase stationnaire à -14.5 dB avec la technique proposée au bout de 100 itérations.

Dans le deuxième cas, et en appliquant des contraintes uniquement au niveau de la fonction d'autocorrélation, des codes quasi-idéaux ont été trouvés tels les codes polyphases vérifiant la condition de Barker ou les codes ayant une fonction d'autocorrélation périodique idéale (Dirac) comme le montre la Fig. 13.

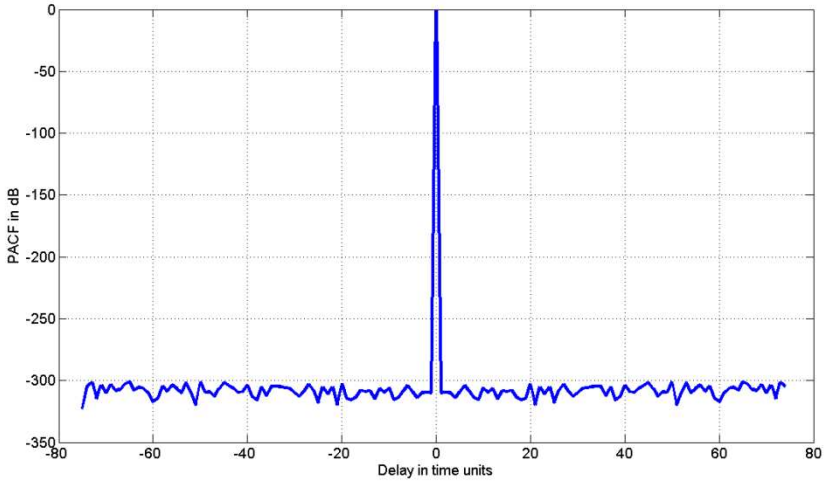

Fig. 13 Une fonction d'autocorrélation périodique quasi-idéale obtenue par les projections alternées pour un code de longueur 150.

Finalement, les deux contraintes de spectre et d'autocorrélation ont été appliquées à notre benchmark de canaux disponibles en bande HF en comparaison avec le résultat de l'algorithme génétique. Pour un niveau maximal de lobe secondaire maintenu à -13 dB, Fig. 14 montre les deux spectres obtenus par les deux algorithmes. Une bonne amélioration de l'occupation spectrale peut être remarquée pour la solution des projections alternées, où on arrive même à discerner visuellement la bande autorisée de la bande interdite.

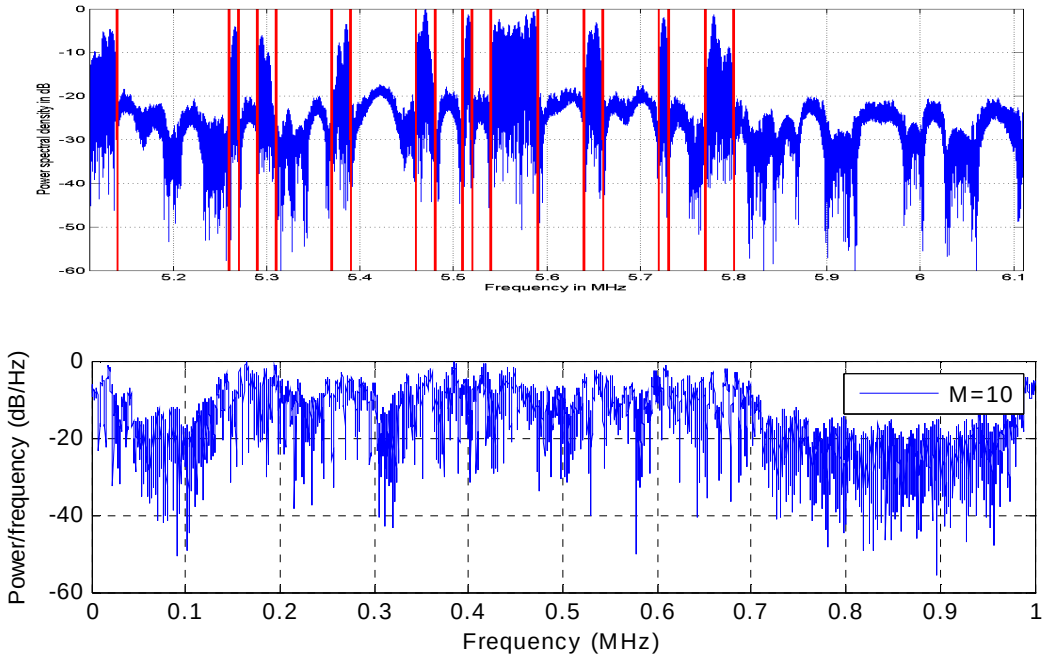

Fig. 14 Densité spectrale de puissance de la solution obtenue par projections alternées en comparaison avec la solution proposée par [5] en utilisant un algorithme génétique avec une contrainte de -13 dB pour les lobes secondaires.

Validation expérimentale

Ce chapitre présente le test des formes d'onde et des techniques de codage décrites précédemment. La capacité de la forme d'onde à rapport cyclique élevé à opérer à courtes et longues distances en présence des pertes d'éclipses est examinée.

Les expérimentations ont été menées au centre de l'Onera, Palaiseau, situé à 10 km de l'aéroport de Paris-Orly. Les avions en décollage ou en atterrissage constituaient des cibles parfaits pour les expérimentations en question.

Le schéma bloc du système de mesure présenté dans la Fig. 15 a été placé sur un toit de l'un des bâtiments et comprenait :

- Deux antennes d'émission et de réception (passive) omnidirectionnelles distantes de 20 m et séparées par la chambre abritant le reste de l'équipement.
- Un Pc industriel muni de deux cartes ICS 554 et 564 servants de convertisseurs Analogique/Digital et Digital/Analogique respectivement, avec une résolution de 14 bits.
- Des amplificateurs et des synthétiseurs de fréquence

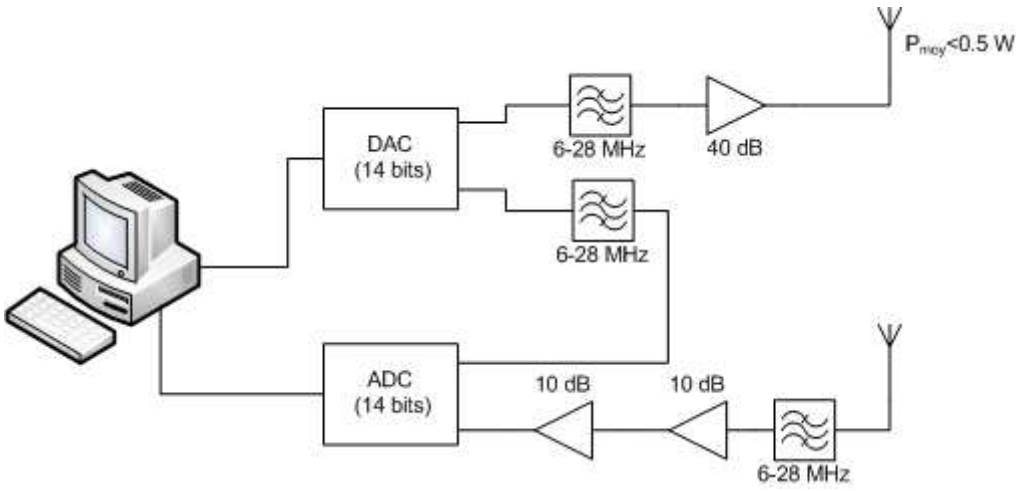

Fig. 15 Le schéma bloc du radar expérimental.

Le test des formes d'onde

Dans le chapitre de gestion du temps d'émission radar, de nouvelles découpes temporelles combinant des impulsions de différentes largeurs ont été présenté. Ces découpes avaient la propriété de résister aux dégradations en résolution qui se produisent à l'intérieur de la zone d'éclipse de la forme d'onde conventionnelle.

Un ensemble de quatre formes d'onde différentes a été constitué à partir d'une des formes d'onde optimisée (Fig. 5) et d'une forme d'onde conventionnelle une fois avec une rampe linéaire en fréquence et une fois avec la PA afin d'occuper une bande de 300 kHz. Les caractéristiques de ces formes d'onde sont présentées dans le tableau suivant :

Forme d'onde	*Enveloppe*	*Largeur d'impulsion*	*Période de rép.*	*Rapport cyclique*	*Bande (kHz)*	*Code Type*
W1	Impulsion	56.4 μs	120 μs	0.47	300	Rampe lin.
W2	Impulsion	56.4 μs	120 μs	0.47	300	PA
W3	Optimisée	-	120 μs	0.47	300	Rampe lin.
W4	Optimisée	-	120 μs	0.47	300	PA

La fréquence centrale a été choisie dans un des canaux libres en bande HF à 24 MHz et dont l'état d'occupation a été vérifié à l'aide d'un analyseur de spectre avant émission. La puissance transmise était de moins de 0.5 Watt en moyenne et chaque acquisition se faisait sur 120 s. Un traitement distance-Doppler classique avec une durée d'intégration de 2s a été appliqué. Ainsi les résolutions vitesses et distance théoriques étaient de :

$$\Delta v = \frac{c}{2Tf_0} = 3.125\ m/s$$

$$\Delta r = \frac{c}{2B} = 500\ m$$

La Fig. 16 montre l'évolution de la résolution mesurée en fonction de la distance pour les différentes formes d'onde. Ces résultats confirment d'une part la dégradation de la résolution prédite pour la forme d'onde conventionnelle et ceci pour deux types de codage différents. Cette dégradation atteint 3 à 5 fois la résolution idéale. D'autre part, la forme d'onde optimisée a réussi à garder une résolution quasi-constante comme prévu autour de 500 m correspondant à la valeur approximative théorique (Fig. 16).

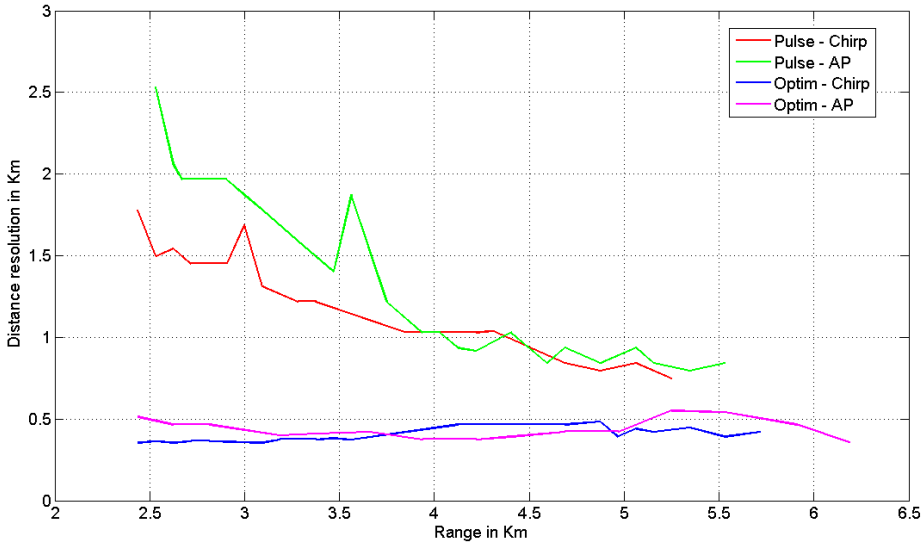

Fig. 16 Evolution de la résolution mesurée en fonction de la distance pour les différentes formes d'onde.

Conclusion

L'objectif de ce travail a été de surmonter les problèmes qui peuvent se poser lors de l'étalement de l'énergie en temps et en fréquence.

Pour le radar monostatique utilisant l'isolation temporelle efficace des canaux d'émission et de réception, l'étalement de l'énergie dans le temps produit une augmentation des pertes d'éclipse qui détériorent les performances du radar pour les distances affectées. Dans ce contexte, le deuxième chapitre a présenté la conception de formes d'onde allant jusqu'à 50% en rapport cyclique et permettant de d'épargner plus les longues distances de ces pertes que les courtes distances qui sont moins affectées par les pertes de propagation. Combinant à la fois des courtes et des longues impulsions, ces formes d'onde résistent ainsi à la dégradation de résolution à l'intérieur de la zone d'éclipse qui a lieu pour la forme d'onde conventionnelle. Cette propriété a été validée expérimentalement au chapitre 4.

L'aspect fréquentiel de la forme d'onde radar a été étudié au chapitre 3. Une nouvelle technique de codage basée sur les projections alternées a été introduite, testée et comparée avec d'autres techniques existantes. Simple à implémenter, pourtant efficace en calcul car utilisant des transformées de Fourier successifs, cette technique permet de répondre à la fois à des contraintes d'allocation spectrale et de contrôler le niveau des lobes secondaires de la fonction d'ambigüité associée. Des codes quasi-idéaux ont été trouvés avec des propriétés similaires aux codes de Barker polyphases ou les codes de Franck, P4 (etc.) dérivés de la rampe en fréquence.

Autre avantage, ces solutions ne figurent à priori dans aucune base de données de forme d'onde ce qui rend leur classification très difficile et empêche ainsi la réalisation d'un récepteur d'interception dédié.

Parmi les perspectives, on peut imaginer une extension de la projection alternée pour un réseau d'antennes, permettant ainsi de privilégier des bandes de fréquences dans des directions particulières et éviter d'autres dans d'autres directions. Finalement, l'utilisation des algorithmes évolutionnaires pour les applications radar demeure un domaine de recherche prometteur surtout avec l'accroissement de la complexité des futurs systèmes radars, ainsi que la quantité d'informations à fournir et traiter en temps réel.

PH.D. THESIS
OF THE UNIVERSITY PIERRE ET MARIE CURIE
PARIS VI

Speciality:

ELECTRICAL ENGINEERING
(SMAER)

Presented by:

Rami KASSAB

For the grade of:

DOCTOR OF PHILOSOPHY OF THE UNIVERSITY OF PIERRE ET MARIE CURIE

DESIGN OF LPI WAVEFORMS FOR MONOSTATIC RADAR

JURY:

Pr. Hugh GRIFFITHS, University College London	Reviewer
Pr. Philippe FORSTER, University Paris X	Reviewer
Pr. Aziz BENLARBI-DELAI, University Paris VI	Examiner
Pr. Marc LESTURGIE, Onera/ Sondra (Director)	Research co-Director
Dr. Jocelyn FIORINA, Supélec	Supervisor
Pr. Walid TABBARA , University Paris VI	Research Director

Université Pierre & Marie Curie - Paris 6
Bureau d'accueil, inscription des doctorants et base de données
Esc G, 2ème étage
15 rue de l'école de médecine
75270-PARIS CEDEX 06

Tél. Secrétariat : 01 42 34 68 35
Fax : 01 42 34 68 40
Tél. pour les étudiants de A à EL : 01 42 34 69 54
Tél. pour les étudiants de EM à ME : 01 42 34 68 41
Tél. pour les étudiants de MF à Z : 01 42 34 68 51
E-mail : scolarite.doctorat@upmc.fr

Contents

List of Figures

List of Acronyms

ACF	Autocorrelation Function
ADC	Analogue to Digital Converter
AF	Ambiguity Function
AP	Alternate Projection
ARM	Anti-Radiation Missile
CS	Cumulative Sum
CW	Continuous Waveform
DAC	Digital to Analogue Converter
ESM	Electronic Support Measures
FMCW	Frequency Modulated Continuous Waveform
FOPEN	FOliage PENetration
HFSWR	High Frequency Surface Wave Radar
ITU	International Telecommunication Union
LO	Local Oscillator
LPI	Low Probability of Intercept
NLFM	Non-Linear Frequency Modulation
NSGA-II	Non-dominated Sorting Genetic Algorithm II
PACF	Periodic Autocorrelation Function
PSL	Peak Sidelobe Level
RCS	Radar Cross-Section
RDD	Radar Detector Detector
SCR	Signal to Clutter Ratio
SINR	Signal to Interference plus Noise Ratio
SNR	Signal to Noise Ratio
WRC	World Radiocommunication Conference

Chapter 1

Introduction

1.1 An electronic war... on the road

One of the many car gadgets available on the market is a speed radar detector. This electronic device, whose usage is prohibited in many countries, warns the driver for a possible presence of speed monitoring so he can avoid being penalised for over-speeding. In fact, the law enforcement authorities often rely on Doppler radars like hand-held radar guns, in order to measure the speed of moving vehicles. These radars could be also mounted on police car patrols or even in strategic places where over-speeding frequently occurs.

The radar detector, on the other hand, uses a super heterodyne receiver in order to detect these radars emissions. The detection should occur far enough to give the driver the time to react and readjust his speed.

Figure 1. Spectre IV+ a radar detector detector from Stealth Micro Systems sensitive to the local oscillator leakage of the common radar detectors.

As a countermeasure to these detectors, the radar guns first used new frequencies which made the detectors ineffective until they were able to update their technology. Next, the radar transmissions have reduced their time and peak power in order to reduce the probability of interception, but the detectors were able to follow up by using more sensitive receivers.

The law enforcement authorities started then to use a new radar gun equipped with radar detector detector (RDD), which is no more than a modified version of

the radar detector, sensitive essentially to the local oscillator (LO) frequency used by the radar detector superheterodyne receiver. Nevertheless, newer versions of the radar detectors managed to fabricate a superhetrodyne detector which does not produce LO leakage - typical of such detectors - which current RDDs, such as the STALCAR/SPECTRE shown in Figure 1, rely upon to alert proximate detector usage.

Now, replace the speed radar by a critical radar application such as altimeter or airborne surveillance and the problem takes another dimension. This time, any interception of the radar transmissions makes it vulnerable to jamming or to the threat of anti-radiation missiles (ARM).

1.1 To see without being seen

The art of designing radar equipment that is hard to intercept started at the end of the World War II and evolved into one of the most important features of modern radar systems known as LPI for the low probability of intercept.

One look at the radar range equation and one could figure out the challenge facing this type of radar. The equation states that a standard intercept receiver will always benefit after one way propagation from a much higher signal level than the radar itself after a two-ways propagation. But it is the very purpose of the LPI design to unbalance this standard situation where the Electronic Support Measure (ESM) and Radar Warning Receivers have this tactical advantage.

The strategy could be summarised by first avoiding transmitting more power than the necessary and then to spread the radar transmissions in all possible dimensions i.e. time, frequency and space (even polarisation).

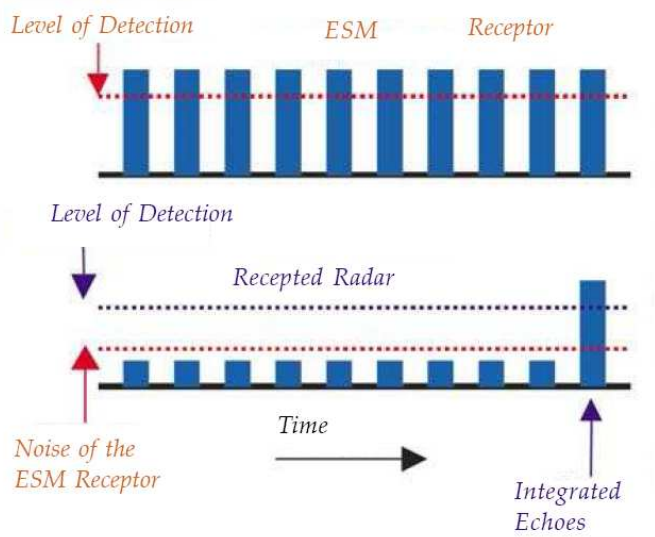

Figure 2. The reduced transmissions of the LPI radar hidden within the noise of the ESM receiver sum up after coherent integration in the Radar.

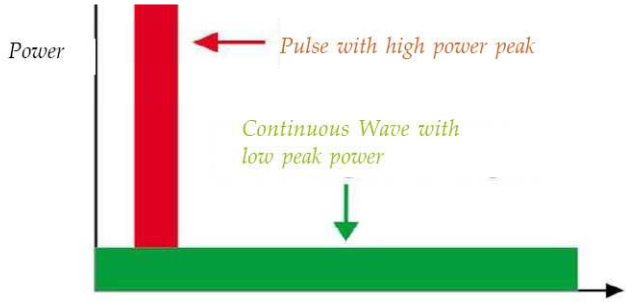

Figure 3. The continuous waveform spreads the transmitted energy through time and therefore having a lower peak power compared to the conventional waveform.

1.2 Time considerations

An LPI radar tries to reduce the peak transmitted power and hide itself within the noise, as seen in Figure 2, since the performance of the intercept receiver is a function of the peak power and depends on the signal to noise ratio (SNR) in order to validate the detection. Nevertheless, this does not affect the performance of the radar whose performance depends on the mean transmitted power and could resort to coherently integrate long enough in order to achieve the desired SNR. In this context the use of continuous waveforms offers the highest mean to peak power, as illustrated in Figure 3, and these waveforms are therefore the best candidates for this purpose.

Figure 4.The PILOT equipment consists of a transceiver unit and a signal processor unit that should be integrated with standard navigation antenna and a display (or Multi-Function Console) to form a complete radar.

One of the firsts and most famous radar system that applied this concept is the PILOT [6] which stands for "Philips Indetectable Low Output Transceiver". This LPI radar was conceived and tested by Philips Laboratories in September 1987. The radar transmitted a frequency modulated continuous waveform (FMCW) in a monostatic configuration with just one antenna, relying on a Reflected Power Canceller technology to cancel the power and noise leaking from the transmitter into the receiver. With a nominal output power of 1W, PILOT achieved ranges of 15 to 20 km against typical naval targets of $100m^2$ which is usually achieved by a conventional pulsed radar with 10-20 kW of peak power and 5-10 W of average power. When it comes to the intercept range, an ESM with a minimum detectable signal of -60 dBmi, could detect the conventional radar at 250 km while the PILOT would be intercepted at only 2.5-3 km.

However, realizing enough isolation between the transmitter and the receiver in continuous monostatic radar remains a severe problem. In fact the leakage power, which typically largely surpasses the radar returns, can saturate the low noise amplifiers in the receiver.

The idea of the power leakage cancellation could be traced back to 1960. It consists in feeding back into the receiver some out-of-phase version of the transmitted signal. The amplitude and phase adjustment of this signal was first made by hand. In 1990, this process was automated by an analogue adaptive cancellation scheme. In 2004, a digital leakage cancellation technology using DSP was proposed in order to achieve a better precision of cancellation [7] [8].

What is even more severe problem is the noise leakage from the transmitter to the receiver [9]. This noise reduces badly the dynamic ranges of the radar. To suppress this noise, delay matching is applied as in the case of the Pilot radar in the microwave frequency. Yet, it is reported in [9], that this technique remains hard to implement in the high frequency.

Nonetheless, for monostatic radar the time isolation between the transmit and the receive channels remains the most effective solution to suppress the power and noise leakage problem, especially for long range radar that need to transmit higher power. This solution also reduces the cost and complexity of the leakage cancellation techniques.

In this particular case the LPI strategy recommends the use of quasi-continuous waveforms with high duty cycle, 50% being the highest reasonable duty cycle to be reached, allowing eventually enough time to receive the whole transmitted power. In fact, when blanking the receive channel while the transmitter is on, partial or even total eclipse of the target returns may occur depending on the waveform and the range of the target.

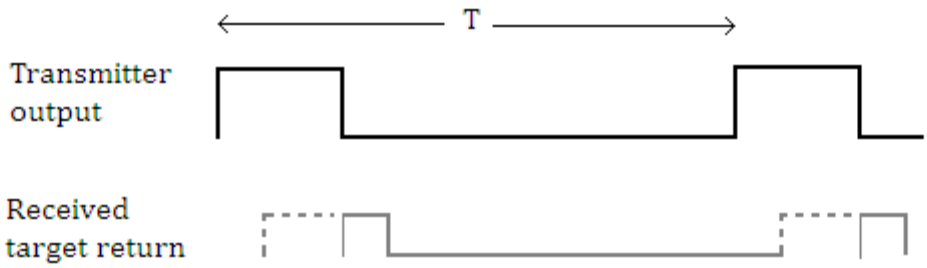

Figure 5. An eclipsing situation for a pulsed waveform of repetition period T where a part of the target return is lost while the transmitter is on and the receiver is off.

Figure 5 illustrates an example of partial eclipsing occurring for a near target return in the case of a pulsed waveform of a repetition period T.

In order to reduce this eclipsing loss, [10] proposed to use particular binary codes having low autocorrelation function. But as the duty cycle of these codes drops rapidly when their length increase, [10] adopted a long repetition of the optimal code, relying on a gold complex code to resolve the distance ambiguity. The resulting eclipsing loss suffers from high fluctuation against the distance due to the repetition of the code. A criticism we would raise is that the previous design makes no allowance for the propagation losses of the signal. These losses would make the eclipsing losses have more critical impact on the SNR of the far distance bins whose returns are more affected by the propagation losses.

1.3 Bandwidth considerations

Spreading the transmitted power in frequency gives more difficulty to the intercepting receiver. In fact, the intercept receiver needs a channel bandwidth to be narrow enough to separate different signals that are close in frequency. On another hand, increasing the bandwidth of the channel leads to a decrease in the SNR of the intercept receiver, as the noise is proportional to the size of the received band. Consequently the detection sensibility of the interceptor is reduced.

In addition, increasing the bandwidth of the radar's waveform improves the distance resolution, particularly for the continuous waveforms relying on the pulse compression to achieve the desired range resolution.

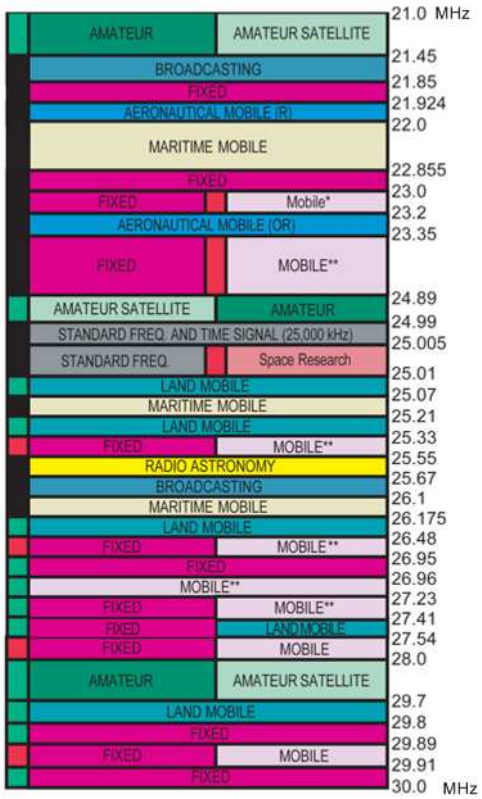

Figure 6. Part of the United States official frequency allocations on October 2003 in the HF band.

However, the bandwidth available for radar use is a precious resource, rare and difficult to find especially for radar applications. For example, Figure 6 shows a portion of the radio spectrum in the HF band as defined officially by the United States National Telecommunications and Information Administration on October 2003. In this table we notice the congestion of the HF band, which is a main limitation for some radar applications like the High Frequency Surface Wave Radar (HFSWR) as well as the presence of strong emitters like the TV broadcast and the mobile applications in the frequency domain of the Foliage Penetration (FOPEN) Synthetic Aperture Radar chosen to reduce the attenuation due to vegetation. In the same time, the radar should also avoid to radiate into some bands used by other radars or dedicated for critical applications like the navigation.

The radar waveform designer investigated in a first step the techniques to suppress the interference in the receiver. The interference signal parameters are first estimated and then subtracted from the original signal [11]. Then came the notch filtering which derives a filter after estimating the interference spectral energy. The side effect of this technique is a potential increase in the sidelobes that could be reduced by a combination of median and apodisation filtering [12]. In [13] the authors present the optimal transmit and receive waveforms construction to maximize the signal to interference plus noise ratio (SINR). By receive waveform, we denote the modified replica used to correlate with the received signal.

Finally, [4] presented a sparse frequency transmit and receive waveform design that allows to transmit in a set of available channels and avoid the transmission in the forbidden bands. The receive waveform is designed also to minimise the reception of the forbidden bands and suppress the range sidelobes of the ambiguity function. During the design a conjugate gradient algorithm is used in order to minimise the linear aggregation of the penalty functions like the Integrated Sidelobe Level (ISL) and the integral of the spectral energy in the stop bands.

The receive waveform proposed in [4] different than the conjugate of the transmitted signal as in the case of match filtering [14], comes at the expense of the SNR due to the mismatch.

In an attempt to prevent the mismatch loss, [5] considered the same optimisation problem using only the transmit waveform and for the case of a matched filtering. In [5], the authors replaced also the gradient algorithm by a genetic evolutionary algorithm.

But since the radar spectral environment could vary rapidly, as in the case of sudden interference in one channel or in the case of a shared channel that became available, the design algorithm is desired to be able to respond in the shortest delays to these changes if not requiring a real-time adaptation to the spectral environment.

1.4 The approach

From all the preceding, we conclude that for the monostatic radar using time isolation between the transmit and receive channels, the waveform to use is a quasi-continuous waveform. The transmit/receive strategy should be carefully chosen to be adapted to the operational range of the radar since the eclipse losses could affect the evolution of the SNR or the signal to clutter ratio (SCR) over the range. Since the transmitters are often peak power limited, the operation in the blocked/saturate states implies that the envelope of the waveform is determined by the transmit/receive strategy (constant amplitude).

The next step is to determine the phase code that should spread the transmitted waveform in frequency, occupy the available channels, avoid the critical bands or the ones with interference and exhibit good performances in terms of resolution and sidelobes level of the ambiguity function, commonly used to evaluate the delay- Doppler match filer response. In contrast to the first step, this step is subject to a computational efficiency constraint due to the dynamic nature of the spectrum in some applications.

Away from the conventional intuitive approach of waveform design where the transmitted waveform is series of periodic impulses whose repetition period is determined by the maximal range of the radar, and whose code is chosen in the catalogue of well known codes (Chirp, Barker, Franck, Costas …), in the following we propose a two parts optimisation in time and then in frequency.

First, we showed how an envelope optimization of a quasi- continuous waveform could manage the shelter loss in distance to limit its effects on the SNR in a noise limited application and on the SCR in another clutter limited application. The results were the subject of [15], [16] and [17]. Next, we considered the phase coding problem under the different spectral and performance constraints and we proposed an efficient and simple algorithm to respond to these constraints. This algorithm was presented in [18] and [19]. Finally, taking advantage of the laboratory facilities available in Sondra and the Onera and the geographical position of the Onera's center in Palaiseau near Orly's airport, the resulting waveforms were tested and compared with the conventional waveforms in a real radar scenario of aircraft detection and localisation.

Chapter 2 presents and explains in details the origin of the LPI strategy. As a consequence of this strategy, the problems resulting from spreading the energy in time are presented for a monostatic radar using time isolation between the transmit and the receive channels. The deterioration of performance due to the consequent eclipse loss is highlighted. Finally noise limited and clutter limited (sea clutter of the HF surface wave radar) cases are considered and new solutions are derived allowing a convenient spread of energy in time.

Chapter 3 deals with radar spectrum management problem. The radar waveform should be able to fit in a given set of available channels and avoid some other forbidden ones. Some existing techniques that allow radar waveform designs under spectral constraints are presented. In addition a new efficient technique is introduced and compared with the previous ones.

Chapter 4 presents the experimentations that were carried out in order to validate the performance of the proposed waveforms and techniques. Using the aircrafts flying nearby as targets different combinations of optimised and conventional codes and envelopes were tested and their performances measured and analysed.

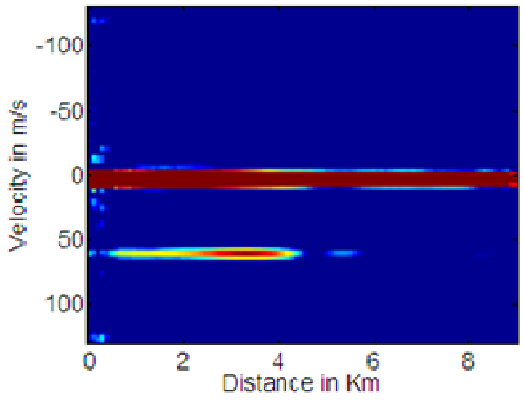

With a conventional waveform

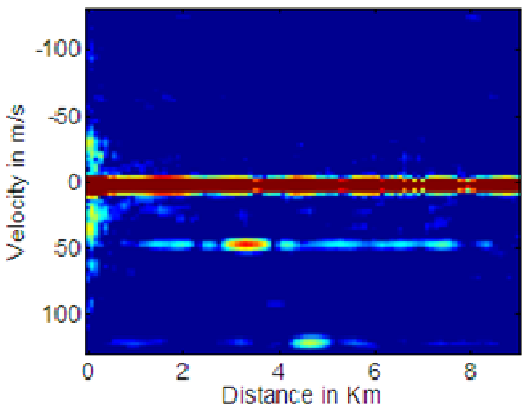

With the new waveform

Chapter 2

Managing Time

2.1 Introduction

In this chapter the LPI strategy and its influence on the waveform design is revisited. In order to achieve good LPI characteristics in a monostatic radar special attention should be paid to the shelter effect when applying the time isolation between the transmit and receive channels. For this, two cases of transmit/receive strategies are presented covering their impact on the SNR and SCR. In every case appropriate waveform design is carried out and the resulting solutions are compared with the conventional pulsed waveforms.

2.2 Radar configurations

Depending on the use or not of active antennas and their location relatively to the receiver, radar could operate in monostatic, bistatic or even multistatic passive or active configurations. This classification depends on the angle formed by the transmitter, the target and the receiver also known as the bistatic angle: when close to zero the configuration tends to be monostatic even with physically separated transmit/receive antennas.

Monostatic radars have some inherent advantages and are considered to be all weather wide area sensors. Their use of active emitters gives them the ability to better operate in noisy environments and then to cover wide areas rapidly.

Bistatic and multistatic radars on another hand benefit from a resilience to countermeasures, since the receiver is separated from the emitter which could be detected and jammed. In addition they benefit from an eventual amelioration of the radar cross section of the target even for stealth targets given the difficulty to reduce echoes in all directions. This naturally comes at the expense of the system complexity and the necessity of synchronisation between sites commonly achieved by means of global positioning system (GPS) (Satellite two way comm. Link, direct path (LOS or wired)) [20]. In passive mode, the system bypasses the need for dedicated transmitter, easing the overall system in terms of related costs (power, maintenance, frequency allocation, etc.) but suffers from the lack of control of performance since it depends on third party transmissions.

In addition it is also possible to combine monostatic and bistatic information of a given area in order to achieve better performances.

2.3 Power leakage

In applications where size and weight are critical such as the unmanned vehicles and satellites, monostatic radar offers more practical solution, especially when high power microwave antenna is the heaviest part of the system, by using it as both emitter and receiver. However, one of the severe challenges in the design of monostatic radar is to realize enough isolation between the transmitted and the received signals. In fact, the power leakage from the circulator which could be used to do the separation, in addition to the reflected power due to the antenna mismatch, could easily surpass the power of the targets returns and saturate the low noise amplifiers in the receiver, especially that these signals are not filtered out since they naturally belong to the same frequency band of the radar. And, if the transmitted signal could leak, so does the noise from the transmitter to the receiver reducing its sensitivity.

This leakage power could be reduced by means of cancellation methods [7] [8] whose aim is to produce a signal with the same amplitude with opposite phase to the leakage signal in order to feed it through the receiving path for cancellation. One could also consider the separation of the transmitter and the receiver despite the difficulty of decoupling between the transmitting and receiving antennas in low frequencies due to their low directivities.

The last resort is to avoid the use of continuous waveforms and allow the time isolation between the transmission and reception. This explains the use of pulsed waveforms in monostatic radar, where the receiver is blocked during the transmission.

2.4 Low probability of intercept (LPI) properties

2.4.1 Introduction

With the improvement of electronic technology, and the integration of new components and signal processing techniques in radars using more complex waveforms, the performance of modern radar is improving significantly. In the same time comes the improvement of radar warning receivers, electronic support measures (ESM) and anti-radiation missiles (ARM) threatening the effectiveness and existence of the radar.

Therefore, an important feature [21] for radar system is to exhibit low probability of intercept.

2.4.2 **The range factor**

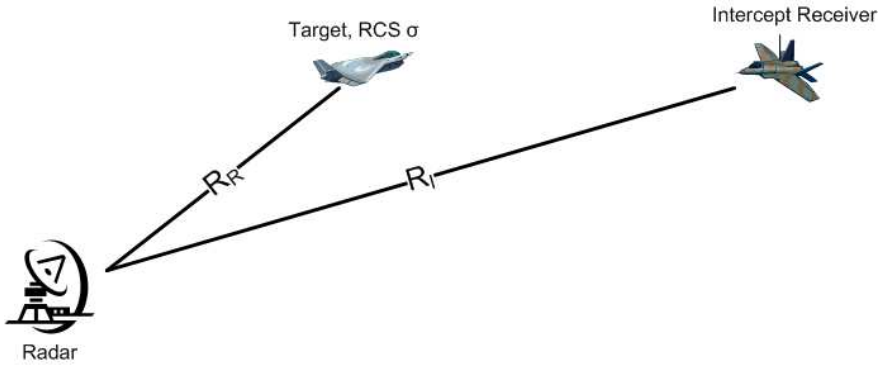

Figure 7. The radar against an intercept receiver scenario.

Let us consider the next scenario shown in Figure 7 where a radar is capable of detecting a target of RCS σ for a range R_R in the presence of an intercept receiver whose intercept range for the radar is R_I. Assuming that the intercept receiver has an RCS σ, we can see that if $R_I > R_R$ the radar is detected by the intercept receiver. In the opposite case, the radar could detect the intercept receiver while keeping itself hidden from interception. It is this kind of feature that we look for and the corresponding radar is qualified as LPI.

Of course, it must be recognised that no matter what, an active sensor will always have a probability of intercept. And it is also evident that radar that has an LPI property would have it to a particular type of intercept receiver and not to all kinds of receivers.

The ratio of the intercept receiver range to the radar range is called the range factor [22] and is used to evaluate the LPI performance of a radar relatively to an intercept receiver:

$$\alpha = \frac{R_I}{R_R}$$

α should be lower than one, and the lower it is, the better is the LPI performance of the radar.

The radar detection range could be expressed by:

$$R_R = \left[\frac{G_T \frac{E_T}{\tau} \sigma G_R \frac{\lambda^2}{L_R}}{(4\pi)^3 K T_R B_R S_R} \right]^{\frac{1}{4}}$$

where G_T and G_R are the radar receiver and transmitter antenna gain respectively, E_T is the radar transmit energy, τ is the pulse width, λ is the radar wavelength, L_R is the radar loss, K is the Boltzmann constant, T_R is the radar noise temperature, B_R is the radar signal bandwidth and S_R is the signal to noise

ratio required at the input of the radar receiver in order to ensure some given probabilities of detection and false alarm.

Now for the intercept receiver, the propagation from the radar towards it is only one-way whereas it is both ways for the radar. Therefore, the intercept range is:

$$R_I = \left[\frac{G_{TI} \frac{E_T}{\tau} G_I \frac{\lambda^2}{L_I}}{(4\pi)^2 K T_I B_I S_I} \right]^{\frac{1}{2}}$$

where G_{TI} is the radar transmitter antenna gain towards the intercept receiver, G_I is the intercept receiver gain, L_I is the intercept receiver loss, T_I is the intercept receiver noise temperature, B_I is the intercept receiver effective bandwidth and S_I is the signal to noise ratio required at the input of the intercept receiver in order to ensure the same probabilities of detection and false alarm as the radar.

The range factor is therefore expressed as:

$$\alpha = \left[\frac{1}{4\pi} \frac{{G_{TI}}^2}{G_T} \frac{{G_I}^2}{G_R} \frac{\lambda^2}{\sigma} \frac{S_R}{{S_I}^2} \frac{L_R}{{L_I}^2} \frac{E_T K T_R}{K^2 {T_I}^2} \frac{B_R/\tau}{{B_I}^2} \right]^{\frac{1}{4}}$$

$$= R_R \left[\frac{4\pi}{\sigma} \frac{T_R}{T_I} \frac{B_R}{B_I} \frac{L_R}{L_I} \frac{G_{TI} G_I}{G_T G_R} \frac{S_R}{S_I} \right]^{\frac{1}{2}} \quad (*)$$

Since the required probabilities of detection and false alarm are the same for both the radar and the intercept receiver, we could assume that the required SNRs at the output of the receivers are also the same. We denote them by S_{oR} and S_{oI} for the radar and the intercept receiver respectively.

The following ratio could be rewritten:

$$\frac{S_R}{S_I} = \frac{S_{oR}/\mathrm{G_{PR}}}{S_{oI}/\mathrm{G_{PI}}} = \frac{\mathrm{G_{PI}}}{\mathrm{G_{PR}}}$$

where $\mathrm{G_{PR}}$ and $\mathrm{G_{PI}}$ are the processing gains of the radar and the intercept receiver respectively.

To give an application to the range factor formula let us consider the performance of a coastal surveillance radar [23] used for ship detection against the performance of a ship mounted radar warning receiver. The radar is able to detect Swerling 3 targets of RCS 100 m^2 up to 15 km with an integration gain of 338 (25 dB) and a resolution of 3m using a 30dB gain scanning antenna. The receiver has an omnidirectional coverage in azimuth with 0 dBi of gain and 25 MHz of bandwidth. By assuming that both the radar and the receiver have the same noise figures and losses and considering sidelobe detection, replacing the values into the range factor formula gives us:

$$\alpha = 15000 \times \left[\frac{4\pi}{100}\frac{50}{25}\frac{1}{10^6}\frac{1}{338}\right]^{\frac{1}{2}} = 0.409$$

From this result, the radar is able to have a safe detection of the ship from 6135 m to the 15 km range without being intercepted.

2.4.3 **The strategy**

A first analysis of the radar range factor (*) first shows that it increases with the radar's range. This results from the one-way free space loss of the intercept receiver while the radar exhibits two ways propagation loss. Therefore, the longer is the radar's range the easier it is for the intercept receiver to detect the radar. But since the radar's range is fixed by the application, the LPI performance mainly depends on the antennas gain and the sensitivity of the receivers.

The ratio $\frac{G_{TI}}{G_T G_R}$ indicates that for better LPI properties, the transmit antenna should have a wide beam in order to hide itself from the intercept receiver. This could also allow the radar to cover a wide zone without scanning, reducing the cost of the transmitter. The radar receiving antenna should be in the contrary as narrow beam as possible and with minimal sidelobes.

The radar bandwidth is determined by the approximate desired range resolution and for coherent integration over a time interval T_C the processing gain of the radar is $B_R T_C$. Now if the intercept receiver succeeds in matching the radar's bandwidth, its incoherent integration will provide it with a lower processing gain, estimated for a same integration time T_C by $(B_R T_C)^{\gamma}$ with γ typically 0.7 to 0.8. Therefore the radar receiver will maintain a processing advantage of $(B_R T_C)^{1-\gamma}$. As a consequence, the LPI radar has all profit in spreading its transmitted energy in frequency and in time.

In brief, the LPI strategy could be resumed by the spread of the radar transmissions in all possible dimensions, i.e. space, time and frequency.

2.5 Eclipsing loss

2.5.1 **Introduction**

Eclipsing loss is the loss of received signal in radar that occurs while the receiver is switched off during the transmission (see Figure 5). For pulsed waveforms this loss usually occurs for the targets that are near the transmitting system and for the targets at the end of the unambiguous range extent. These two regions i.e. at the beginning and the end of the radar extent are also known by the first and the second eclipsing zones respectively [24].

This eclipsing effect results in a degradation of the performance, since the waveform is partially received, a degradation that usually occurs on two levels. First the shelter loss reduces the SNR, which is most delicate in the second

eclipsing zone for the pulsed waveforms where the echoes are already weakened by the propagation losses, whereas it contributes in reducing the high response of the targets in the first eclipsing zone. Second, since the waveform is partially sheltered, the occupied spectrum is reduced and the resolution therefore becomes poorer. We witness wider mainlobe and higher sidelobes of the ambiguity function into the eclipsing zone [24]. Figure 8 depicts the impact of a half eclipse on a pulsed chirp after pulse compression in comparison with the uneclipsed case just at the frontier of the eclipsing zone marked by R_z.

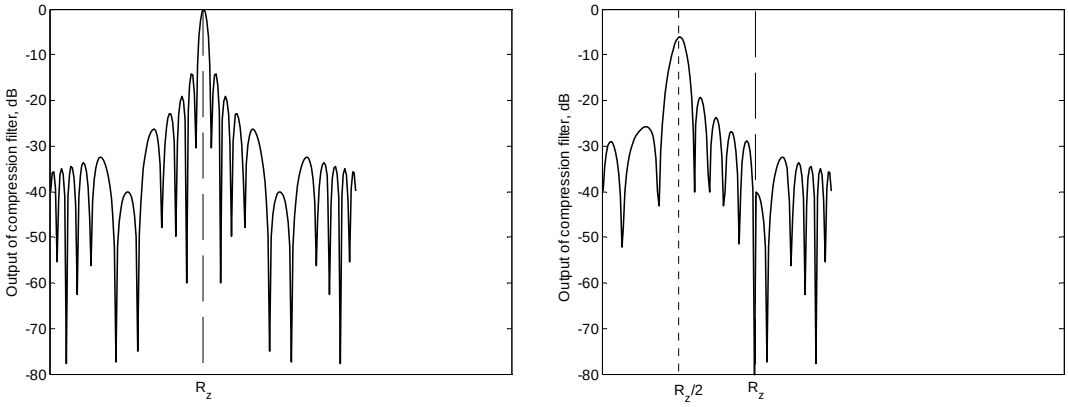

Figure 8. Compression filter output with no eclipsing (on the left) and after half eclipse in the middle of the first eclipse zone (on the right).

Shelter loss increases eventually with waveforms having high duty cycles. A high duty cycle could be an interesting feature for a waveform in order to lower the peak transmitted power and therefore the probability of intercept or simply in order to increase the transmitted mean power to achieve higher ranges.

2.5.2 **The loss function**

In order to evaluate the loss that exhibits an interrupted waveform due to the blanking, a loss function is introduced, also known as the eclipsing loss or shelter loss function. It reflects the portion of the transmitted waveform that is blanked for a particular distance.

Let $x(t)$ be the transmit switch taking values 1 and 0 for the saturated and blocked states of the transmitter as it is often peak power limited. The receive channel operates in an opposite way and the receive switch is therefore $1 - x(t)$. Considering that the transmitted energy over the time integration T is A, the expression of the shelter loss function for a timeshift τ corresponding to a distance d is written:

$$l(\tau) = \frac{1}{A}\int_0^T x(t-\tau)x(t)dt, \tau = \frac{2d}{c}$$

Figure 10 shows the resulting shelter loss function for a pulsed waveform shown in Figure 9. The function evolution shows clearly how the close targets and the ones at the end of the unambiguous range extent are affected by the loss.

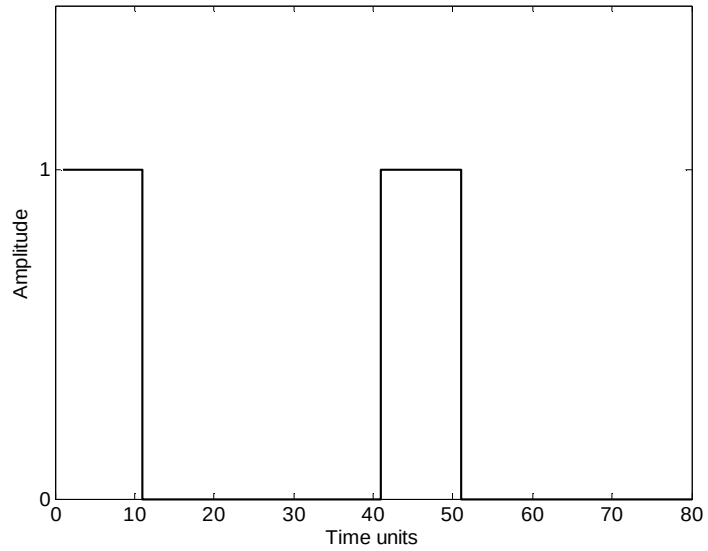

Figure 9. Pulsed waveform of ¼ duty cycle.

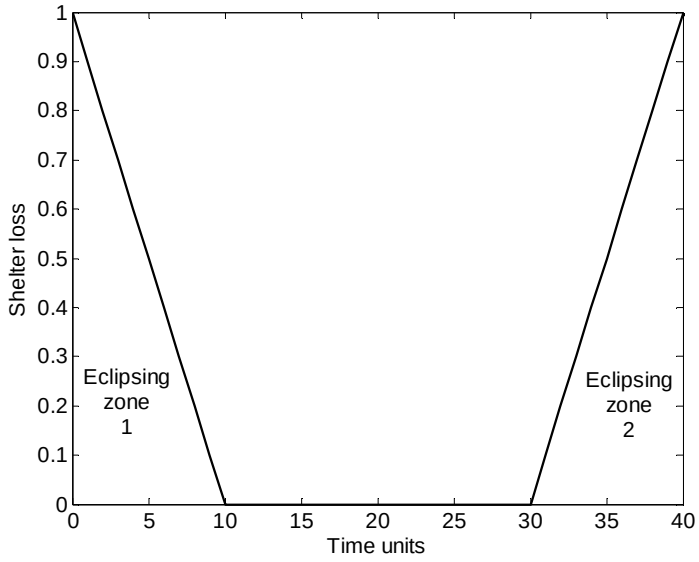

Figure 10. Shelter loss for the ¼ duty cycle pulsed waveform.

Another example is of a random waveform made by equiprobable pulses of duty cycle ½ and 1/3 [25], shown in Figure 11. The energy loss relatively to continuous waveform is by 3.8 dB. The shelter loss function for this type of waveform is given in Figure 12. The function shows that the mean value of shelter is around 0.4 i.e. additional 4 dB of losses.

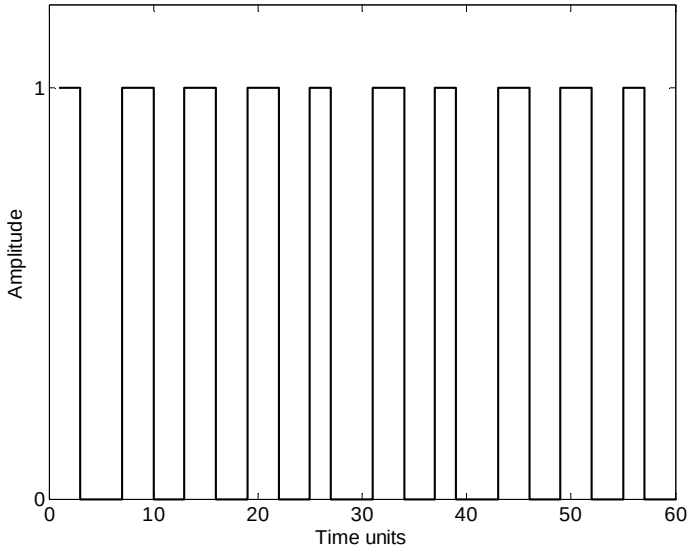

Figure 11. Random ½- 1/3 duty cycle waveform.

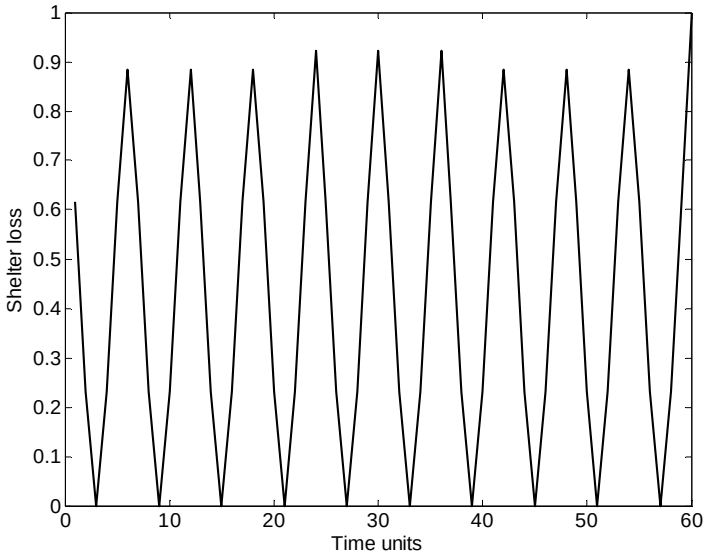

Figure 12. Shelter loss for the random ½- 1/3 duty cycle waveform.

In an attempt to reduce the shelter loss probability, an alternative is to use special binary codes that exhibit low autocorrelation. Some optimal codes [10] have the properties of "superposition not exceeding one". The autocorrelation function for such a code $\mu = \{\mu_k : k = 0,1,..,N-1\}$ with $\mu_k \epsilon \{0,1\}$ is as follows:

$$\phi(m) = \sum_{k=0}^{k=N-m-1} \mu_k \, \mu_{k+m} = \begin{cases} N_0 & m = 0 \\ 1 \; or \; 0 & m \neq 0 \end{cases}$$

with N_0 the number of impulses in the code.

This optimised code has been found to exist for $4 \leq N_0 \leq 46$ [10]. Figure 13 gives the relation between N_0 and its duty cycle. As it could be seen, the duty cycle drops rapidly with the size of the code reflecting the difficulty of finding long code, with a good duty cycle that exhibits at the same time a low shelter loss for all the distances.

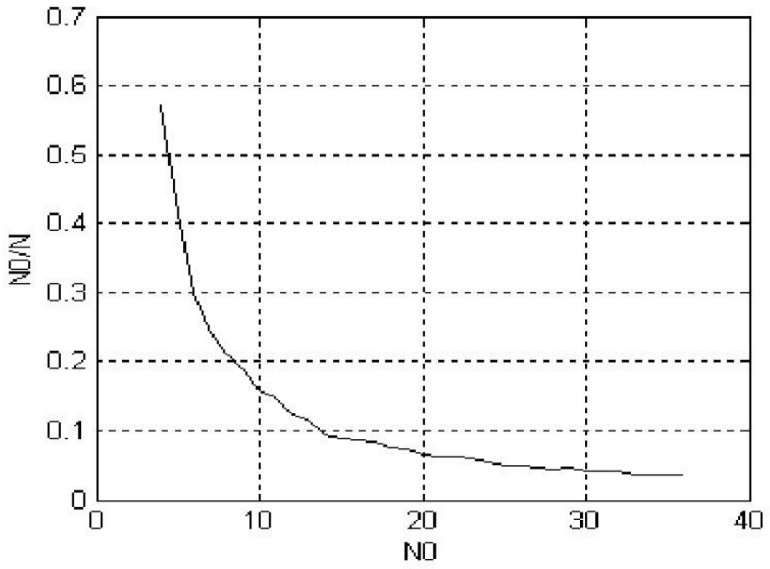

Figure 13. The relation of the impulse number and the duty cycle for the "superposition not exceeding one" codes.

However, for the radar application two additional issues have to be taken into consideration. First, the shelter effect alters the ambiguity function of the transmitted waveform, making it range dependant [26]. Second, the propagation loss that affect the echoes contributes on one hand into increasing their dynamics and on another hand, makes it more difficult to tolerate the shelter loss for the far targets as much as for the closer ones.

In the following we propose to deal with the design of the interruption scheme of the waveform taking into account the propagation losses that affect the received echoes.

2.6 Problem Formulation

2.6.1 The match filtering

Let $a(t)$ be the complex envelope of the waveform whose magnitude takes the values 0 and K for the blocked and saturated states of the transmitter respectively. This signal is shifted in time and frequency and attenuated by a complex factor α_0 before reaching back the radar. Therefore, the envelope of the received signal is:

$$s(t,\theta_0) = \alpha_0 a(t,\theta_0)[1 - |a(t)|/K]$$

where $\theta_0 = (d_0, v_0)$ is the shift in time and frequency due to the distance d_0 and the velocity v_0 of the target $a(t,\theta_0)$ is the corresponding shifted envelope. Without loss of generality, in the following we will consider $K = 1$.

The optimal receiver, in the presence of an additive white Gaussian noise (AWGN) $b(t)$ of power spectral density N_0, is based on a matched filtering therefore a normalised correlation with the model of the echoes whose output is:

$$Q(\theta,\theta_0) = (1/Pr(\theta)) \left| \iint [\alpha_0\, a(t,\theta_0) + b(t)][1 - |a(t)|] a^*(t,\theta) dt \right|^2$$

where the energy profile $Pr(\theta)$ is:

$$Pr(\theta) = \int |a(t,\theta)|^2 [1 - |a(t)|]\, dt$$

As the samples of the received signal are forced to zero during transmission, noise is also cancelled over this period.

Let

$$\chi(\theta,\theta_0) = \int a(t,\theta_0) a^*(t,\theta)[1 - |a(t)|] dt$$

and

$$X(\theta) = (1/|\alpha_0|) \int b(t) a^*(t,\theta)[1 - |a(t)|] dt$$

then

$$Q(\theta,\theta_0) = (|\alpha_0|^2/Pr(\theta)) |\chi(\theta,\theta_0) + X(\theta)|^2$$

$\chi(\theta,\theta_0)$, known as the ambiguity function (AF), reaches its maximum for $\theta = \theta_0$:

$$\chi(\theta_0,\theta_0) = \int |a(t,\theta_0)|^2 [1 - |a(t)|] dt = A - \int |a(t,\theta_0)|^2 |a(t)| dt$$

$$= A[1 - l(\theta_0)] = Pr(\theta_0)$$

with A the energy of the transmitted signal over the integration interval and $l(\theta_0)$ the shelter loss function. Hence, if we denote by E the expected value operator then:

$$E[Q(\theta,\theta_0)] = \big(|\alpha_0|^2/Pr(\theta)\big)\big(|\chi(\theta,\theta_0)|^2 + E[X(\theta)X^*(\theta)]\big)$$
$$= \big(|\alpha_0|^2/Pr(\theta)\big)|\chi(\theta,\theta_0)|^2 + N_0$$

In the absence of noise we could verify that this function has a maximum for $\theta = \theta_0$ (unbiased estimator). In fact:

$$|\chi(\theta,\theta_0)|^2/Pr\,(\theta) = \frac{|\int a(t,\theta_0)a^*\,(t,\theta)[1-|a(t)|]dt|^2}{\int|a(t,\theta)|^2[1-|a(t)|]\,dt} = \frac{\left|\int_S\ a(t,\theta_0)\,a^*(t,\theta)dt\right|^2}{\int_S\ |a(t,\theta)|^2\,dt}$$

where $S = \{t : |a(t)| = 0\}$

Applying the Cauchy-Schwartz inequality gives us:

$$\frac{\left|\int_S\ a(t,\theta_0)\,a^*(t,\theta)dt\right|^2}{\int_S\ |a(t,\theta)|^2\,dt} \leq \frac{\int_S\ |a(t,\theta_0)|^2\,dt\int_S\ |a(t,\theta)|^2\,dt}{\int_S\ |a(t,\theta)|^2\,dt}$$

$$\Rightarrow \frac{\left|\int_S\ a(t,\theta_0)\,a^*(t,\theta)dt\right|^2}{\int_S\ |a(t,\theta)|^2\,dt} \leq \int_S\ |a(t,\theta_0)|^2\,dt$$

And since

$$\left.\frac{\left|\int_S\ a(t,\theta_0)\,a^*(t,\theta)dt\right|^2}{\int_S\ |a(t,\theta)|^2\,dt}\right|_{\theta=\theta_0} = \int_S\ |a(t,\theta_0)|^2\,dt$$

which is an upper bound, therefore the maximum is indeed reached for $\theta = \theta_0$.

2.6.2 **Performance of detection**

The detection decision is made by comparing Q to a threshold T [27]. The probability of detection P_d is affected by the energy profile, while the probability of false alarm P_{fa} remains unchanged. Their expressions, for a non fluctuating target, are given by:

$$P_d = \left[\int_T^{+\infty} exp\big(-\big(x+|\alpha_0|^2Pr(\theta)\big)/N_0\big)\,I_0\left(2\sqrt{\big(x|\alpha_0|^2Pr(\theta)\big)/N_0}\right)dx\right]/N_0$$

$$P_{fa} = \left[\int_T^{+\infty} exp(-x/N_0)\,dx\right]/N_0 = exp(-T/N_0)$$

where I_0 is the zero order modified Bessel function of the first kind.

2.6.3 **Output dynamic range**

The dynamic range of the output and for a good signal to noise ratio (>10 dB) could be evaluated in the operating range of the radar by the ratio:

$$R = \left[\max_{\theta} Q(\theta,\theta)\right] / \left[\min_{\theta} Q(\theta,\theta)\right] = \left[\max_{\theta}\left(|\alpha|^2 Pr(\theta)\right)\right] / \left[\min_{\theta}\left(|\alpha|^2 Pr(\theta)\right)\right]$$

Reducing this dynamic range is particularly beneficial if separate digital processing follows the matched filtering e.g. in the case of analog match filtering. Otherwise, a lower dynamic could prevent the response of a close strong target from hiding in its sidelobes a weaker farther one.

Since $|\alpha|^2$ is generally proportional to d^{-4} this ratio will be minimal when the product of $|\alpha|^2\ Pr(\theta)$ becomes constant and $Pr(\theta)$ is proportional to d^4.

Eventually, $Pr(\theta)$ should be maximal in the operating range of the radar, and in some cases places a null at the range position of a strong scatterer as for the nadir echo in the case of the synthetic aperture radars. Given these different criteria of optimisation of the waveform in addition to the duty cycle and given the binary nature of $|a(t)|$ which defines $Pr(\theta)$, in the following we will adopt the genetic algorithm that seems to be a suitable optimisation technique.

2.7 Noise limited waveform optimisation

Our first objective function as set before is the dynamic range of the output to be minimised. In the same time we are looking for a high duty cycle waveform. The highest reasonable duty cycle to be achieved is 0.5. In fact, any waveform of a higher duty cycle DC will be equivalent from the shelter loss point of view to its complementary waveform, obtained by inversing the on-off states, and therefore having (1-DC) duty cycle.

Now an interesting case would be to have no shelter loss for the maximal desired range of the radar, which is related to the minimal SNR necessary to ensure a given probability of detection and false alarm. In the same time, if we make sure that this minimal SNR is not affected by excess shelter loss at shorter ranges, loss would become without effect on the power budget of the radar.

To elucidate the previous statements, let us consider a periodic codeword a_p of length N, and consider a maximal range corresponding to a spatial shift of half the codeword. We propose a penalty function to be minimised using genetic algorithm:

$$F_1(a_p) = \left| 10 \log\left(\min_{i=1..N/2} Q(i) / (N/2) \right) \right|$$

with

$$Q(i) = \left(\frac{2i}{N}\right)^{-4} Pr(i)$$

The penalty function evaluates any additional loss of the matched filtering output for the considered operational range of the radar, relatively to the best minimal value that we could expect, meaning for a 50% duty cycle waveform, with no shelter loss for the maximal range corresponding here to a shift of $N/2$.

Figure 14 shows a result of the optimisation with $N = 100$, for which the penalty function has attained zero. The resulting waveform has therefore 50% duty cycle with zero shelter at maximal range (Figure 15), and the shelter loss has no effect on the radar power budget as intended (Figure 16).

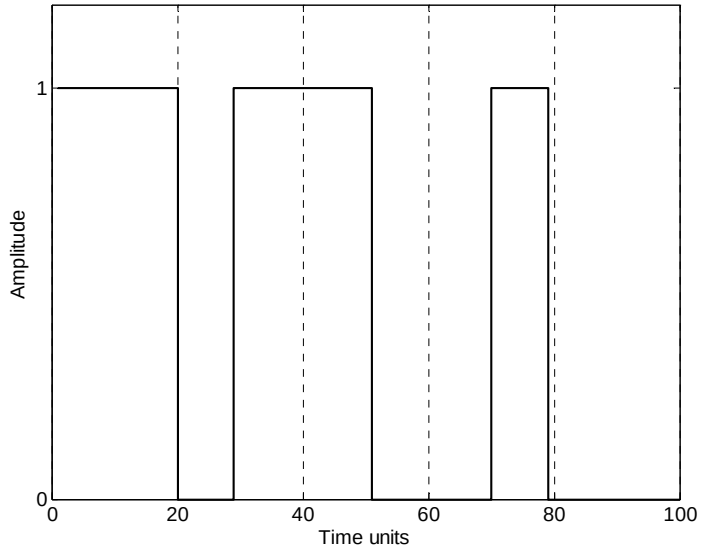

Figure 14. An optimised waveform solution.

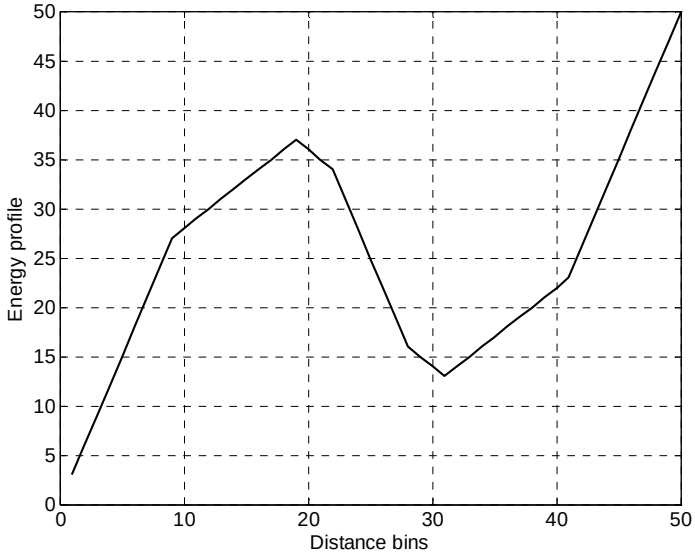

Figure 15. The energy profile of the optimised waveform vs. distance bins.

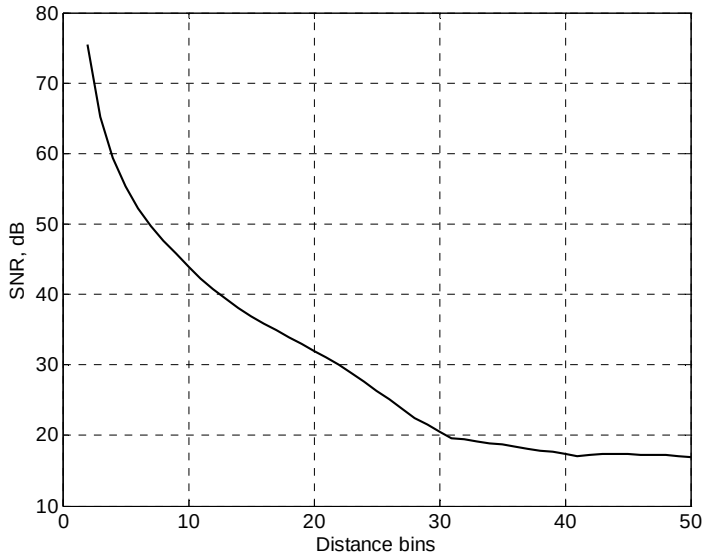

Figure 16. The SNR evolution of the optimised waveform vs. distance bins.

From Figure 16, we see that the total dynamic range of the output is 56 dB whereas a reference value of 68 dB must be considered for the dynamic due to the free propagation loss between the first and the 50th distance bin if there was no eclipse.

However, another waveform solution that could also nullify our given penalty function, is a conventional long 50% duty cycled pulsed waveform. Figure 18 and Figure 19 give the resulting performances in terms of energy profile and evolution of SNR vs. distance bins.

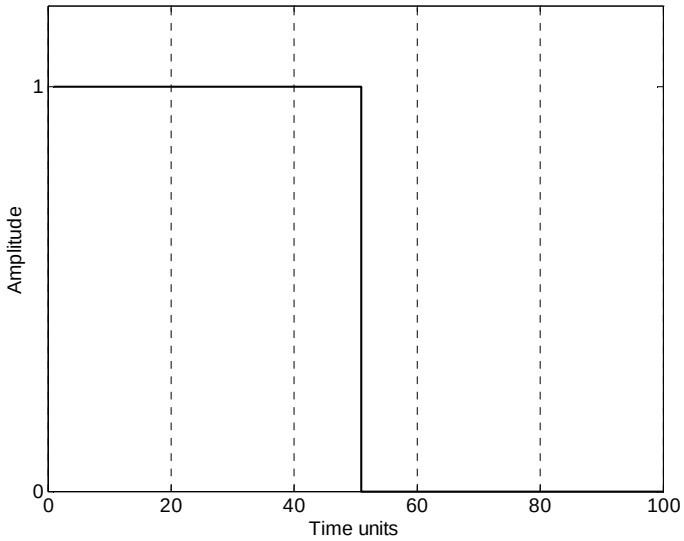

Figure 17. The monopulse 50% duty cycle waveform.

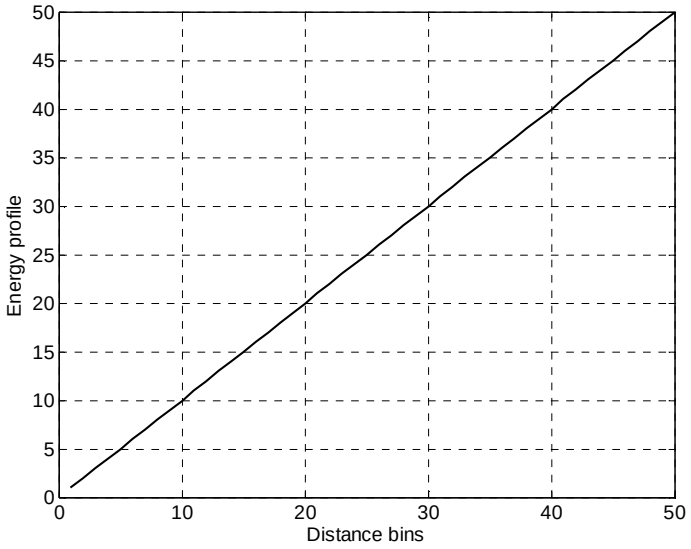

Figure 18. The energy profile of the monopulse 50% duty cycle waveform vs. distance bins.

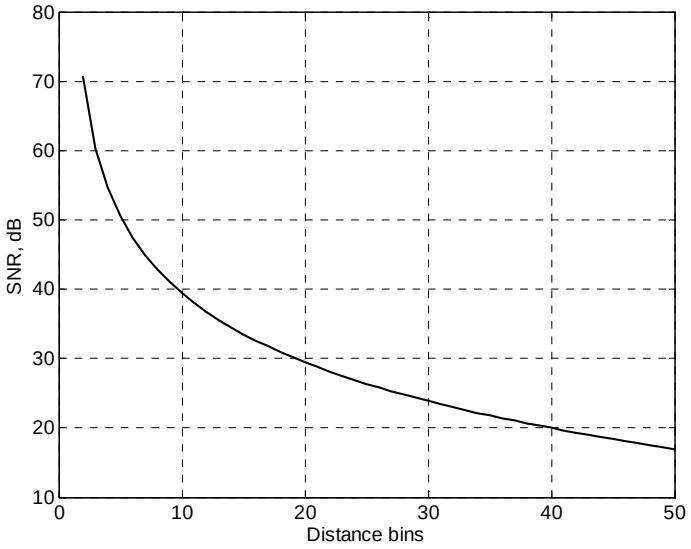

Figure 19. The SNR evolution of the monopulsed 50% duty cycle waveform vs. distance bins.

But if we examine the localisation performance of such a waveform in case of a conventional chirp modulation for pulse compression we see that the first distance bins of such a waveform suffer from a severe deterioration of the resolution. Figure 20 gives the mainlobe width at -3dB level for the waveform in question in comparison with the previous waveform shown in Figure 14 having the same chirp pulse compression factor here taken as 20. The frequency history of both codes is presented in Figure 21.

Since the proposed waveform was decomposed into three shorter pulses than the equivalent monopulse waveform, the close range was less affected by the deterioration of resolution due to the eclipse. At its peak around the tenth

distance bin, the monopulse waveform has approximately 4 times wider mainlobe than the proposed solution. However, both waveforms has almost the same spectral occupation as it could be seen in Figure 22 despite the higher frequency sidelobes due to the chirp time decomposition on three separate pulses in the GA solution.

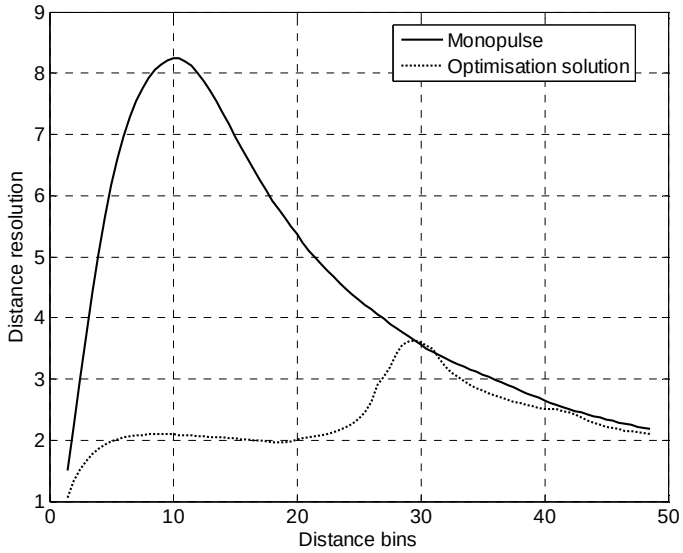

Figure 20. Comparison of the resolution evolution vs. distance bins between the monopulse waveform and another optimised waveform for a linear frequency compression factor of 20.

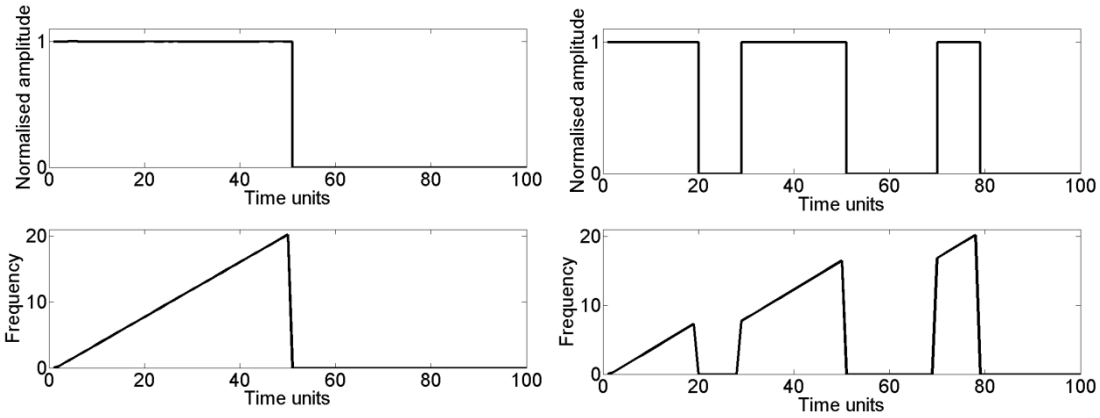

Figure 21. The frequency history of the monopulse waveform (left) and the optimised waveform (right) for a linear frequency compression factor of 20.

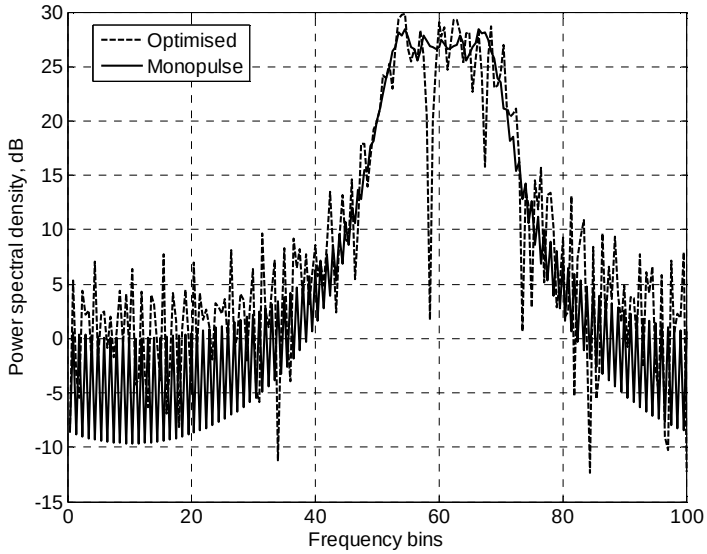

Figure 22. Power spectral densities of the monopulse waveform and another optimised waveform for a linear frequency compression factor of 20.

Another measure of performance is the effective pulse width vs. clutter [24]. It's the width of a pulse having the same peak power as the waveform, and same energy as a uniform clutter response to that waveform. The effective pulse width is written:

$$\tau_c(d) = \frac{\int |\chi(d,r)|^2 dr}{|\chi(d,d)|^2}$$

To give a reference example we consider the effective pulse width of a non coded rectangular pulse of a duration τ without eclipse. The normalised autocorrelation function is a triangle function:

$$tri(t/\tau) = \begin{cases} 1 - |t/\tau|, & |t| < \tau \\ 0, & otherwise. \end{cases}$$

And the effective width is:

$$\tau_c = \int_{-\tau}^{\tau} (1 - |t/\tau|)^2 \, dt = \frac{2}{3}\tau$$

Figure 23 shows the evolution of this indicator for the two waveforms in question. We notice that despite the fact that the monopulse waveform has better effective width in the second half of the range extent, its first half deteriorates badly due to the shelter effect.

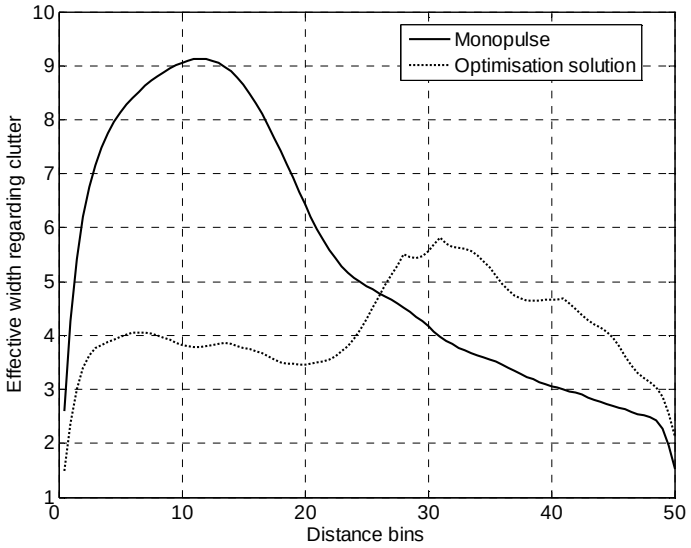

Figure 23. Comparison of the effective width regarding clutter vs. distance bins between the monopulse waveform and another optimised waveform for a linear frequency compression factor of 20.

Although the previous performance factors evolution depends also on the used pulse compression, it is clear that the use of a long pulse badly deteriorates the localisation at close ranges. Consequently, an additional factor is added to the penalty function, in order to penalise the long pulses in the code. The latter is a simple counter that is incremented and decremented for a 1 or 0 respectively while sweeping the values of the bits of the code. The maximal absolute value reached for this counter is then taken into consideration. By means of a sum aggregation [28] this new factor is added to the previous one with a weight δ. The resulting penalty function becomes:

$$F_2(a_p) = \left|10\log\left(\min_{i=1..N/2} Q(i)/(N/2)\right)\right| + \delta\left|\max_{i=1..N/2}\left(CS(i)\right)\right|$$

with CS (Cumulative Sum) defined as:

$$CS(i) = \left|\sum_{k=1}^{k=i}\left(2a_p(k)-1\right)\right|$$

In order to investigate the impact of this additional factor, GA is used to minimise the new penalty function for different values of δ. The algorithm applied a uniform mutation of probability of 0.05 and a single point crossover on a population of 2000 individuals for 100 iterations. In each run, the best half of the population is used to produce the other half for the next iteration (relative elitism of 0.5).

The next pages show the obtained results. The optimised waveforms are phase coded with the same linear chirp of a compression factor of 20 and compared with the monopulse version having the same duty cycle (see Figure 21).

With the increase of weight factor δ, the energy becomes more spread in the codeword, and the waveform becomes increasingly segmented. The improvement in the mainlobe width relatively to the monopulse case is increased as well as the effective width especially in the 30 first distance bins. However the chirp decomposition into smaller pulses increased the sidelobes in frequency domain relatively to the monopulse. This overall increase of the overall occupied bandwidth explains the gain of the resolution at the end of the range extent of the radar where the entire waveform and therefore the enter bandwidth is evaluated. This could be most seen in the last case (d).

Nevertheless, when defining in a later stage constraints to the bandwidth occupation, special phase coding techniques could fit the waveform into the available spectrum. This issue will be discussed in details in the next chapter.

The preceding optimisation focused on the SNR loss due to the eclipse and adapted it to the free space propagation while maintaining high duty cycle. Next, we will try to adapt the waveform for a clutter limited case, the HFSWR.

Case (a):

δ	$F_1(a_p)$	Duty cycle	Dynamic range (dB)
0.01	0	0.5	55.9

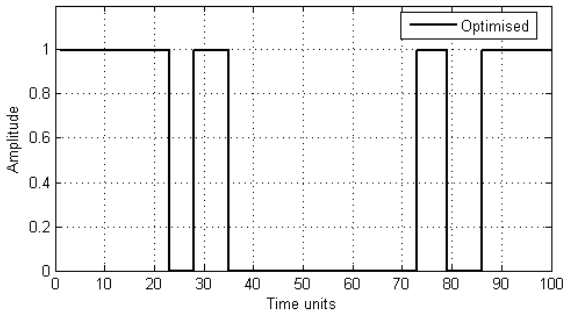

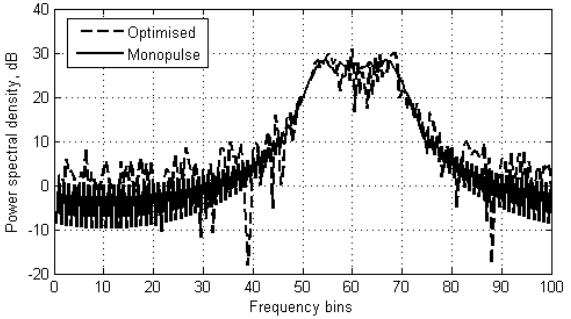

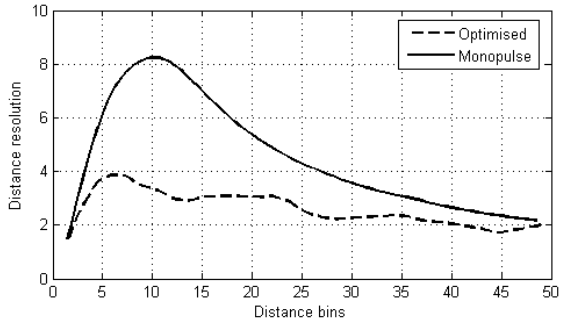

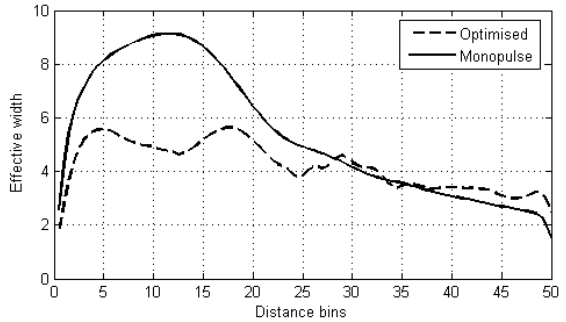

Case (b):

δ	$F_1(a_p)$	Duty cycle	Dynamic range (dB)
0.01	0.1066	0.5	58.1

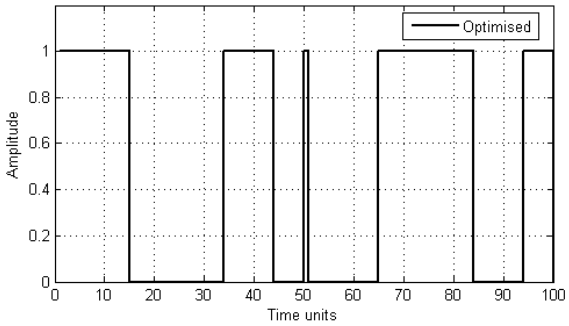

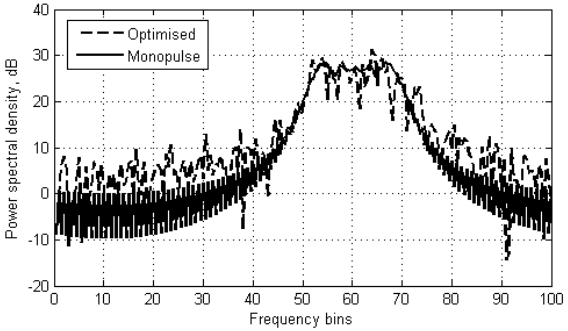

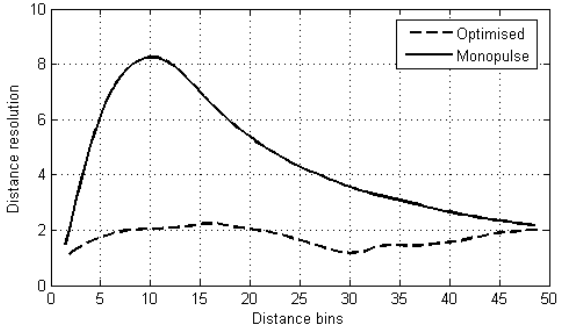

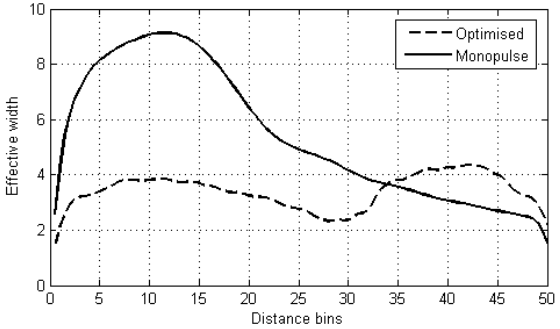

Case (c):

δ	$F_1(a_p)$	Duty cycle	Dynamic range (dB)
0.03	0.1773	0.47	58.14

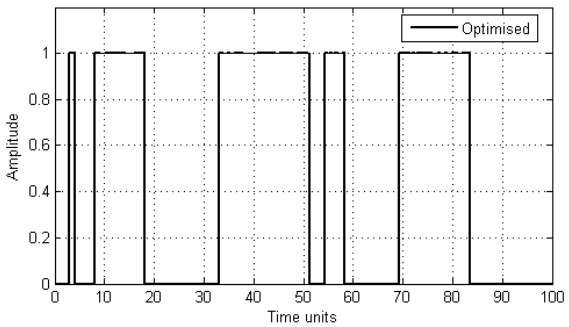

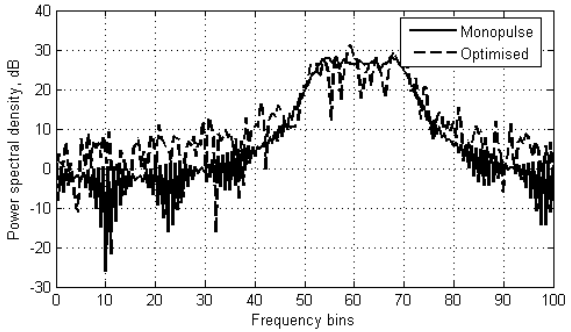

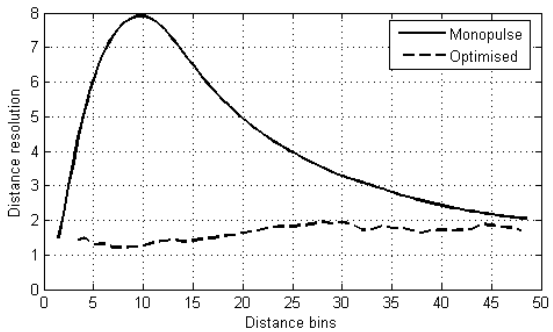

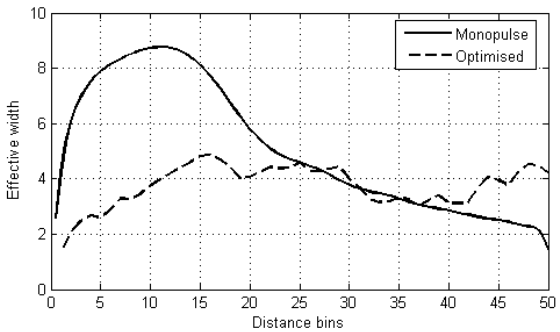

Case (d):

δ	$F_1(a_p)$	Duty cycle	Dynamic range (dB)
0.05	0.5675	0.48	61.54

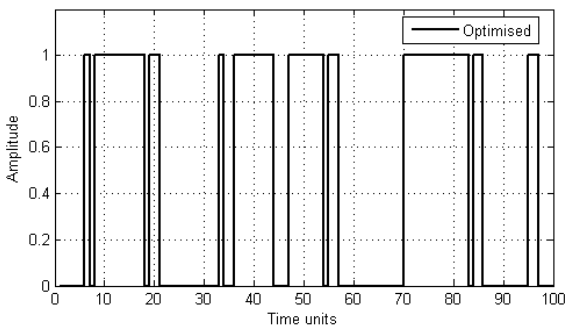

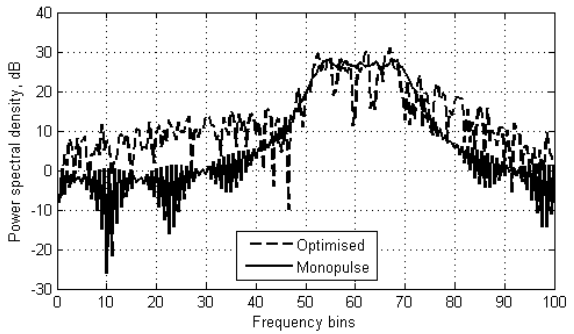

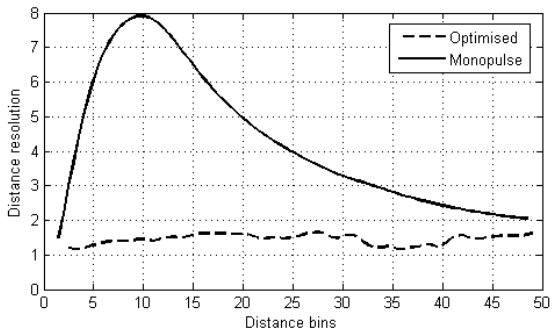

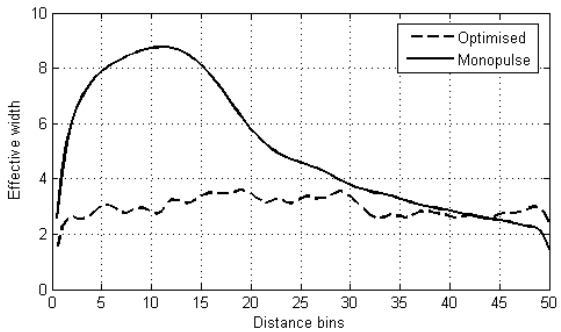

2.8 Clutter limited waveform optimisation

2.8.1 Introduction

HFSWR is the radar technology that benefits from the conducting properties of the sea surface in the HF band [3-30] MHz in order to propagate the electromagnetic waves beyond the line of sight.

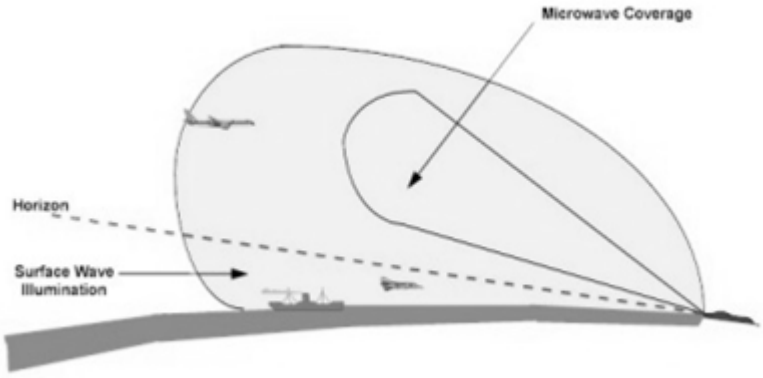

Figure 24. The coverage of the surface wave radar in comparison with a conventional microwave coverage.

Low cost and rapidly deployed, this kind of radar provides detection and tracking of ships and low flying aircrafts beyond the horizon (Figure 24). Therefore it could be used for coastal surveillance, sea state monitoring and ship traffic control, to provide protection of the maritime resources or to protect from illegal entries.

But in order to be fully operational, HFSWR should face many challenges. First, it has to operate in the highly congested HF spectrum where it is very difficult to find a clear channel for its transmissions. Second, it has to operate in the presence of the sea clutter, the ionospheric interference as well as the ambient natural noise.

In this context, the transmitted waveform has a major role, since it affects the power budget, the resolution and the resulting signal to noise and clutter ratio. Now, in its monostatic configuration the common used waveform for the HFSWR is a pulsed waveform such as the FMICW shown in Figure 25.

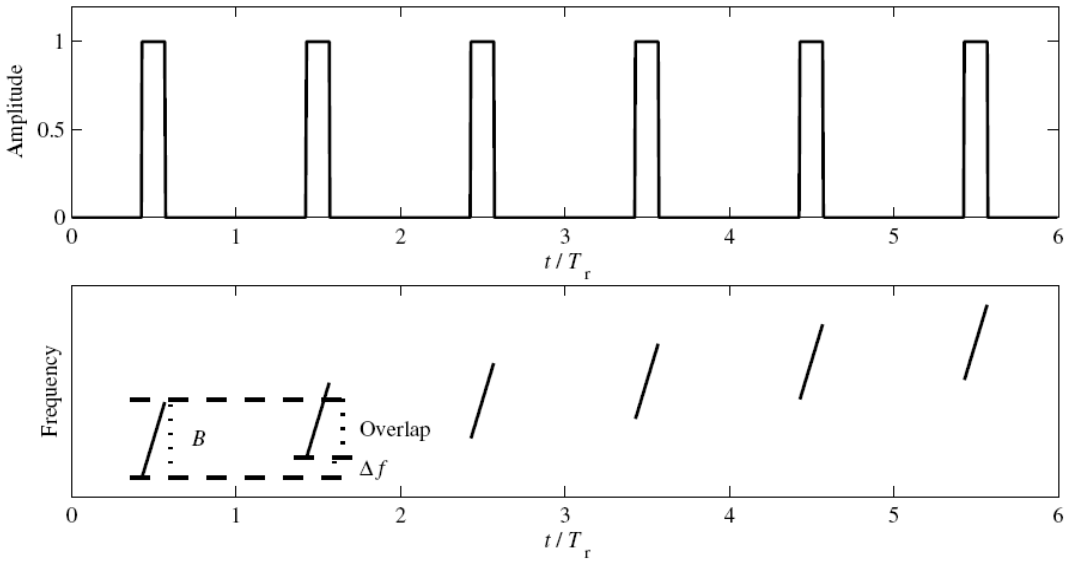

Figure 25. A conventional FMICW waveform used for the HFSWR.

The waveform consists of a train of equally spaced pulses whose repetition period is related to the maximal range of the radar, with a linear frequency coding covering the available frequency channel. The integration time, depending on the application, is determined in order to guarantee the desired SNR while avoiding the range cell migration. Both the range resolution and the maximal velocity of the target set an upper limit for this integration time.

However, the pulsed waveform is not necessarily the best interruption scheme, although it's intuitively the easiest to construct. In the following, the design of an advanced interruption scheme is presented taking into consideration the surface wave propagation losses and the presence of the sea clutter.

2.8.2 **Sea clutter properties**

In maritime environment, the radar backscatter from the sea surface, usually known as the sea clutter is a very important factor to be considered in sea surveillance and remote sensing. Depending on the application, this sea return is used to derive useful information about the sea state or could be considered as competing with the target useful return echo and is therefore wished to be suppressed. In both cases, the modelling and characterisation of this clutter gain an importance that is reflected through its intensive study in the literature.

Figure 26 shows an averaged sea spectrum at 7 MHz measured by the Onera's HFSWR at the Bay of Biscay [29].

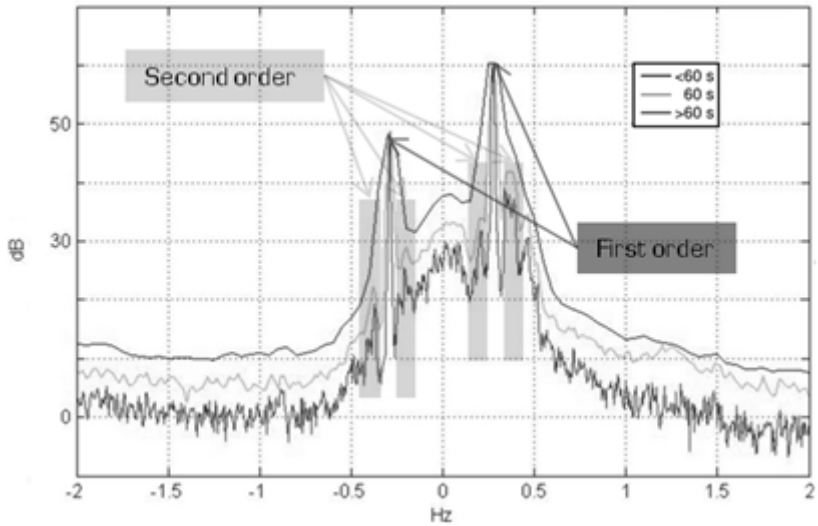

Figure 26. Averaged sea spectrum at 7 MHz for different coherent integration durations, Onera's HFSWR, France.

The spectrum is characterised by two strong spikes known as the Bragg lines and are due to the gravity waves having a spatial wavelength of half the radar wavelength for which resonance occurs. These lines are surrounded by a second order signal due to the superposition of different gravity waves responses.

Now depending on its velocity, target can be more or less affected by the sea clutter. For example at 7 MHz the 1 Hz Doppler shift corresponds to 77 km/h. Therefore, the slow moving targets are generally strongly affected by the sea clutter that risks of preventing their detection especially in the case of low RCS targets such as the small boats.

Another property is that the area of the sea patch surrounding a target in a given range cell increases linearly with distance as it could be seen in Figure 27.

The expression of the RCS of the sea patch at distance r is given by:

$$\sigma_{sea}(r) = \sigma_{00}\, r\, \delta r\, \delta\theta$$

where σ_{00} is the sea reflectivity, δr the radar range resolution and $\delta\theta$ the azimuth angular beamwidth.

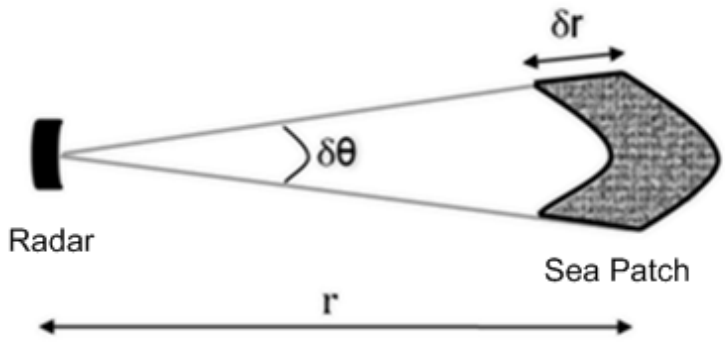

Figure 27. The geometry of sea clutter patch for a given range cell at distance r.

2.8.3 **Surface propagation losses**

Due to the high conductivity of the sea water in the operational frequencies of the HFSWR, the image theory implies that the only polarisation to propagate is the vertical one. The propagation losses for such a polarisation are given by the Bremmer's model [1] [2] with Barrick's [3] adjustments of the sea roughness.

Figure 28 is an example plot of the power level evolution with the distance of propagation for a frequency of 5.5 MHz, the sea parameters being ε=80 and σ=4 S/m for the relative permittivity and the intrinsic conductivity respectively. The transmitter and receiver heights in the Bremmer's equations are one quarter of a wavelength above the sea level. Eventually and for the radar application, the round-trip propagation should exhibit twice the losses witnessed here for the single trip propagation.

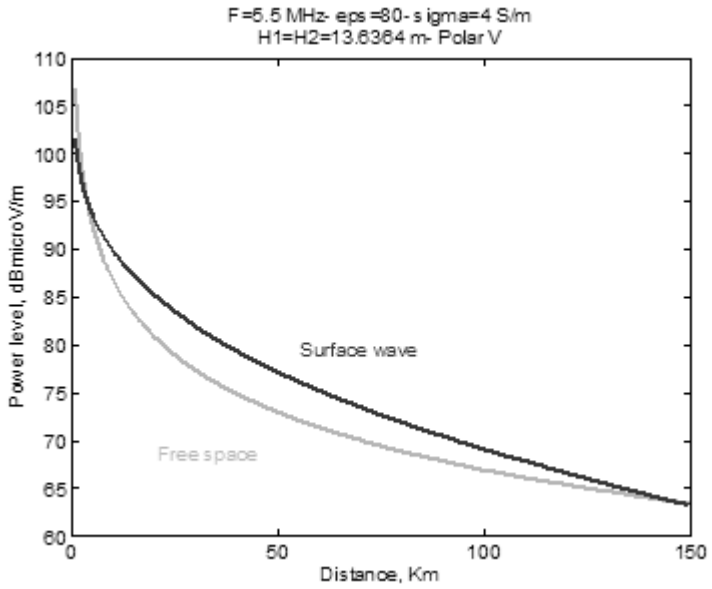

Figure 28 . Power level in dB above the sea surface in function of distance in km for single trip propagation.

2.8.4 **Clutter performance evaluation**

Assuming the transmit code $x[k]$ is a periodic bits series taking values 0 and 1 for the blocked and saturated states of the transmitter respectively.

If we denote by T_c the sub-pulse timewidth, the transmitted signal may be expressed as:

$$x(t) = \sum_k x[k]\, rect_{T_c}\,(t - kT_c)$$

with

$$rect_{T_c}(t) = \begin{cases} 1 \;\; if \;\; 0 \le t \le T_c \\ 0 \;\; elsewhere \end{cases}$$

We consider here the worst case scenario where the sub-pulses are not yet phase or frequency coded. And by supposing that the coded waveform bandwidth will be mainly due to the pulse compression, we could leave apart, at this stage of waveform design, the spectral allocation constraints of the congested HF spectrum. This could be seen as a first step optimisation, where we decide *when* we transmit before deciding *what* to transmit in terms of frequency or phase codes. For this assumption to remain reasonable, the product of the sub-pulse timewidth and the final available bandwidth should be larger than one.

As we are operating in the HF band, the Doppler shifts of the cruising vessels and grazing angle aircrafts do not exceed few tens of hertz. Hence, the performance of a waveform is studied here through the zero-Doppler cut of its ambiguity function [27] i.e. its cross-correlation function.

The latter's expression, by taking into account the time isolation between the transmitting and receiving channels, is as follows:

$$A_x(D,r) = \int_0^T x\left(t - \frac{2D}{c}\right)\, x\left(t - \frac{2r}{c}\right)\, \left(1 - x(t)\right) dt$$

where T is the intended waveform repetition period after coding and it is considered here to be a multiple of $\frac{2D_{max}}{c}$, with D_{max} the maximal operational range of the radar.

An estimation of the contrast ratio [30] [31] [32] for the distance D would be

$$CR_x(D) = \frac{\sigma}{\sigma_{00}\ \delta\theta} \frac{A_x^2\ (D,D)P(D)}{\int_0^{D_{max}} A_x^2\ (D,r)P(r)\ r\ dr} = \frac{\sigma}{\sigma_{00}\ \delta\theta}\ \frac{1}{K_x(D)}$$

where σ is the target's radar cross section, $P(D)$ is the round-trip power loss for the distance D and $K_x(D)$ is the waveform dependent contribution.

2.8.5 **The objective functions**

The waveform optimisation we are here dealing with is a two conflicting objective functions optimisation. In fact, and with the increase of the duty cycle, the energy is more spread in time, and the cross-correlation function extends to integrate more clutter echoes through its sidelobes. This trend will be next confirmed when analysing the evolution of the objective functions defined as follows:

$$f_1(x) = \max_{0 \le D \le D_{max}} \left(10\ log\left(K_x(D)\right)\right)$$

$$f_2(x) = 100\ \left(1 - \frac{1}{T}\int_0^T x(t)\ dt\right)$$

These objective functions are intended to be minimised. When so, the first one contributes to maximising the minimal contrast ratio in the operational range of the radar, while the second one enhances the duty cycle.

2.8.6 **Algorithm choice**

As the number of possible codes grows exponentially with the code length, a sequential search for optimal codes becomes quickly unreasonable.

After a survey [28] within the area of evolutionary multi-objective optimisation, the Non-dominated Sorting Genetic Algorithm II (NSGA-II) [33] has been retained to solve this optimisation problem as it has widely proved its robustness for multi-objective problems i.e. problems with no more than three objectives and its superiority for two objectives problems [34], [35].

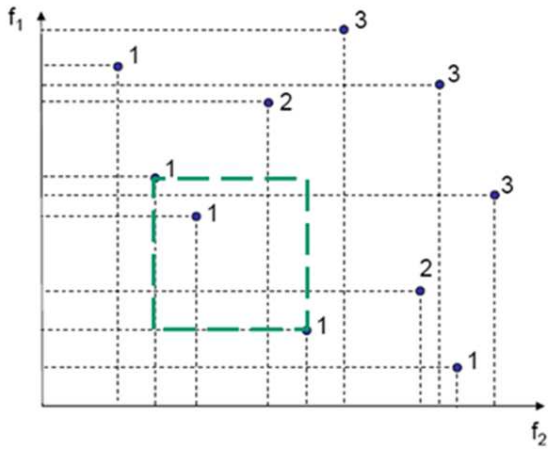

Figure 29. The ranking of individuals based on Pareto non-dominance criterion. Visually, an individual is non-dominated if no other individual belongs to the cuboid it forms with the origin. The crowding distance of an individual is the average side of the cuboid it forms with its nearest neighbors on the same front (dashed).

NSGA-II is a Pareto-based algorithm incorporating elitism and non-dominated sorting as a primary selection criterion (see Figure 29). Individuals of a particular rank become non-dominated once all individuals of better ranks are removed from the population. An additional parameter called the crowding distance is calculated in conjunction with the fitness value. It is a measure of how close an individual is to its neighbours and it is used to evaluate individuals with the same rank. The rest of the procedure is the common application of genetic operators before recombination and selection (see Figure 30).

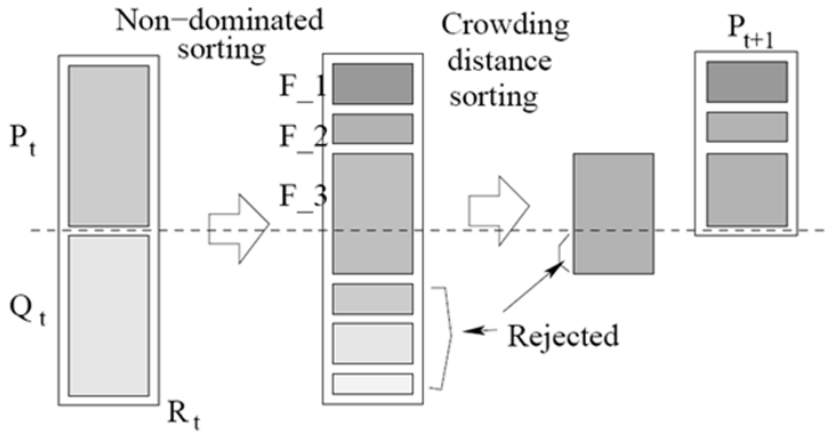

Figure 30. The flowchart of the NSGA-II iteration.

In the following a binary version of NSGA-II is applied to our problem since an individual x of the population representing the transmit code is by definition a binary sequence and therefore we apply the original genetic operators for the single point crossover and uniform mutation.

2.8.7 **The Pareto front**

For this numerical application, we consider a maximal range D_{max} of 150 km divided into 50 range bins. Moreover, we consider two cases of code repetition periods corresponding to 100 and 250 range bins (time units), i.e. 2 and 5 times the maximal range. NSGA-II is then used to generate the optimal set of solutions from a Pareto point of view. The performance of this set is then compared to the one of the conventional train of pulses in the same conditions and with a duty cycle ranging up to 50%.

Figure 31 shows the variation of the minimal achievable values of the contrast ratio maximal loss for the different values of the duty cycle. The evolution of these plots confirms the conflict between these two objectives as it was interpreted previously in this paper. In the case of the pulse train the maximal loss increases in a steady rate of 1dB per additional 3 % of duty cycle between 10% and 50%.

When it comes to the optimised waveforms, we first notice a slight improvement of the second objective by 0.7 dB on average when compared to the pulse train performance, in the case where the repetition period corresponds to twice the maximal range.

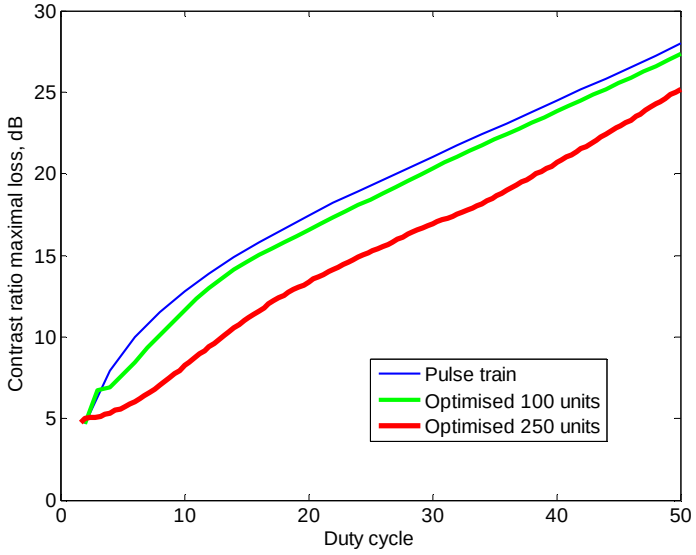

Figure 31. Pareto fronts with NSGA-II in comparison with the pulse train performance.

However, when this repetition period grows to 5 times the maximal range, the improvement raises to 4 dB on average. This could be seen as a direct result of the increase in the degrees of freedom in the design of the waveform thereby expanding the space set of solutions.

Another interesting observation concerns the uniqueness of the code-solution in the final population. This means that no change in bit positions could be done to a code-solution while preserving the optimal performance in terms of minimal contrast ratio.

2.8.8 **Performance analysis**

Figure 32 shows the code solution of 250 time units and 30% duty cycle in comparison with the conventional pulse train used for the same scenario. We see that the optimised waveform breaks the periodicity of width and position of the envelope pulses which causes the blind range.

The evolution of the contrast ratio loss vs. the distance is shown in Figure 33. The study of this evolution shows that the optimised code succeeds in keeping a rather steady contrast ratio between 60 km and 150 km. It starts to perform better than the

pulse train in the far zone beyond 120 km while the latter performs better between 45km and 120 km. The optimised code outperforms the conventional one by guaranteeing a lower maximal loss in the contrast ratio.

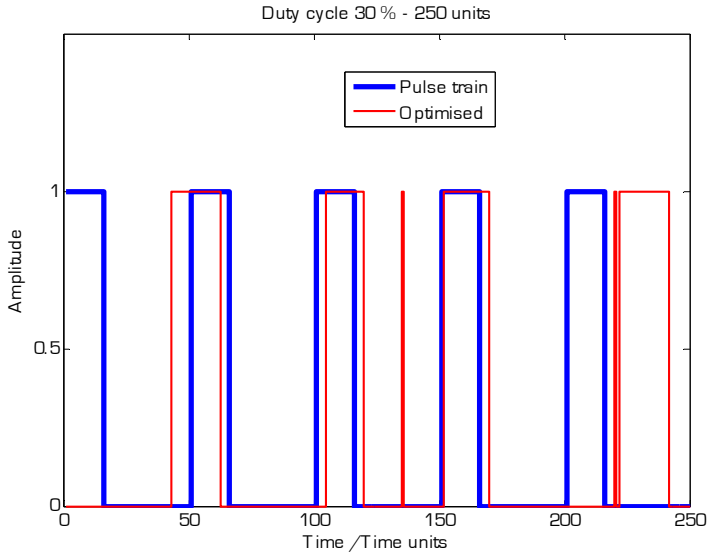

Figure 32. Optimised waveform and its equivalent pulse train for a duty cycle of 30% and 250 time units.

Of course, we here set the limit for the worse case, as these performances are strongly expected to ameliorate by use of pulse compression technique with a higher chance for the optimised code to keep the lead with its performance in terms of minimal contrast ratio.

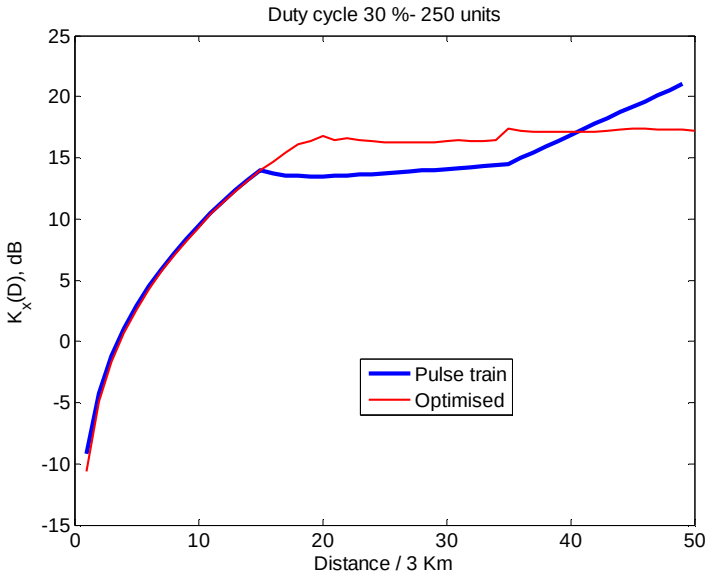

Figure 33. The loss in the contrast ratio in dB vs. distance for the optimised waveform and its equivalent pulse train for a duty cycle of 30% and 250 time units.

2.9 Conclusion

The theory behind the LPI strategy was presented showing the need of spread of energy in the different dimensions. The effects of shelter loss hindering the spread in time were then studied for the monostatic configurations to allow the time isolation between the transmit and receive signals. New waveforms envelopes were then derived in order to overcome the deterioration of performances that occur in the blind zone of the conventional pulsed waveforms. The specific case of HFSWR was considered, and given the sea clutter power density function, a set of optimal waveforms were found to approximate the Pareto front linking the minimal contrast ratio encountered in the range extent of the radar and the duty cycle.

As the time envelopes were now defined, the next step is to find the phase code that allows spreading the waveform in frequency. But since the spectrum is a precious resource and is subject to regulations, a non contiguous band could be the only available band for radar and the waveform should still be able to occupy it and keep in the same time the adequate range resolution and sidelobe level. The techniques allowing such coding are the subject of the next chapter.

Chapter 3

Managing Frequency

3.1 Introduction

In this chapter the frequency aspect of the waveform is studied. When spreading the transmissions in frequency, radar transmissions have to avoid some channels with high interference or some bands with critical operations (e.g. safety applications). First we start by presenting the situation of the radar spectrum. Some existing techniques that allow fitting the radar transmissions into the available frequency channels are then presented and compared. Finally, a new technique based on alternate projections (AP) is proposed and compared to the previous techniques for the same study-cases. The efficiency of this technique is also studied especially that it is important for the radar to react quickly to a sudden change in the spectral environment.

3.2 The international spectrum allocation

Every two or three years the International Telecommunication Union (ITU) organizes the World Radiocommunication Conference (WRC). Based on an agenda of the ITU council which takes into considerations the recommendations of the previous WRCs, the conference aims to revise the radio regulations that govern the use of the radio-frequency spectrum for the three ITU regions (see Figure 34) as well as the use of the satellite orbits.

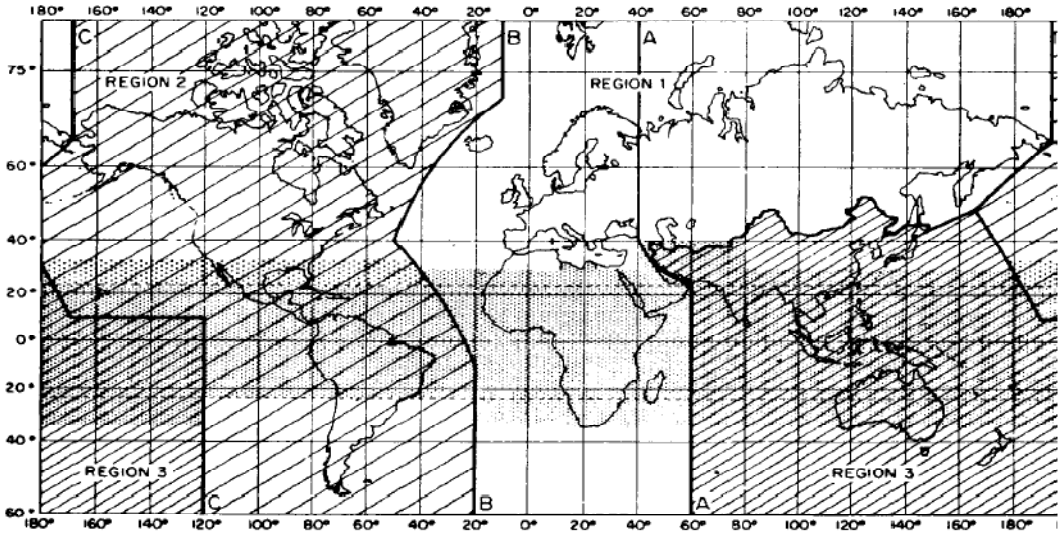

Figure 34. For the allocation of frequencies internationally, the world has been divided into three regions according to the ITU regulation [36].

In this regulation, a basic plan allocates the available spectrum to the different radio applications in terms of blocks of frequencies. Each block provides a band of contiguous frequencies to be used by one or more radio services. When sharing a same block of frequencies the different applications may have two levels of protection: primary or secondary. While the primary services have equal rights within the same band, the secondary services could only operate on a non interference basis to the primary services.

Radars on their hand could benefit from the frequency bands reserved for radiodetermination, earth exploration-satellite and the meteorological aids services. The term radiodetermination by definition [36] covers "The determination of the position, velocity and/or other characteristics of an object or the obtaining of information relating to these parameters, by means of the propagation properties of the wave".

In this context the frequency bands that provide the best quality of service are those which are primarily allocated for the radar use without any other primary applications sharing the band. In the second level comes the case where there is sharing especially with other users of the same status. And finally comes the case where the radar applications are sharing the spectrum on a secondary basis with others applications.

3.3 Radar frequency selection

In theory radar could operate anywhere in the electromagnetic spectrum. Any device that relies on electromagnetic radiation, no matter what frequency it uses, to detect and locate a target based on its scattered echoes could be classified as a radar.

However, the best frequency to use for a given radar application involves tradeoffs among numerous factors. In fact, the choice of frequency has a direct impact on the physical size of the system, the transmitted power, the atmospheric attenuation and the antenna beamwidth. For example at low frequencies (wavelengths are long) the hardware is usually large and heavy while at higher frequencies (shorter wavelengths), the radar comes in smaller packages and lighter weight. But on the other hand, the smaller the hardware the lower the power it can handle. For this reason the large and heavy metric-wave radars could transmit megawatts of average power while the smaller millimetre-wave radars are limited to only hundreds of watts.

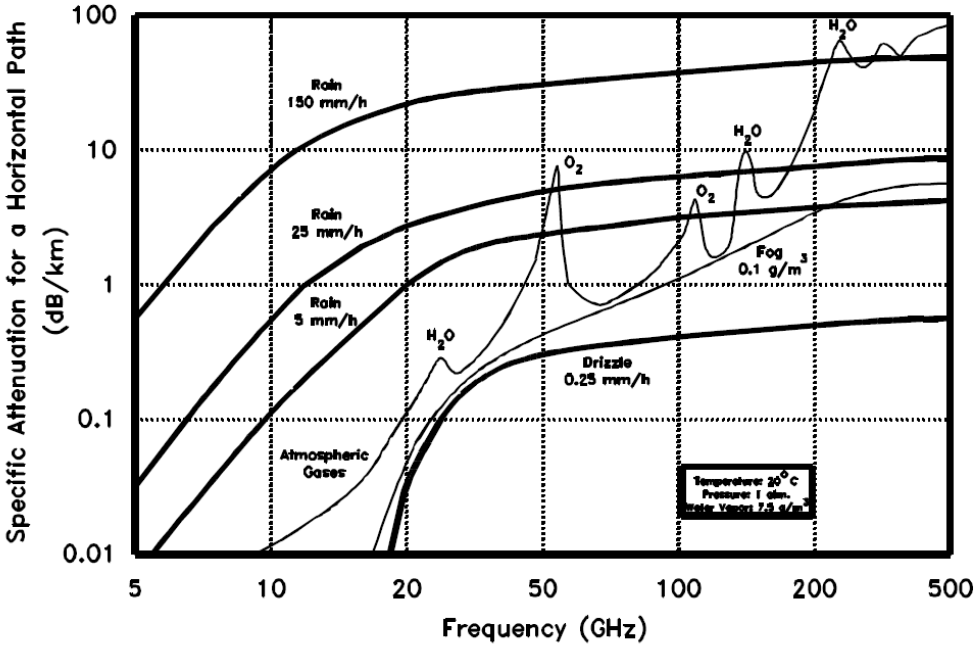

Figure 35. Attenuation due to atmospheric gases and liquid hydrometeors [36].

Table 1. Frequency bands and radar operational propagation limitations [36].

Band	***Description***
LF 30–300 kHz	Allocations are provided in the frequency range but no radar usage or applications have been identified.
MF 300–3000 kHz	Used by continuous wave (CW) radar systems for accurate position location. Very high noise levels are characteristic of this band.
HF 3–30 MHz	Refractive properties of the ionosphere make frequencies in this band attractive for long-range radar observations of areas such as over oceans at ranges of approximately 500–2000 nautical miles. Only a few radar applications occur in this frequency range because its limitations frequently outweigh its advantages: very large system antennas are needed, available bandwidths are narrow, the spectrum is extremely congested with other users, and the external noise (both natural noise and noise due to other transmitters) is high.
VHF 30–300 MHz	For reasons similar to those cited above, this frequency band is not too popular for radar. However, long-range surveillance radars for either aircraft or satellite detection can be built in the VHF band more economically than at higher frequencies. Radar operations at such frequencies are not affected by rain clutter, but auroras and meteors produce large echoes that can interfere with target detection. There have not been many applications of radar in this frequency range because its limitations frequently outweigh its advantages.
UHF 300–3000 MHz	Larger antennas are required at the lower end than at the upper end of the UHF band. As compared to the above bands, obtaining larger bandwidths is less difficult and external natural noise and weather effects are much less of a problem. At the lower end, long-range surveillance of aircraft, spacecraft, and ballistic missiles is particularly useful. The middle range of this band is used by airborne and spaceborne SAR's. The higher UHF end is well suited for short to medium-range surveillance radars.
SHF 3 GHz–30 GHz	Smaller antennas are generally used in this band than in the above bands. Because of the effects of atmospheric absorption, the lower SHF band is better for medium-range surveillance than the upper portions. This frequency band is better suited than the lower bands for recognition of individual targets and their attributes. In this band, Earth observation efforts employ radars such as SAR's, altimeters, scatterometers, and precipitation radars.
EHF 30–300 GHz	It is difficult to generate high power in this band. Rain clutter and atmospheric attenuation are the main factors in not using this frequency band. However, Earth observation efforts are made in this band employing radars such as altimeters, scatterometers, and cloud profile radars.

The expression of the half power beamwidth of a radar's antenna shows that it is directly proportional to the ratio of the wavelength to the width of the antenna in question. This means that in order to achieve good resolution larger antennas should be used in lower frequencies. Even when passing through the atmosphere the radar transmissions are attenuated differently according to their frequency, the absorption and scattering being the major mechanisms causing this

attenuation. Figure 35 shows how the attenuation due to the atmospheric gases and liquid hydrometeors increases with frequency.

Due to the above mechanical and geophysical limitation the Table 1 gives the broad categories of spectrum used by radar and states the attractiveness of each category to particular radar application.

3.4 Radar spectrum erosion

The importance of the international spectrum allocation resides in the fact that many countries around the globe use the ITU table of frequency allocation as a template for their national frequency use. Therefore the decisions taken during the WRCs have a profound impact on the use of specific frequency bands worldwide. And if countries could readapt the ITU allocations to meet their national needs, it is still strategically important for some radar systems to be able to operate globally without prior coordination with the host countries.

However the operational use of the radiolocation differs from one country to another. In many cases the potential use of commercial application of the radiolocation bands creates strong pressure to reallocate these bands to other services.

For example, the World Administrative Radio Conference of 1979 (WARC-79) made changes for 856 MHz of the spectrum allocated for radar applications, by moving the status from primary to secondary and removing previous allocations. In WRC-97, 2,435 MHz of radiolocation and radionavigation spectrum became sharing with non-radar primary radio services [36] [37].

However, as the radar systems are progressing so does the amount of information they provide which often necessitates an increase in the required bandwidth. Such systems include features of multi-function operations as well as improved intrusion detection and space surveillance. By processing a wider bandwidth, it is possible to provide better target recognition capabilities.

3.5 Sparse frequency Coding

When the available spectrum offers a sufficient contiguous bandwidth for radar transmissions, the waveform designer could choose to transmit among well-known frequency or phase codes depending on the application and the required ambiguity function properties in terms of resolution and sidelobes level in the range- Doppler map. These frequency or phase codes are the results of years of studies and improvements even many years before the radar was able, from complexity and hardware point of view, to implement them.

Table 2. Typical radar codes and their inventors.

Name	*Inventor*	*Year*	*Type*
Barker Code	R. H. Barker	1953	Phase Codes
Complementary Code	M. J. E. Golay	1961	Complementary Phase Codes
Huffmann Code	D. A. Huffmann	1962	Phase Codes
Frank Code	R. L. Frank, S. A. Zadoff	1962	Chirplike Phase Codes
Zadoff- Chu Code	S. A. Zadoff	1963	Chirplike Phase Codes
Gold Code	R. Gold	1967	Phase Codes based on binary sequence
Minimum Peaksidelobe Code	J. Linden, N. Cohen et al.	1975	Phase Codes based on binary sequence
Welti Code	R. Sivaswamy	1978	Subcomplementary Codes
P1 and P2 Codes	B. L. Lewis, F. F. Kretschmer	1981	Phase Codes
Frank Polyphase Codes	B. L. Lewis, F. F. Kretschmer	1983	Phase Codes
Costas Array	J. P. Costas	1984	Frequency Codes
Quadratic Congruential Coding	J. R. Bellagrada, E. L. Titlebaum	1988	Frequency Codes
Polyphase Barker Codes	L. Bomer, M. Autweiler	1989	Phase Codes
Generalised P4 Code	F. F. Kretschmer, K. Gerlach	1992	Phase Codes
Biphase Perfect Code	S. W. Golomb	1992	Biphase Codes
Ipatov	V. P. Ipatov	1992	Code with minimum peak response loss
P(n,k) Code	T. Felhauer	1994	Phase Codes
Px Code	P. B. Rapajic, R. A. Kennedy	1998	Phase Codes
PONS Based Complementary Code	P. Zulch, M. Wicks et al.	2002	Complementary Codes
Multicarrier Phase Coded Pulse	N. Levanon, E. Mozeson	2002	Multicarrier Phase Radar Signals
Orthogonal Codes	N. Levanon, E. Mozeson	2003	Train of Orthogonal Coded Pulses

Table 2 gives a non exhaustive list of well known radar codes through history as well as their inventors [38].

Nevertheless, whenever the available spectrum for radar use is reduced to a set of non contiguous channels, special attention should be paid to the waveform design in order to be able to benefit from the combined channels bandwidth while avoiding the interference with the other applications operating between these channels. The resulting codes are qualified “Sparse in Frequency”.

3.6 Gradient algorithm based coding

In [4], the author proposed an algorithm to design optimal transmit and receive waveforms with the property of frequency notching in the transmit bands.

The transmit waveform is designed by minimising the weighted transmitted energy in the forbidden bands, and the transmit power deviation from unity in order to keep acceptable peak to average ratio, since the transmitters are often peak power limited. These two cost functions are aggregated into a single cost function by means of a weighted sum and then minimised by applying the iterative steepest descent method.

Let h_n be the transmit waveform samples and $\hat{h}(f)$ the corresponding Fourier transform. Given a set of N_b frequency forbidden bands, the first penalty function could be written as:

$$J_{T1} = \sum_{k=1}^{N_b} w_k \int_{f_{k1}}^{f_{k2}} \left|\hat{h}(f)\right|^2 df = \boldsymbol{h}^{\dagger} \boldsymbol{R}^{(2)} \boldsymbol{h}$$

$$\boldsymbol{R}_{\boldsymbol{mn}}^{(2)} = \sum_{k=1}^{N_b} w_k \begin{cases} \dfrac{exp[2\pi i(m-n)f_{k2}\Delta t] - exp[2\pi i(m-n)f_{k1}\Delta t]}{2\pi i(m-n)\Delta t}, & m \neq n \\ (f_{k2} - f_{k1}) \qquad\qquad\qquad\qquad\qquad\qquad\qquad\qquad , & m = n \end{cases}$$

with $\boldsymbol{h}$ the vector of elements h_n, Δt the sampling interval, f_{k1} and f_{k2} the start and end frequencies of the k^{th} stop band. In [4], some diagonal loading is incorporated into $\boldsymbol{R}^{(2)}$ by replacing $\boldsymbol{R}^{(2)}$ by $\boldsymbol{R}^{(2)} + \lambda_T \boldsymbol{I}$ in order to penalise the samples magnitude and ensure that the matrix is definite positive.

The second penalty function penalises the deviation of the transmitted power from unity:

$$J_{T2} = \sum_{k=1}^{N_t} (|h_n|^2 - 1)^2$$

The total penalty function becomes:

$$J_T = \alpha J_{T1} + (1-\alpha) J_{T2} \text{ , } 0 < \alpha < 1$$

The iterative steepest descent method gives:

$$\boldsymbol{h}^{(p+1)} = \boldsymbol{h}^{(p)} - \mu \boldsymbol{\nabla}_{\boldsymbol{h}^{(p)}} J_T$$

Another alternative is to set $|h_n|$ to 1 and to do a phase-only design where $J_{T2} = 0$.

The receive waveform on its hand is calculated in order to filter out the energy received from the forbidden bands and in the same time reduce the range sidelobes of the cross-correlation function. It is the mismatched filter principle that aims to reduce the ambiguity sidelobes but with a loss of SNR since the filter is no more matched to the transmitted waveform.

If we denote by $\boldsymbol{g}$ the vector samples of the receive waveform, the first penalty function is also a frequency penalty function:

$$J_{R1} = \boldsymbol{g}^{\dagger} \boldsymbol{R}^{(2)} \boldsymbol{g}$$

As in the case of the transmitted waveform an additional diagonal loading could be added in the form of $\lambda_R \boldsymbol{I}$ to $\boldsymbol{R}^{(2)}$.

The second penalty function is an integrated range sidelobes of the cross-ambiguity function:

$$J_{R2} = \boldsymbol{g}^{\dagger} \boldsymbol{R}^{(1)} \boldsymbol{g}$$

with

$$\boldsymbol{R}^{(1)} = \boldsymbol{H}^{\dagger} \boldsymbol{H}$$

$$\boldsymbol{H} = \begin{pmatrix} h_1 & 0 & \dots & 0 \\ h_2 & h_1 & \dots & 0 \\ \vdots & \vdots & \vdots & \vdots \\ h_{N_t} & h_{N_t-1} & \dots & h_1 \\ \vdots & \vdots & \vdots & \vdots \\ 0 & 0 & \dots & h_{N_t} \end{pmatrix}$$

The total penalty function for the receive waveform becomes:

$$J_R = \beta J_{R1} + (1-\beta) J_{R2}, 0 < \beta < 1$$

The steepest descent algorithm gives again:

$$\boldsymbol{g}^{(p+1)} = \boldsymbol{g}^{(p)} - \mu \boldsymbol{\nabla}_{\boldsymbol{g}^{(p)}} J_R$$

3.7 Genetic algorithm based coding

Another alternative to the gradient algorithm is to use an evolutionary algorithm to design. In fact this technique has been successfully applied to similar design problems such as the array pattern synthesis [39] [40]. In [5], the authors divide the transmitted pulses into subpulses in which they transmit frequency chirps each corresponding to the available channel in frequency. The aim of the genetic

algorithm in this case would be to select the best distribution of the chirps over the subpulses in order to get the lowest integrated range sidelobes of the ambiguity function.

The use of chirps each corresponding to an available channel, helps to reduce the spectrum power leakage into the forbidden bands. However this condition requires that the subpulse duration is long enough for the chirp to respect the available channel in frequency. The limitation is therefore bounded by the bandwidth of the narrowest available channel.

In this context, the use of different lengths subpulses for the different bandwidths available channels could be a better solution to reduce the power leakage especially for the narrow channels. Another possible amelioration we could consist of transmitting upward and downward chirps since these two could exhibit low cross-correlation provided enough time bandwidth product.

Table 3. An example of the available radio frequency in Canada for the summer of 1999 according to the Canadian technical report of the defence R&D.

Channel	*Frequency Range*
1	5.11~5.14 (MHz)
2	5.26~5.27 (MHz)
3	5.29~5.31 (MHz)
4	5.37~5.39 (MHz)
5	5.46~5.48 (MHz)
6	5.51~5.52 (MHz)
7	5.54~5.59 (MHz)
8	5.64~5.66 (MHz)
9	5.72~5.73 (MHz)
10	5.77~5.80 (MHz)

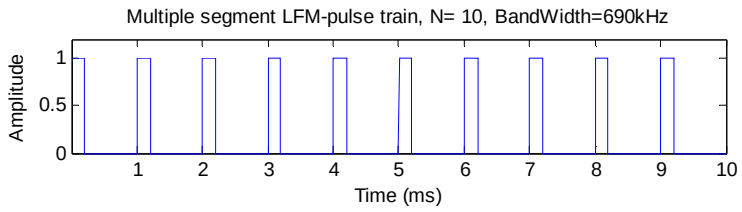

Figure 36. The transmitted waveform consisting of a train of 10 pulses with a duty cycle of 20%.

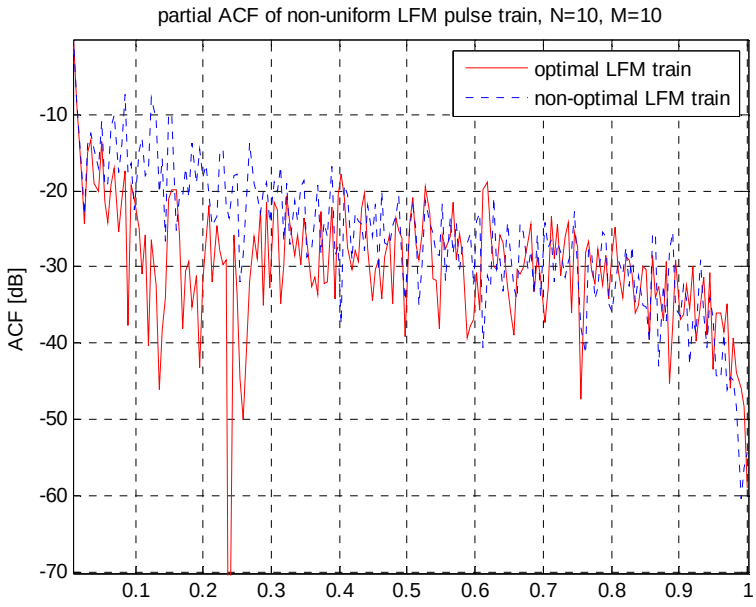

Figure 37. In [5] after optimally coding each transmitted pulse with 10 chirps using the genetic algorithm, the peak sidelobe of the autocorrelation function has been reduced to -13 dB.

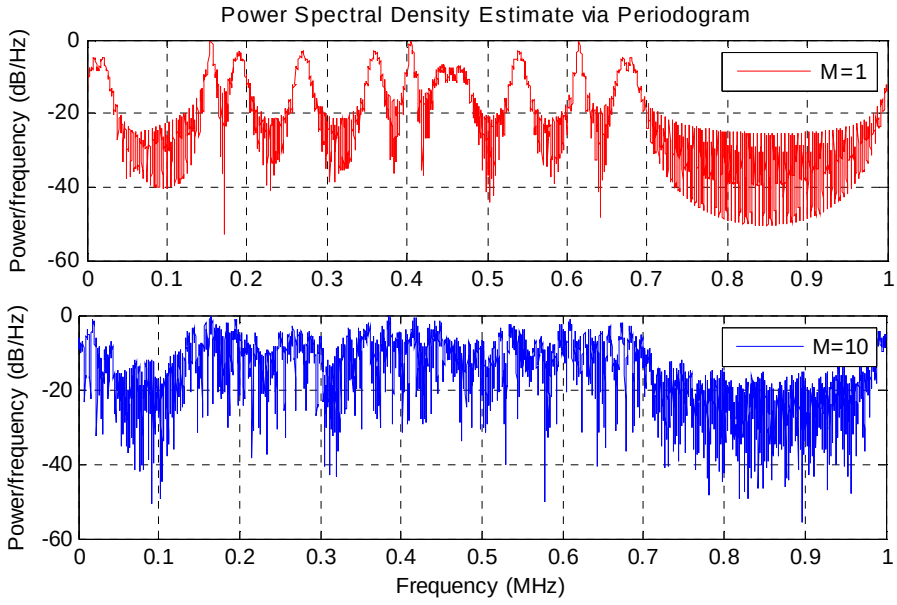

Figure 38. In [5] the reduction of the sidelobes apparently came with an increase of the power leakage into the forbidden bands due the increase of the subpulse number from one to ten.

As an application, [5] studied the case of the HFSWR with 10 noise free channels (see Table 3) presented by [41]. The transmitted waveform is a train of 10 pulses as depicted in Figure 36. First, each pulse was assigned a different chirp code corresponding to one of the available channels. In a second step, the pulse is divided into ten subpulses and the GA is used to get the best assignment

reducing the integrated sidelobes. Figure 37, shows how the peak sidelobe was reduced from the first non-optimal case at -9 dB to around -13 dB. However, this gain came at the expense of an increase in the power leakage in the forbidden bands as it could be noticed in the power spectral density of the resulting waveform shown in Figure 38.

3.8 The stationary phase approximation

The stationary phase method was developed by Lord Kelvin in the 1800s to calculate integrals encountered in the study of hydrodynamics [42]. The approximation is a principle of the asymptotic analysis of the behaviour of oscillating integrals defined as:

$$I(\lambda) = \int_a^b f(t)\, e^{i\lambda\, g(t)} dt, \lambda \gg 1$$

where f and g could be developed into Taylor's series near some appropriate points in $[a, b]$, and g is a real valued function.

Suppose that:

$$\exists!\, c \in [a,b] /\ g'(c) = 0, g''(c) \neq 0\ and\ f(c) \neq 0$$

Let μ be the sign of $g''(c)$.

$I(\lambda)$ could be rewritten as follows:

$$I(\lambda) = e^{i\lambda\, g(c)} \int_a^b f(t)\, e^{i\lambda\,[g(t)-g(c)]} dt$$

Since $e^{i\lambda\,[g(t)-g(c)]}$ is very oscillatory under the condition of $\lambda \gg 1$ for $t \neq c$, the integral will be rapidly decaying except for a small neighbourhood of c. Therefore:

$$I(\lambda) \approx e^{i\lambda\, g(c)} \int_{c-\varepsilon}^{c+\varepsilon} f(t)\, e^{i\lambda\,[g(t)-g(c)]} dt$$

and with the Taylor's approximation around c we get:

$$\begin{aligned} I(\lambda) &\approx f(c) e^{i\lambda\, g(c)} \int_{c-\varepsilon}^{c+\varepsilon} e^{i\frac{\lambda}{2} g''(c)(t-c)^2} dt \approx f(c) e^{i\lambda\, g(c)} \int_{-\infty}^{+\infty} e^{i\frac{\lambda}{2} g''(c)(t-c)^2} dt \\ &= f(c) e^{i\lambda\, g(c)} \int_{-\infty}^{+\infty} e^{i\frac{\lambda}{2} g''(c) s^2} ds = f(c) e^{i\lambda\, g(c)} \sqrt{\frac{2\pi i}{\lambda g''(c)}} \\ &= f(c) e^{i\lambda\, g(c)} \sqrt{\frac{2\pi}{\lambda |g''(c)|}} (i\mu)^{\frac{1}{2}} = f(c) e^{i\lambda\, g(c)} \sqrt{\frac{2\pi}{\lambda |g''(c)|}}\, e^{\frac{\pi i \mu}{4}} \end{aligned}$$

Hence

$$I(\lambda) \sim f(c) e^{i\lambda\, g(c)} \sqrt{\frac{2\pi}{\lambda |g''(c)|}}\; e^{\frac{\pi i \mu}{4}}, \lambda \to \infty$$

Finally we see why it's called the stationary phase approximation since the main contribution of the integral comes from the region where the phase $g(t)$ is stationary.

Now if we go back to our waveform code design problem, it could be stated as follows: For a given time envelope the problem consists in finding the phase code that provides the signal with the desired spectrum amplitude, i.e. finding $\varphi(t)$ satisfying $\left| \mathcal{F}\left(a(t) e^{j\varphi(t)}\right)\right| = A(f)$ with known amplitudes $a(t)$ and $A(f)$, $\mathcal{F}$ being the Fourier transform operator.

$$\mathcal{F}\left(a(t) e^{j\varphi(t)}\right) = \int_{-\infty}^{+\infty} a(t)\, e^{j[-2\pi f t + \varphi(t)]} dt = A(f) e^{j\phi(f)}$$

Applying the stationary phase principle to the above integral results in:

$$A(f_k) \approx a(t_k) \sqrt{\frac{2\pi}{\varphi''(t_k)}}$$

for

$$f_k = \frac{1}{2\pi} \varphi'(t_k)$$

If we denote by ψ the instantaneous frequency

$$\psi = \frac{\varphi'}{2\pi}$$

we could write the condition $\psi = f$

$$\frac{d\psi}{dt} = \frac{a^2(t)}{A^2(f)}$$

An integration of the previous equation gives:

$$\int_{-\infty}^{\lambda} a^2(t) dt = \int_{-\infty}^{\psi(\lambda)} A^2(f) df$$

Therefore, by the evaluation of the area under $a^2(t)$ and the one under $A^2(f)$ it is possible to know $\psi(\lambda)$ and then get back to φ by simple integration.

One application to this method could be found in [43] for array pattern synthesis. Similarly this approach could be used to shape the spectrum of radar signals in order to reduce the sidelobe levels as in the case of the non linear frequency modulation (NLFM) [44].

One example is a generation of a NLFM with a constant amplitude and a spectrum following a square root of a raised cosine to the power n:

$$A(f) = \left[k + (1-k)\cos^{\mathrm{n}}\left(\frac{\pi f}{B}\right)\right]^{\frac{1}{2}}$$

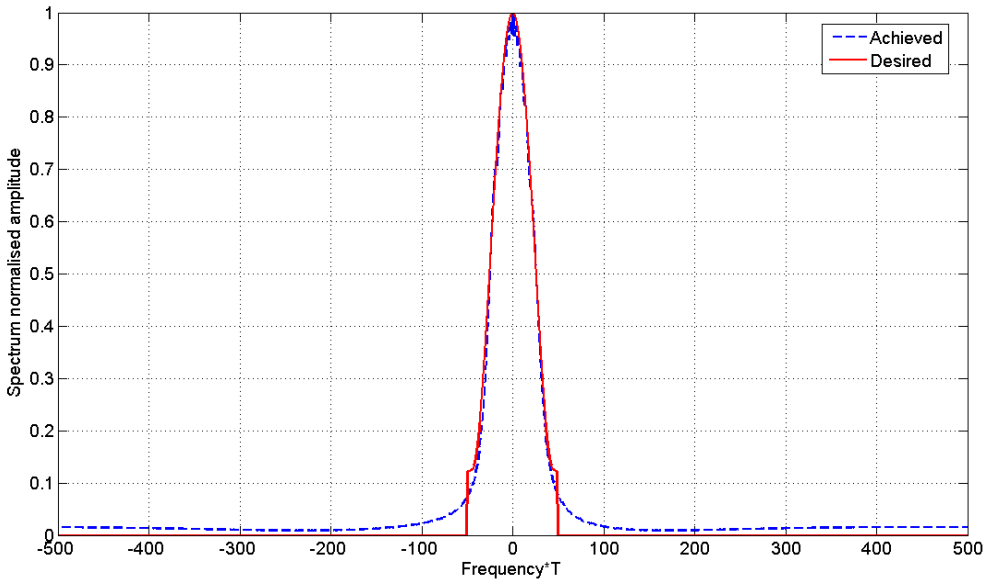

Figure 39. A very good accordance between the desired (solid) and the achieved (dashed) raised cosine spectrum (n=4, k=0.015, B=1) of a uniform amplitude signal with a time bandwidth of 100.

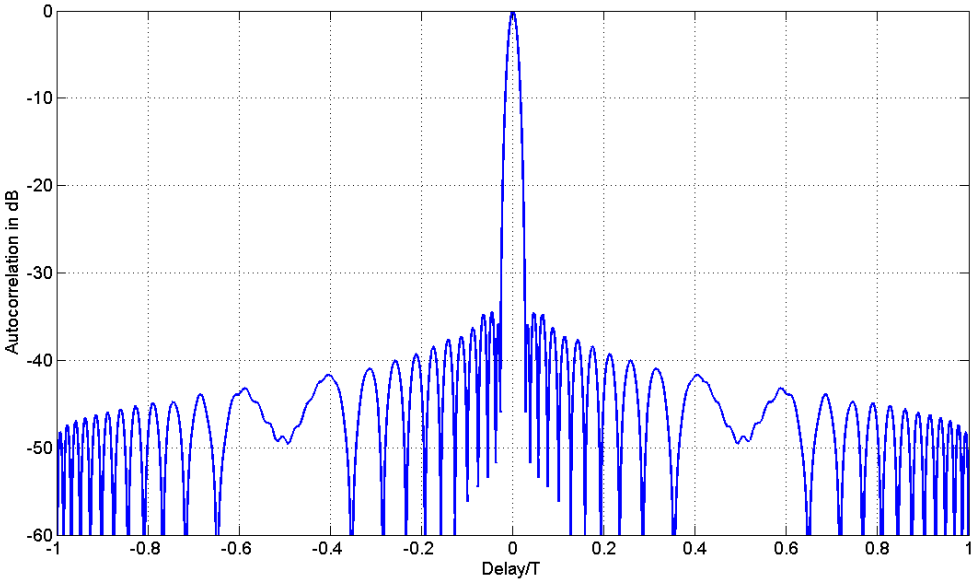

Figure 40.The autocorrelation function of the NLFM whose spectrum appears in Figure 39 (dashed line).

For k=0.015, n=4 and B=1, yields the spectrum depicted in Figure 39 for both the desired and the resulting spectrum. The time bandwidth product is 100 and we could notice that a good match has been achieved between the two spectra.

But as the amplitude of the transmitted signal is constant, the peak range sidelobe level could not be suppressed more than $-20\log(BT)+3$ dB according to [45]. In Figure 40 the autocorrelation function of the resulting NLFM shows that the peak sidelobe reached is -35 dB while the limit is -37 dB as set by the latter rule for our case where the time bandwidth product is 100.

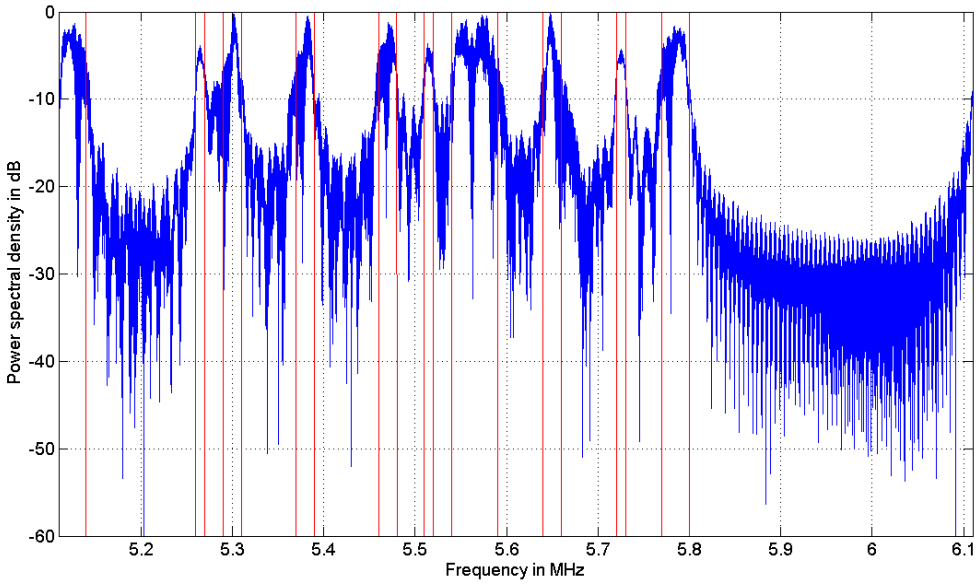

Figure 41. Real case available spectrum reported in Table 3 filled with the stationary phase approximation.

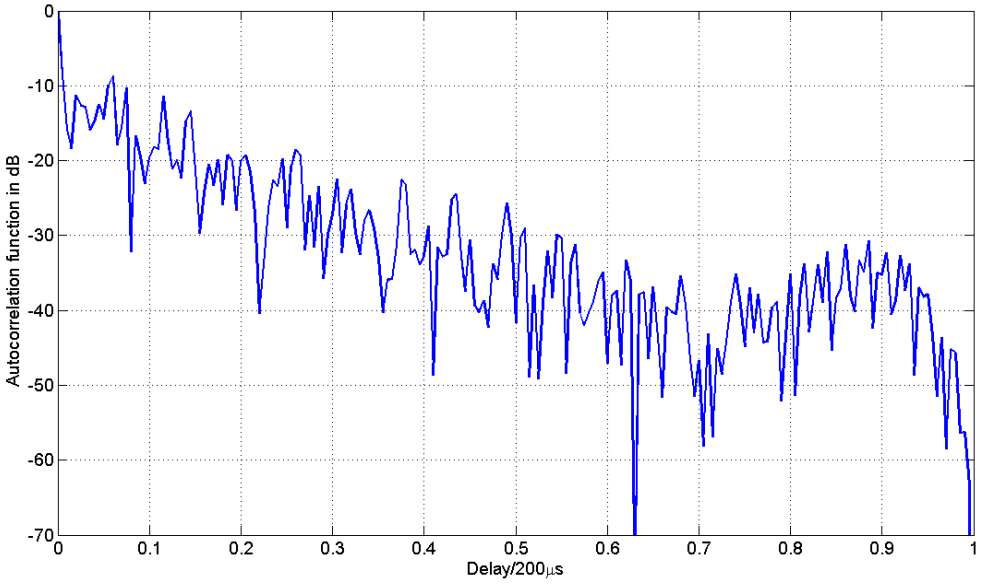

Figure 42.The partial autocorrelation of function for the signal whose power spectral density shown in Figure 41 with a peak sidelobe at -8.7 dB.

Now if we consider the same configuration of signal shown in Figure 36 and available spectrum reported in Table 3 we see in Figure 41 that the resulting spectrum after the stationary phase approximation is quite similar to the previous case where each pulse is coded with one sub-chirp corresponding to one available channel as reported in [5] for the non-optimal case. The sidelobe level in Figure 42 is still high reaching -8.7 dB. Therefore, the stationary phase approximation has no advantage in the sparse frequency coding especially that it does not offer any solution for the sidelobe reduction.

As we are looking at improving the suppression level in the forbidden frequency bands of the stationary solution, we notice that by nullifying the spectrum at the forbidden bands, the amplitude of the waveform becomes distorted. However, if we correct again the waveform envelope and keep only the phase code, the spectrum of this new signal has no more zeros in the forbidden bands, but interestingly a lower power level than previously. Repeating this iteration achieves even more suppression level in the forbidden bands.

What seems at the first sight as a discovery turns out to be based on the principle of alternate projections applied to a mathematical feasibility problem. However, the application to the radar waveform design remains as a major contribution of this thesis. Next we will present in details this alternative solution combining efficiency and efficacy and based on successive Fourier transforms.

3.9 The alternate projections technique for radar coding

3.9.1 Introduction

The radar phase coding under spectral constraints also falls in the category of the well-known mathematical feasibility problems.

The feasibility problem [46] could be described as follows: In the general estimation problem of an object h belonging to a space Ξ under a family of propositions $\psi_{i,i\epsilon I}$ representing all the available informations about the problem, the problem consists in finding the feasibility set:

$$S = \bigcap_{i\epsilon I} S_i$$

where S_i is the set of all the estimates being consistent with the information carried by the proposition ψ_i.

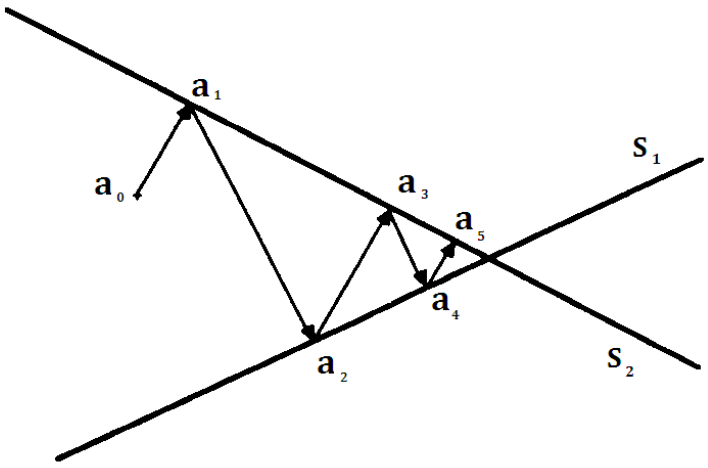

Figure 43. An illustration of the alternate projections algorithm as proposed by Kaczmarz in 1937.

Although historically the first alternating projection algorithm could be traced back to Schwarz around 1870 and his work on the integration of partial differential equations, the first feasibility algorithm based on projection could be attributed to Kaczmarz in 1937 and Cimmino in 1938 for their work on solving systems of linear equations. Figure 43 illustrates the operation of Kaczmarz's algorithm. The case of two subspaces is also known as the Von Neumann's Alternating Projection Theorem. The algorithm's proceeds by cyclic projections onto the m subspaces as follows:

$$\forall n \in \mathbb{N}, a_{n+1} = \mathcal{P}_{l_n}(a_n), l_n = n\ (modulo\ m)+1$$

where $\mathcal{P}_{l_n}$ is the projector on the $l_n{}^{\text{th}}$ subspace.

This technique based on the set theoretic framework has been applied to a wide range of engineering problems: signal recovery, image reconstruction, filter design, array signal processing, electron microscopy, speckle interferometry, antenna array design [47] [48], topography, spectral estimation, neural networks and colour systems etc…

In the case of the radar phase coding, a general signal space that could model the underlying physics is the Hilbert space $\mathcal{L} = L^2[\mathbb{R}, \mathbb{C}]$ of all the square-integrable functions x mapping a continuous variable $t \in \mathbb{R}$ to a complex number $x(t) \in \mathbb{C}$.

3.9.2 Application to waveform design for radar

The set of all the signals bounded in amplitude by the two functions m_L and m_U is defined as:

$$S_1 = \{a \in \mathcal{L} | (\forall\, t \in \mathbb{R})\ \ m_L(t) \leq |a(t)| \leq m_U(t)\}$$

The case where $m_L \equiv m_U$ corresponds to the phase only design.

In the same way if we denote by $\hat{x} = \mathcal{F}(x)$ the Fourier transform of x we could define the set of signals bounded in magnitude in the spectral domain by the two functions M_L and M_U as follows:

$$S_2 = \{a \in \mathcal{L} | (\forall\, f \in \mathbb{R})\ M_L(f) \leq |\hat{a}(f)| \leq M_U(f)\}$$

The last set is the set defined by the requirement of the autocorrelation function of the signal, for which we will define an upper bound not to exceed Γ_U. The autocorrelation function of x is calculated from the inverse Fourier transform of the square modulus of the signal's spectrum $\gamma_x = \mathcal{F}^{-1}(|\mathcal{F}(x)|^2)$

$$S_3 = \{a \in \mathcal{L} | (\forall\, \tau \in \mathbb{R})\ \ |\gamma_a(\tau)| \leq \Gamma_U(\tau)\}$$

Note that these three sets are not convex. The reason for S_1 and S_2 is the presence of a lower (non-zero) bound whereas for S_3 it is possible to verify that depending on Γ_U, the convex combination of two elements of S_3 has not necessarily an autocorrelation function respecting the same upper bound. We could give as an example the average of one rectangular pulse and its shifted version in time where the upper bound is the autocorrelation function of the rectangular pulse itself. This average signal has for sure an autocorrelation that extends beyond the original one.

To these three sets we associate three operators:

$$\mathcal{T}_m a(t) = \begin{cases} m_U(t) \exp\left(j.\angle\big(a(t)\big)\right) & |a(t)| > m_U(t) \\ a(t) & m_L(t) \leq |a(t)| \leq m_U(t) \\ m_L(t) \exp\left(j.\angle\big(a(t)\big)\right) & |a(t)| < m_L(t) \end{cases}$$

$$\mathcal{T}_M \hat{a}(f) = \begin{cases} M_U(f) \exp\left(j.\angle(\hat{a}(f))\right) & |\hat{a}(f)| > M_U(f) \\ \hat{a}(f) & m_L(f) \le |\hat{a}(f)| \le M_U(f) \\ M_L(f) \exp\left(j.\angle(\hat{a}(f))\right) & |\hat{a}(f)| < M_L(f) \end{cases}$$

$$\mathcal{T}_\Gamma \gamma_a(\tau) = \begin{cases} \Gamma_U(\tau) \exp\left(j.\angle(\gamma_a(\tau))\right) & |\gamma_a(\tau)| > \Gamma_U(\tau) \\ \gamma_a(\tau) & |\gamma_a(\tau)| \le \Gamma_U(\tau) \end{cases}$$

where $\angle$ is the angle operator.

The projection algorithm we propose is the following:

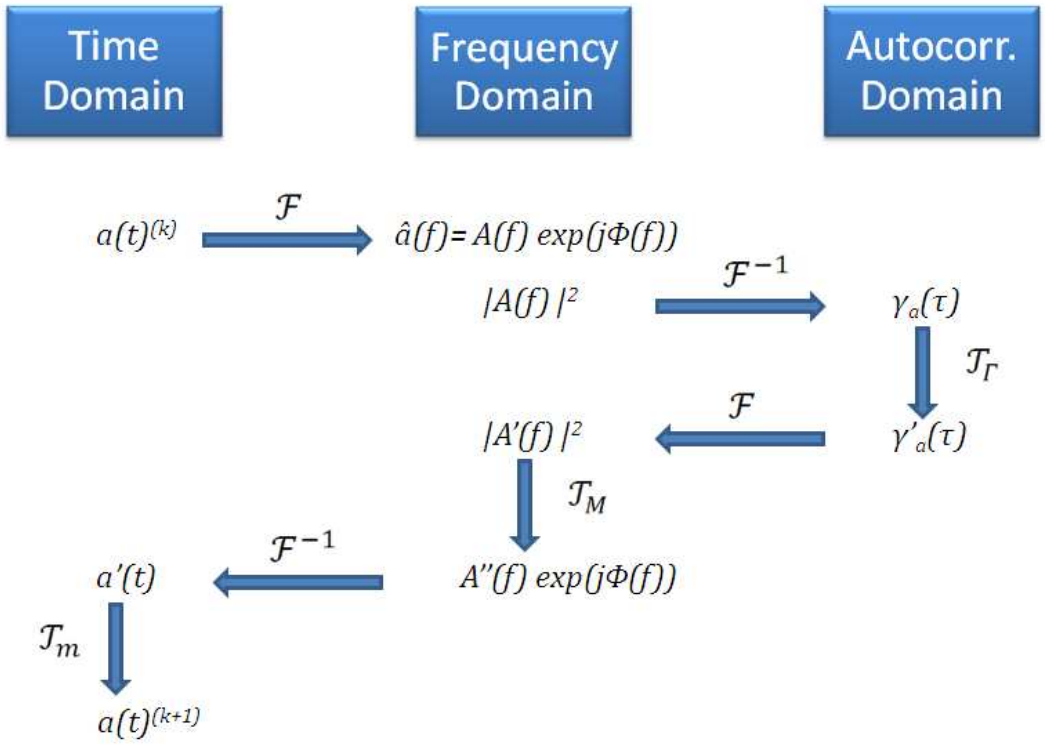

Figure 44.The flow diagram describing the alternate projections applied to radar code design.

Starting with an initial phase vector and an initial signal amplitude midway between $m_L(t)$ and $m_U(t)$, we first calculate the corresponding spectrum using Fourier transform. The square modulus of the spectrum is then inverse Fourier transformed in order to calculate the autocorrelation function to which we apply the correction operator $\mathcal{T}_\Gamma$ before going back by Fourier transform to the spectral domain where the new modulus of the spectrum is now adopted along with the old one phase. To this new spectrum we apply the spectral correction operator $\mathcal{T}_M$ and then one more time use the Fourier transform to go back to the time

domain where we apply the last correction operator $\mathcal{T}_m$ and proceed to the next iteration. The whole procedure is depicted in Figure 44.

3.9.3 **Phase coding under only spectral constraints**

In this first application we will investigate the ability of the proposed technique to fit the radar signal in a rectangular channel window. Practically, the radar has to limit its transmission into well defined frequency channels and not to exceed a level of leakage of power into the adjacent channels where other critical applications may operate.

In the first example we consider a sampled continuous periodic radar signal of 1000 time units with constant amplitude and an available channel of 100 frequency bins. The maximal level of transmission in the stop bands is limited to -20 dB. As no constraint is applied at the moment on the autocorrelation function an additional lower bound constraint is added inside the available channel to make sure the signal occupies the totality of the available channel. This lower bound is set to -0.4 dB.

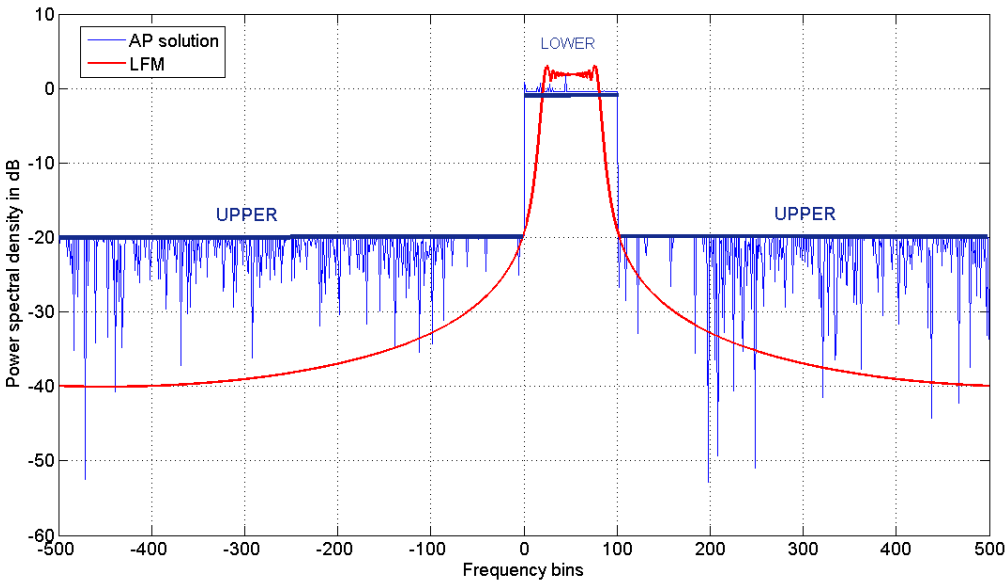

Figure 45.The power spectral densities of the AP solution and a chirp (LFM) respecting the same level of rejection (-20 dB) outside the available channel.

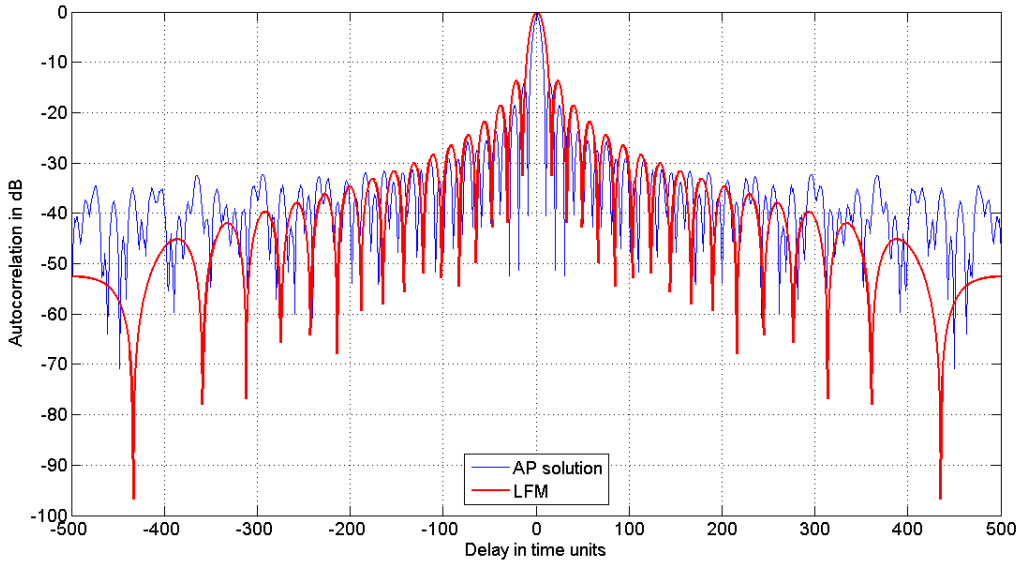

Figure 46.The periodic autocorrelation functions of the AP solution and the equivalent chirp respecting the spectral allocation constraint as seen in Figure 45.

Figure 45 shows the power spectral densities of the resulting code in comparison with a linear frequency modulation (LFM) solution that meets the same spectral occupation criterion. One could notice the rectangular shape of the spectrum obtained after the AP with a nearly flattened top, while the rejection level has been rigorously respected outside the window. On another hand, the swept bandwidth of the LFM had to be reduced in order to respect the spectral constraint. A practical solution would have been to use a filter to suppress the transmission outside the window but the resulting waveform won't keep a constant envelope in that case. As a result of this reduction, we notice in Figure 46 that the mainlobe of the LFM is nearly 1.6 times larger than the AP solution with a slightly higher PSL.

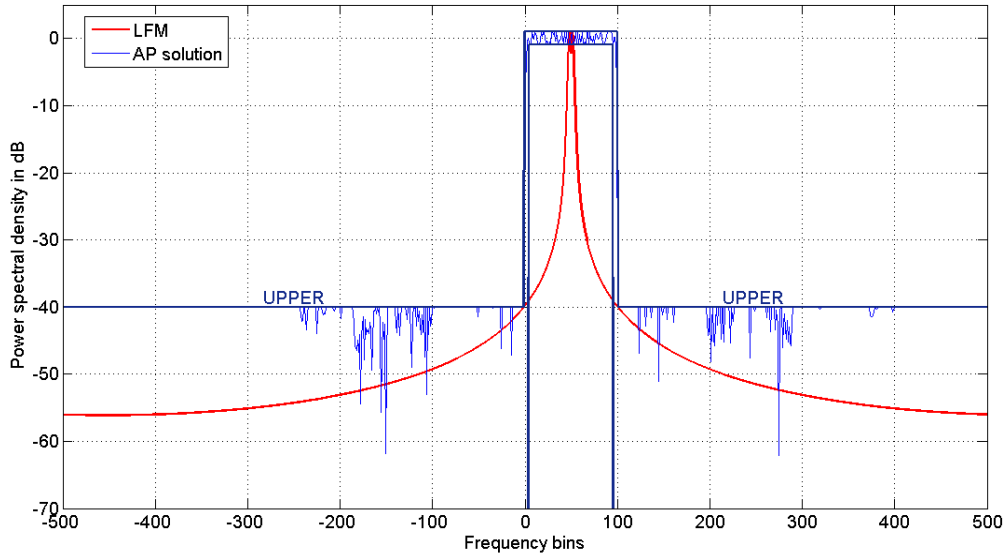

Figure 47. The power spectral densities of the AP solution and a chirp respecting the same level of rejection (-40 dB) outside the available channel.

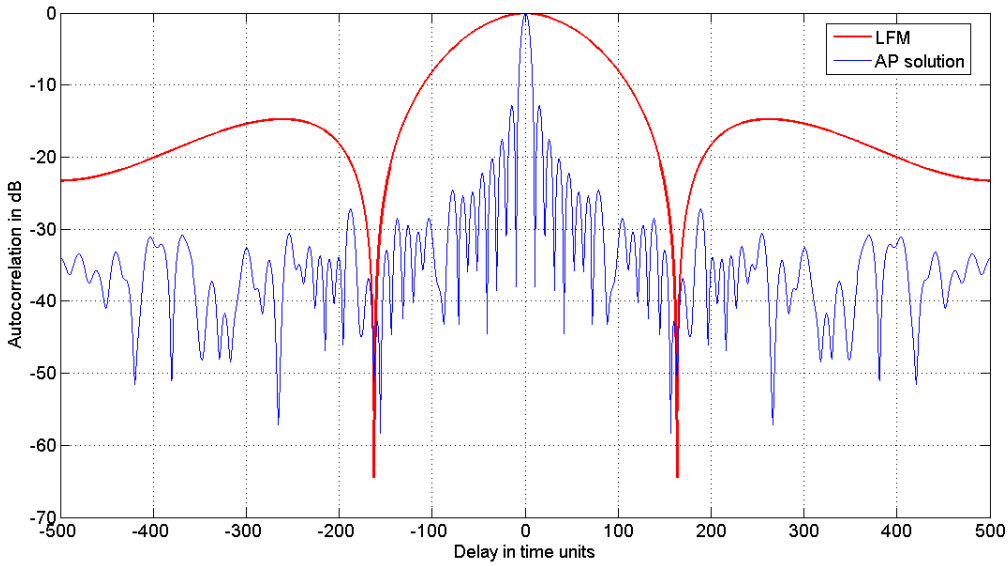

Figure 48. The periodic autocorrelation functions of the AP solution and the equivalent chirp respecting the spectral allocation constraint as seen in Figure 47.

However, if we raise the bar of the suppression level outside the available window this time to -40 dB, the LFM solution by itself could not be appropriate anymore. The LFM waveform that would respect this constraint should be very narrow in bandwidth as it could be seen in Figure 47 which induces a very high loss in resolution as depicted in Figure 48. We could also notice that the higher suppression level here reached by the AP solution came with a stronger fluctuation in the pass-band where we left a margin of 2 dB for the spectrum to fluctuate.

Now, in order to compare the performance of the AP with the stationary phase approximation, we consider again the case of the HF channels we mentioned in 3.8 and apply the AP technique this time to fill in the available channels.

As a criterion of comparison we will evaluate the ratio of the total energy transmitted in the forbidden frequencies to the energy transmitted in the available channels. Given two sets F_a and F_b of allowed and forbidden frequency bands respectively this ratio is written:

$$R_x = \frac{\int_{f \epsilon F_b} |\hat{x}(f)|^2 \, df}{\int_{f \epsilon F_a} |\hat{x}(f)|^2 \, df}$$

We denote by R_x the rejection ratio.

Starting from an initial arbitrary phase vector representing the samples phase, chosen as uniform random variables in $[0,2\pi[$ the proposed algorithm doesn't converge every time towards the same solution due principally to the non-convexity of the sets. For this we applied the algorithms for 200 initial random phase vectors and after 1000 iterations evaluated the rejection ratio that has been achieved.

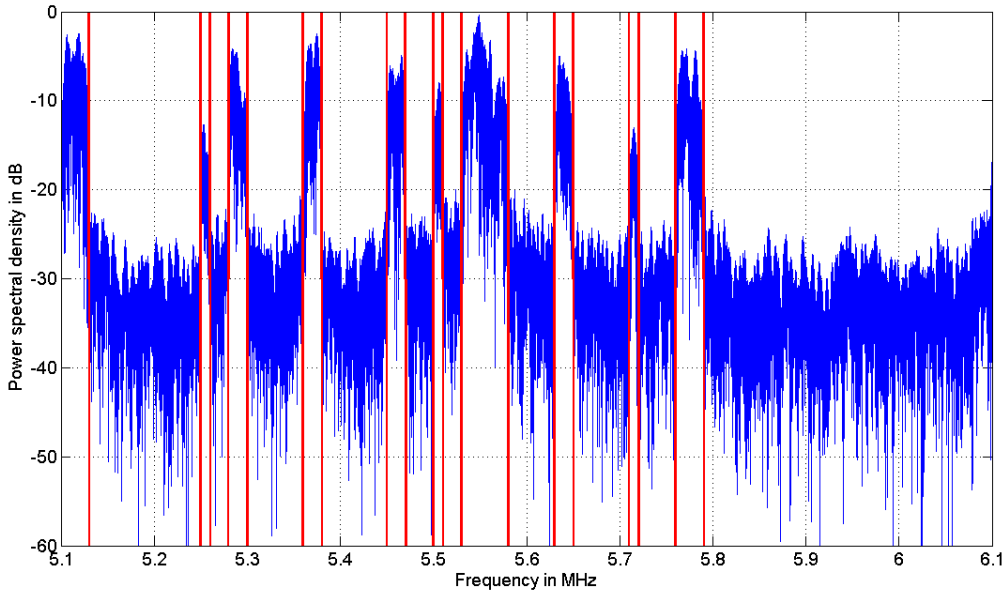

Figure 49.The available channels reported in Table 3 occupied using the alternate projection technique starting from an arbitrary phase and yielding around -14.4 dB of stop to pass band energy ratio.

The statistics shows that on average the AP algorithm reaches -14.43 dB for the rejection ratio with a standard deviation of 0.35 dB while the stationary phase solution presented in 3.8 has only achieved -6.22 dB. Figure 49 shows an example of the power spectral density obtained in this case with the AP.

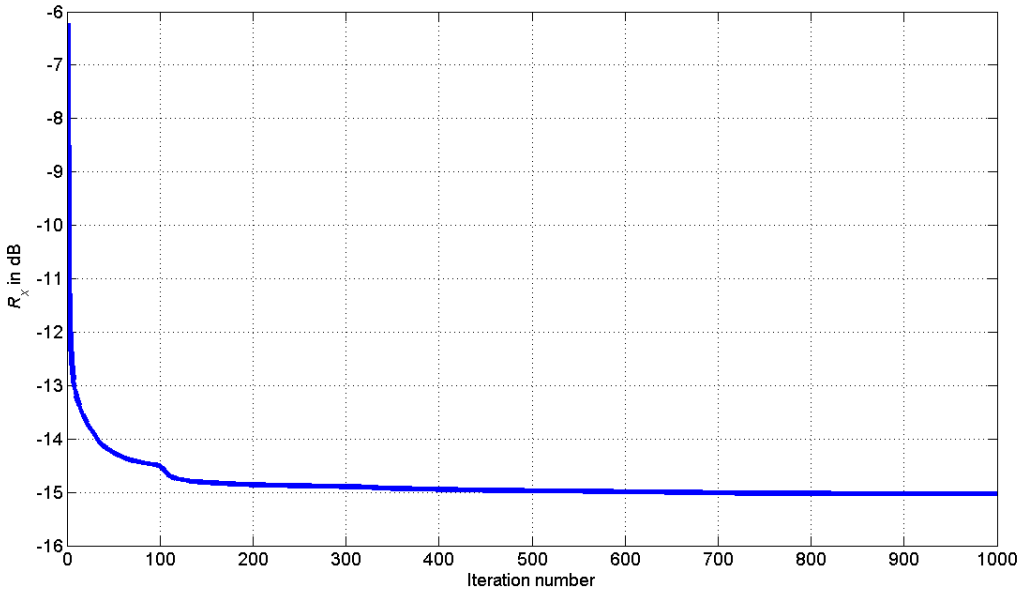

Figure 50.The evolution of the rejection ratio through the iteration of the alternate projections algorithm starting from the stationary phase solution as initial phase.

Now rather than starting from a totally arbitrary phase, if we use the stationary phase solution as an initial phase for the AP, the algorithm reaches after 1000 iterations -15 dB of rejection. Figure 50 shows the fast convergence of the algorithm in this case since in just 100 iterations the rejection went from -6.22 to -14.5 dB.

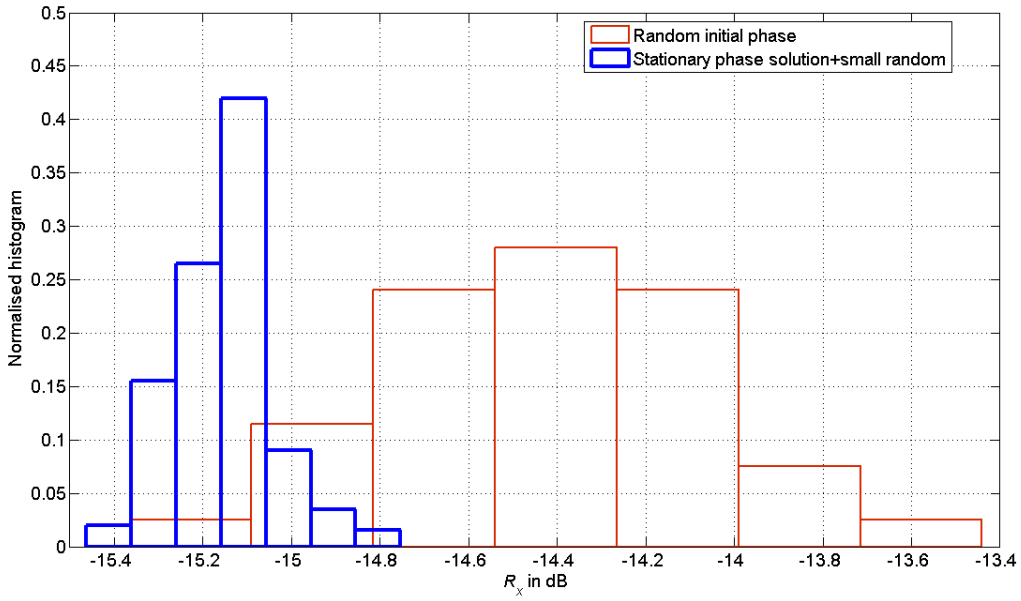

Figure 51.The normalised histograms of the rejection ratio results when starting from an arbitrary phase or the stationary phase solution with a small random variation.

The last alternative we tested was to add a random phase uniformly distributed in $[0,2\pi/10[$ to the stationary phase solution. This time the AP reached -15.15 dB on average with 0.1152 dB of standard deviation. In Figure 51 the normalised histograms of the two cases of totally random initial phase and the initial stationary solution phase with small random variations are shown together. We notice the improvement in the mean and the standard deviation when the stationary phase solution is used. However we notice that we didn't achieve a lot of gain when we added the small variations to the stationary phase solution before proceeding with the alternate projections.

3.9.4 Phase coding under only autocorrelation constraints

The research for codes that exhibit the lowest sidelobes levels has been carried out through history as it was reported in [38] going back to the most famous radar codes, the Barker codes in 1953. In a continuation of these works, [49] extended in 2005 the Barker polyphase sequences up to length 63 and extrapolated that at length 64 calculations carried out using 50 machines of 1.2 Gig might find one Barker code at this length every three weeks.

In this section we will try to investigate the ability of the proposed algorithm to suppress the range sidelobes until achieving ideal like performance. The first case we consider is the case of the periodic autocorrelation function (PACF). Codes like Franck codes, Zadoff-Chu codes and P4 codes exhibit ideal PACF. They could be used for CW radars like those with LPI properties.

By applying the AP technique, it turns out we are able to find quasi-ideal codes by setting the PACF upper bound Γ_U to be a Dirac function.

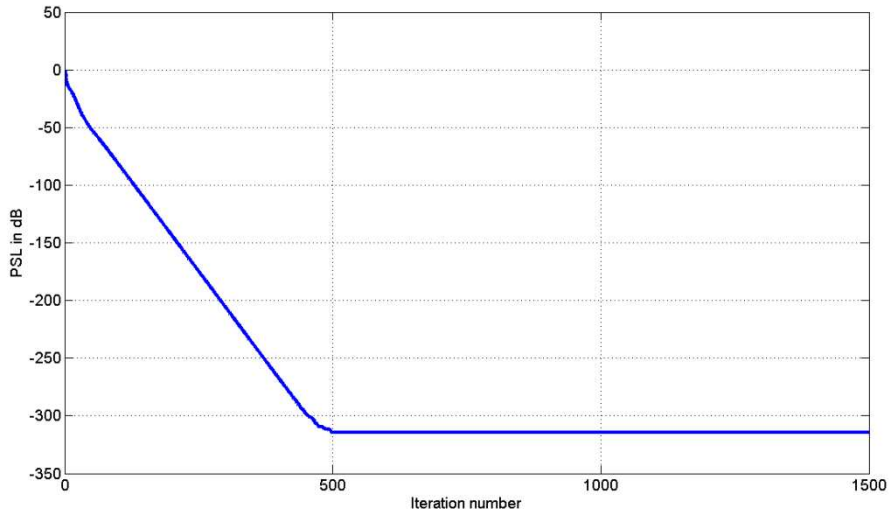

Figure 52. The evolution of the peak sidelobe level of the periodic autocorrelation function through iterations of the alternate projections algorithm for a codeword of length 15.

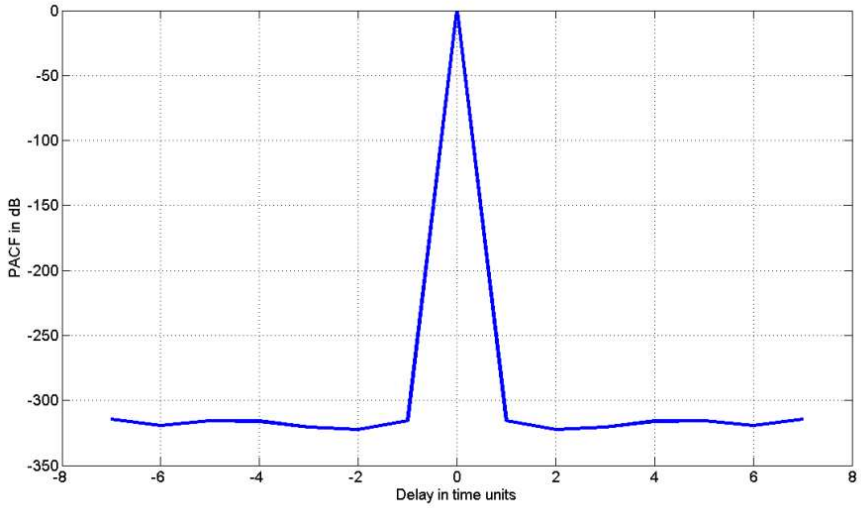

Figure 53. A quasi-ideal periodic autocorrelation function obtained by the alternate projection technique for a codeword of length 15.

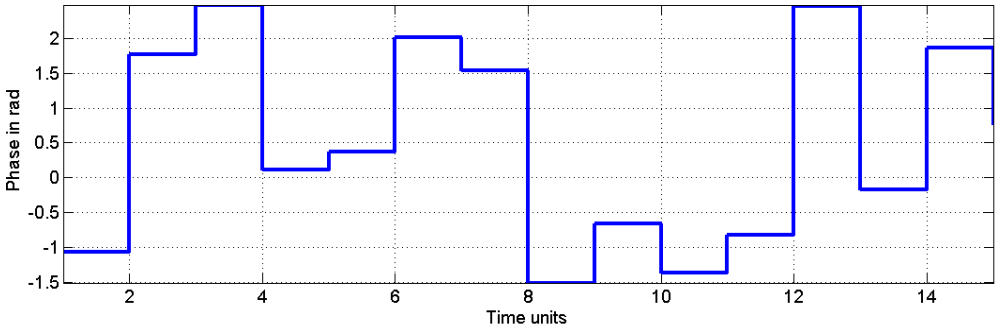

Figure 54. Phase history of one alternate projection solution of length 15 having quasi-ideal periodic autocorrealtion function.

Figure 52 shows us the evolution of the peak sidelobe level (PSL) of the PACF for a code of length N=15. In 500 iterations the algorithm could converge to a quasi-ideal PACF waveform with more than 300 dB of sidelobe rejection. The PACF of this resulting waveform is plotted in Figure 53 and its phase in Figure 54.

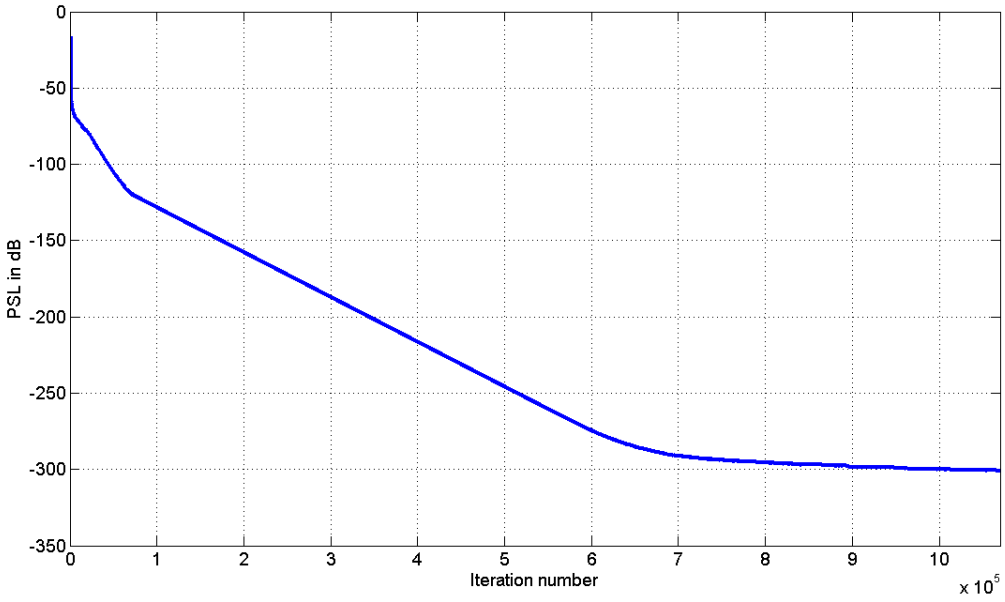

Figure 55. The evolution of the peak sidelobe level of the periodic autocorrelation function through iterations of the alternate projections algorithm for a quasi-ideal codeword of length 150.

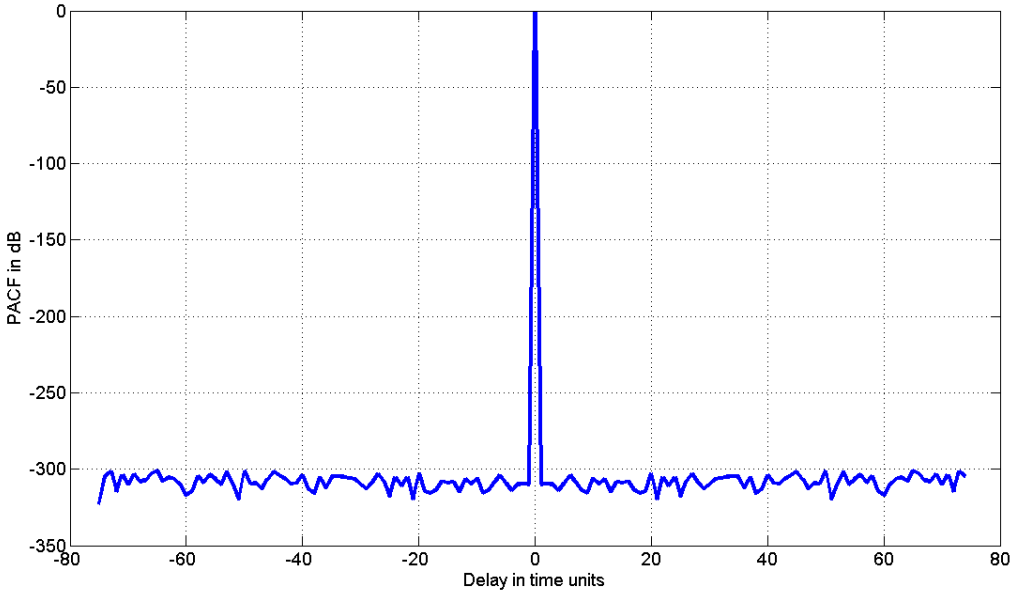

Figure 56. A quasi-ideal periodic autocorrelation function obtained by the alternate projection technique for a codeword of length 150.

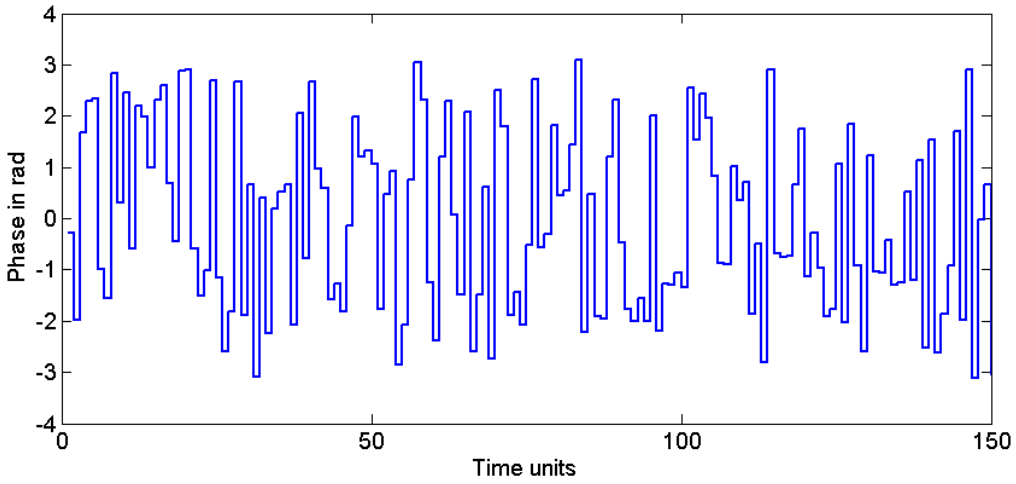

Figure 57. Phase history of one alternate projection solution of length 150 having quasi-ideal periodic autocorrealtion function.

Now if we consider a longer sequence of 150 phase elements, it takes approximately 1000 times the previous number of iterations for the code to achieve -300 dB of PSL as it could be seen in Figure 55. The PACF and the phase history of the resulting code are shown in Figure 56 and Figure 57. If the convergence time for such length code could be hindering the implementation in a real time phase coding scenario, one could not neglect the utility of these kinds of codes that do not fall in any classification category of the previously mentioned ideal PACF codes with known phase history characteristics and derived from linear frequency modulations.

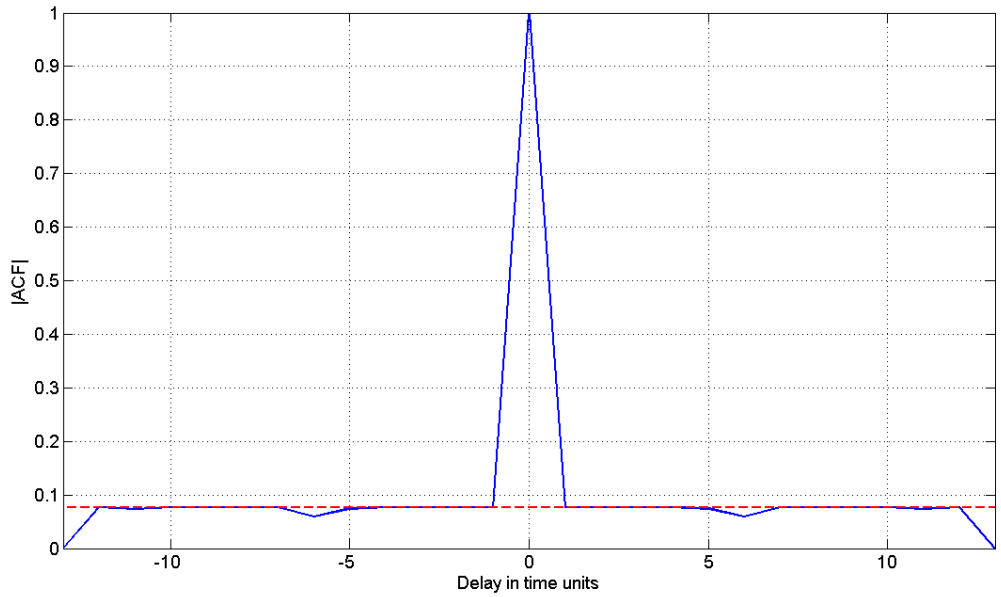

Figure 58. The autocorrelation function of a length 13 polyphase code verifying Barker condition obtained by the alternate projection technique.

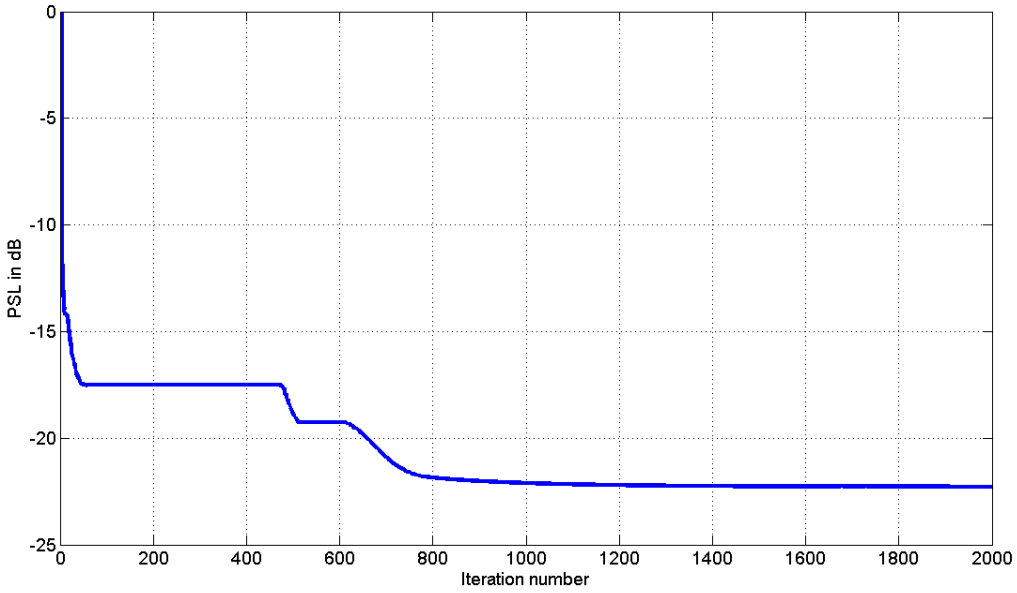

Figure 59. The evolution of the peal sidelobe level of the autocorrelation function of a length 13 polyphase code verifying Barker condition.

The second case we consider is the one of codes exhibiting low aperiodic autocorrelation functions. The first case we present is a synthesis of a polyphase code of length 13 verifying Barker condition i.e. a PSL of 1/13. For this construction we set the upper autocorrelation bound to 1/13 outside the center peak. This upper bound is indicated in dashed line in Figure 58 as well as the resulting ACF. We show the convergence to this result in Figure 59 reached in about 1000 iterations.

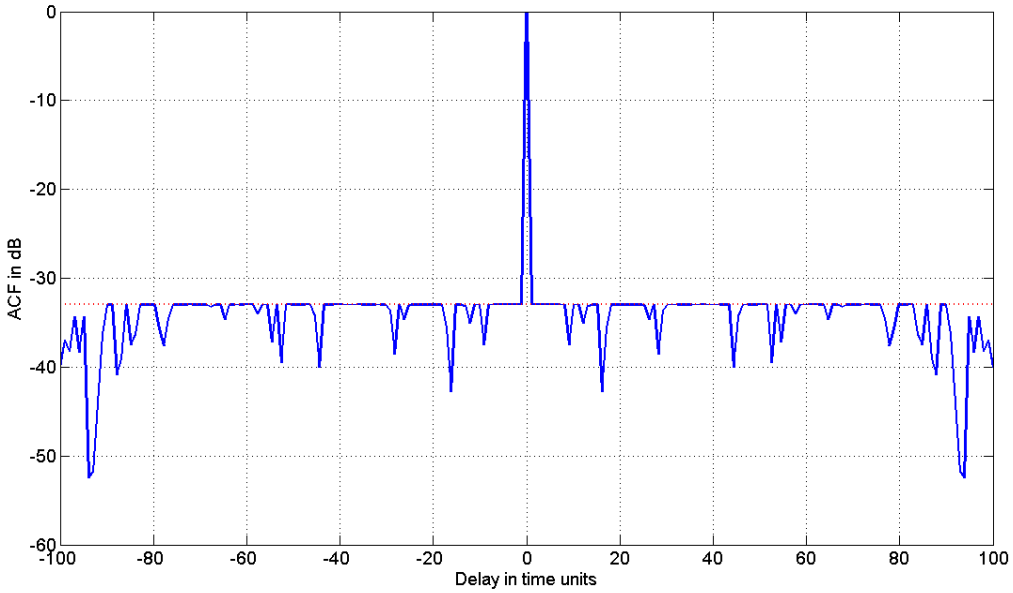

Figure 60. The autocorrelation function of a length 100 code obtained by alternate projections (solid line) respecting an upper bound (dashed line) of -33 dB for the peak sidelobe level.

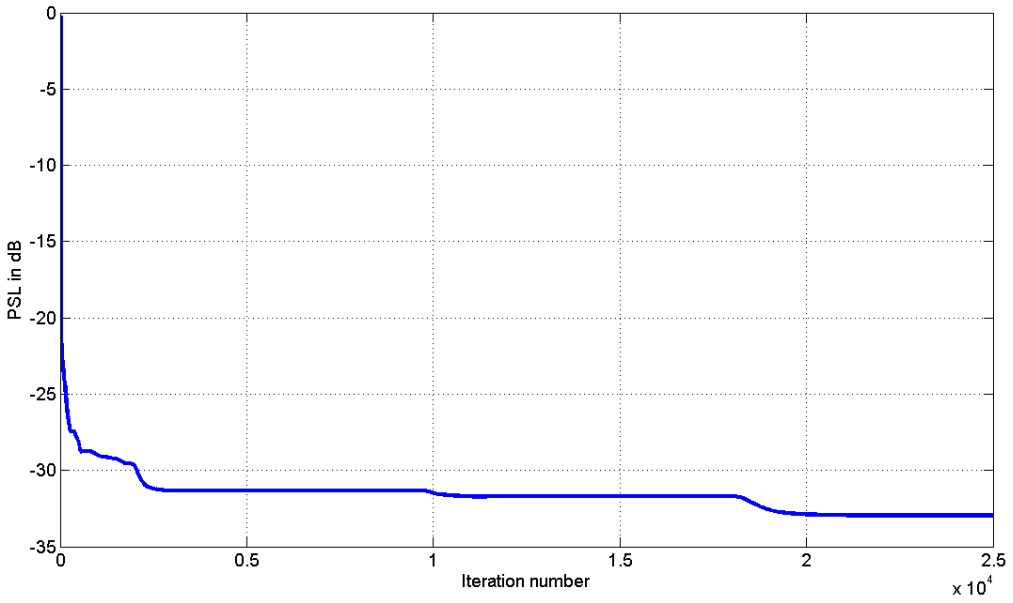

Figure 61.The convergence of the peak sidelobe level of synthesised code towards the upper bound set during the alternate projections.

Yet, if we extend the length of the designed code, the design process seemed to have more difficulty to achieve the Barker condition. Therefore we softened the constraint on the PSL until we were able to achieve a solution that respects the constraint. For a code of length 100 this was achieved by setting the upper bound of the PSL to -33 dB as it could be see in Figure 60. For the same length and mainlobe width, Frank code reaches 29.9 dB and Chu code 26.2 dB. The P (1,

0.01) code has similar peak sidelobe level but with a 1.5 time wider mainlobe [14]. Figure 61 shows that the convergence was 20 times slower than the case of length 13.

N=100		
Phase Code	*Mainlobe width*	*PSL*
Frank	1	-29.9 dB
Chu	1	-26.2 dB
P (1, 0.01)	1.5	-33 dB
AP	1	-33 dB

3.9.5 Phase coding under spectral and autocorrelation constraints

Here we consider the last case of application, an UWB SAR hypothetical scenario presented in [4] which consists of two pass-bands at [420-450] and [475-572] MHz. As presented in §3.6, the author first optimises the transmit waveform in order to fit the amplitude and spectral constraints. Next, a receive waveform is designed in order to furthermore filter the energy from the forbidden bands as well as to reduce the sidelobe levels of the cross-correlation function. However, we consider here the matched filtering case, so our transmitted pulse of 20µs should exhibit in the same time good sidelobe level and enough suppression in the forbidden bands, in contrast with the mismatched filtering case where a receive waveform helps reducing the sidelobes of the transmitted waveform at the expense of a mismatch loss.

The pulse is sampled at 160MHz and the alternate projection algorithm is iterated for 2000 times. We set an upper bound for the ACF sidelobes at -17 dB and considered strict suppression in the stop-bands i.e. we nullified the frequency samples belonging to these bands during the spectrum correction phase.

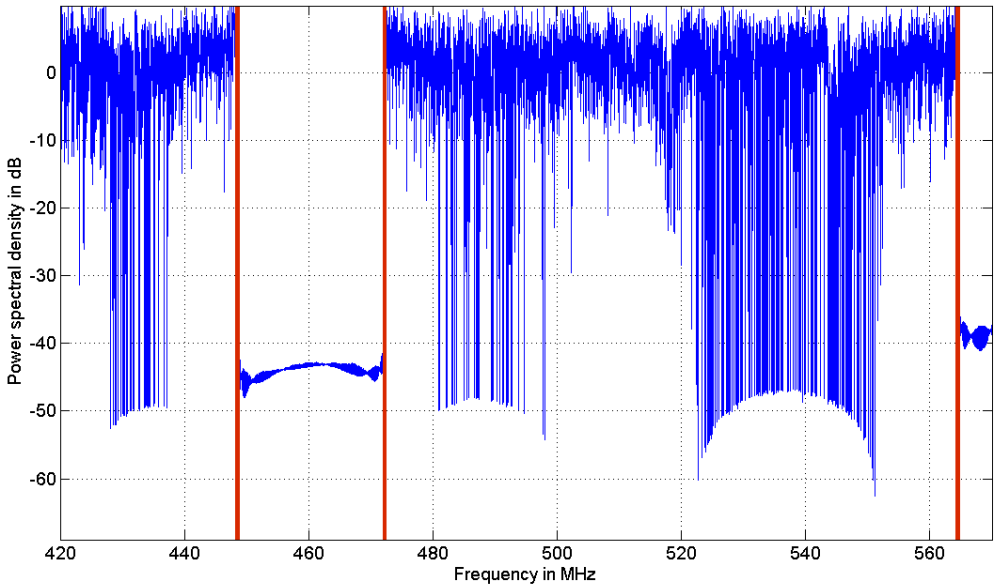

Figure 62.The power spectral density of the alternate projections solution achieving 40 dB of suppression level outside the [420-450] and [475-572] MHz windows.

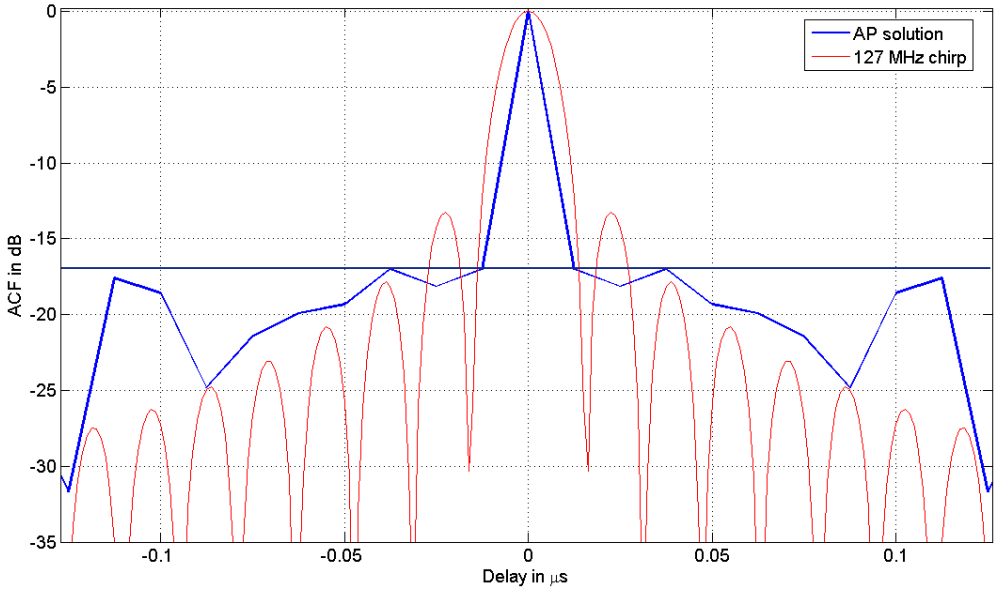

Figure 63.The autocorrelation function of the alternate projections solution whose power spectral density id shown in Figure 62 along with the response of a chirp having the same total spectral occupancy.

As a result the power spectral density has achieved around 40 dB of suppression level in the stop-bands as it can be seen in Figure 62. The zero-Doppler cut of the resulting ambiguity function shows that the sidelobe level has been lowered to the upper bound at -17 dB as seen in Figure 63. The ACF of a chirp signal having the same total occupied bandwidth i.e. 127 MHz is also traced for comparison.

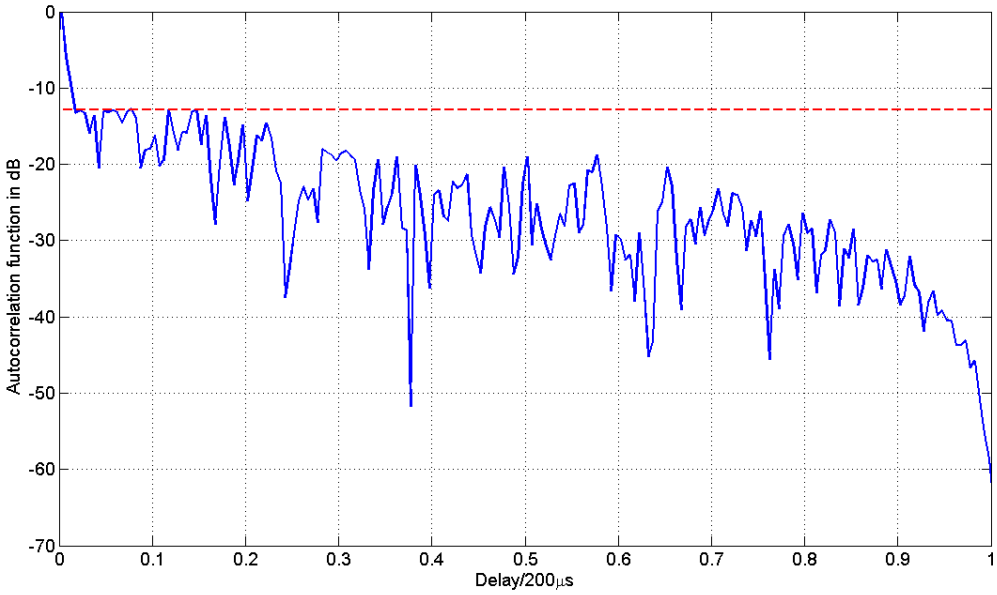

Figure 64.The autocorrelation function of the alternate projection solution for the HF channels reported in Table 3 and respecting a -13 dB of peak to sidelobe level (shown in dashed line).

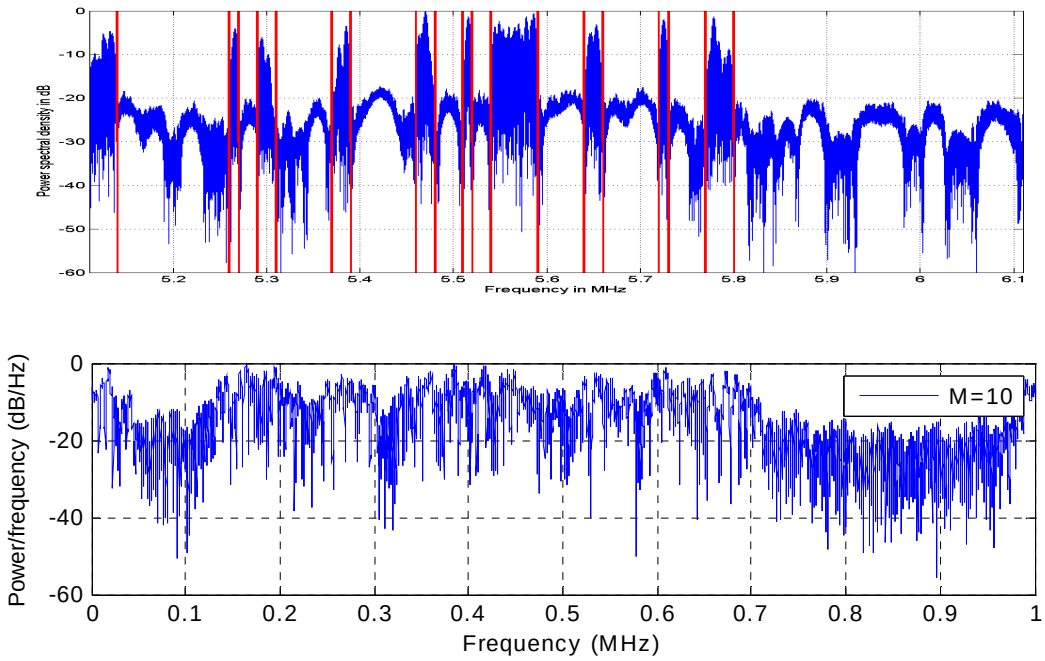

Figure 65.The power spectral density of the alternate projections solution when trying to occupy the available channels reported in Table 3 under a -13 dB sidelobe constraint (Top) in comparison to the equivalent spectrum obtained by GA in [5].

The next example we consider is the set of available channels in HF that we presented previously in 3.7, 3.8 and 3.9.3. Now we apply an additional constraint on the sidelobe level not to exceed -13 dB relatively to the main peak.

After 200 iterations and with an autocorrelation function respecting the constraint in question as shown in Figure 64, the power spectral density achieved a rejection ratio of -6.7 dB. When comparing this PSD shown in Figure 65 to the one presented in [5] satisfying the same sidelobe level, even that we don't have the value of the rejection ratio for exact comparison we see a good improvement in the isolation between the available and forbidden channels.

3.10 Evaluation of the clutter performance of the HFSWR waveforms

In order to reduce the complexity of the waveform design for the monostatic HFSWR, we have proposed in the previous chapter to optimise in a first step the transmit/receive strategy in order to guarantee the best minimal contrast ratio over the operational range of the radar and for different duty cycles.

Here we always consider a monostatic HFSWR operating in the blocked/saturated states. Performances of the Doppler ambiguity, especially in terms of sidelobes, are governed by the properties of the periodic waveform (giving a "Sinc" function profile in the Doppler frequency domain) similarly to a conventional waveform: the longer the integration time, the lower the sidelobes and the narrower the resolution. Hence, we focus the study on the design of the code and its properties in time (range). Note that the Doppler effect within a code duration can be neglected in HFSWR applications. The cross-correlation function of a transmitted signal $x(t)$ for distances D and r is:

$$A_x(D,r) = \int_0^T x\left(t - \frac{2D}{c}\right)\, x^*\left(t - \frac{2r}{c}\right)\left(1 - \frac{|x(t)|}{M}\right) dt$$

where T is the integration time and M is the amplitude of the transmitted signal during the saturated state of the transmitter.

The contrast ratio (See 2.8.4) could be therefore estimated by:

$$CR_x(D) = \frac{\sigma}{\sigma_{00}\,\delta\theta}\frac{A_x^2\,(D,D)P(D)}{\int_0^{D_{max}} A_x^2\,(D,r)P(r)\,r\,dr} = \frac{\sigma}{\sigma_{00}\,\delta\theta}\,\frac{1}{k_x(D)}$$

where σ is the target's radar cross section, σ_{00} is the sea reflectivity corresponding to the Doppler shift of the target, $\delta\theta$ is the angular beamwidth, $P(D)$ is the round-trip power loss for the distance D, D_{max} the maximal operational range of the radar and $k_x(D)$ a waveform dependent loss of contrast ratio factor.

The clutter performance indicator is defined by the maximal loss of contrast ratio encountered over the operational range of the radar defined as:

$$K_x = \max_{0 \le D \le D_{max}} k_x(D)$$

As for the spectral performance we use the usual ratio of the total energy in the forbidden bands to the energy in the allowed ones:

$$R_x = \frac{\int_{f \epsilon F_b} |\hat{x}(f)|^2 \, df}{\int_{f \epsilon F_a} |\hat{x}(f)|^2 \, df}$$

For this numerical application, we consider again the set of ten available channels found in the Canadian technical report of 2001 [41].

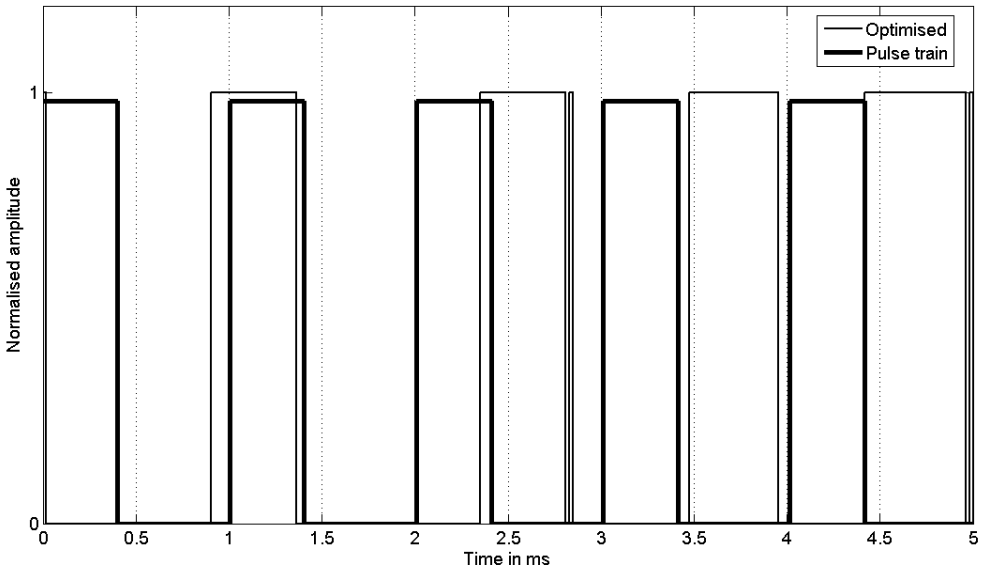

Figure 66. A 40% duty cycle optimised waveform belonging to the Pareto front in Figure 31. Pareto fronts with NSGA-II in comparison with the pulse train performance along with its equivalent pulse train.

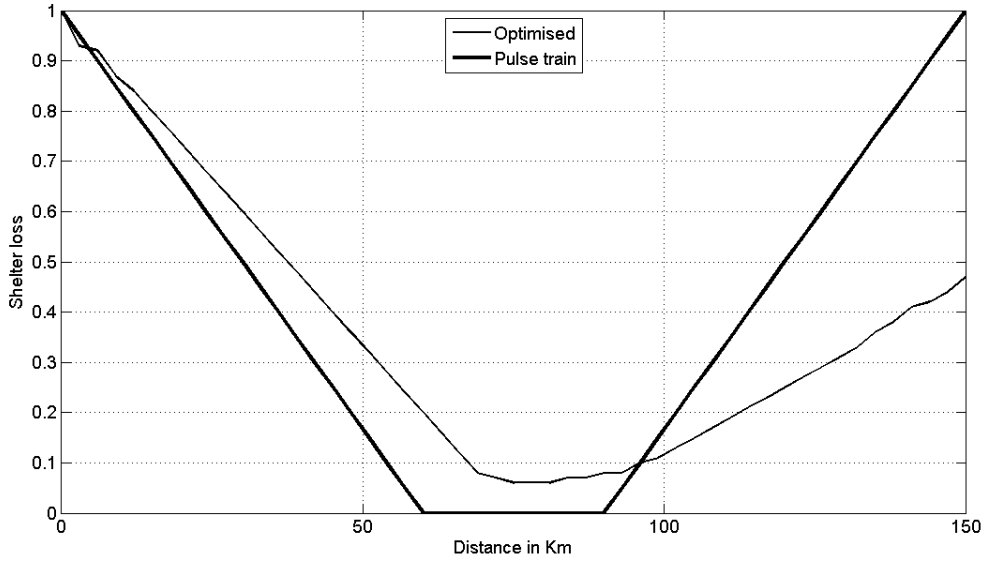

Figure 67.The shelter loss function of both waveforms shown in Figure 66 where the optimized waveform benefits from an advantage at the end of the radar range extent.

For the waveform's time envelope, we use a 40% duty cycle optimised solution [17], and as reference its equivalent train of 5 pulses of a total duration T_p = 5 ms sampled at F_s = 3.45 MHz. Figure 66 shows both waveforms variations over time for one repetition period (with slightly modified amplitude for ease of distinction), while their resulting shelter loss (or eclipsing loss) function over the 150 km, corresponding to the maximal range of the radar, could be seen in Figure 67.

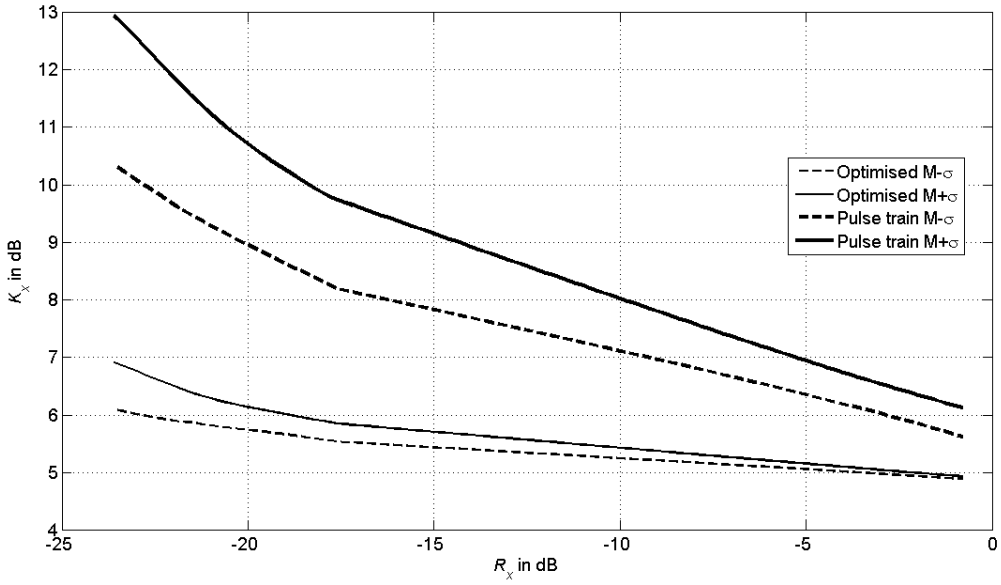

Figure 68.The statistical evolution of the contrast ratio maximal loss vs. the rejection ratio when applying the alternate projections under the spectral constraint.

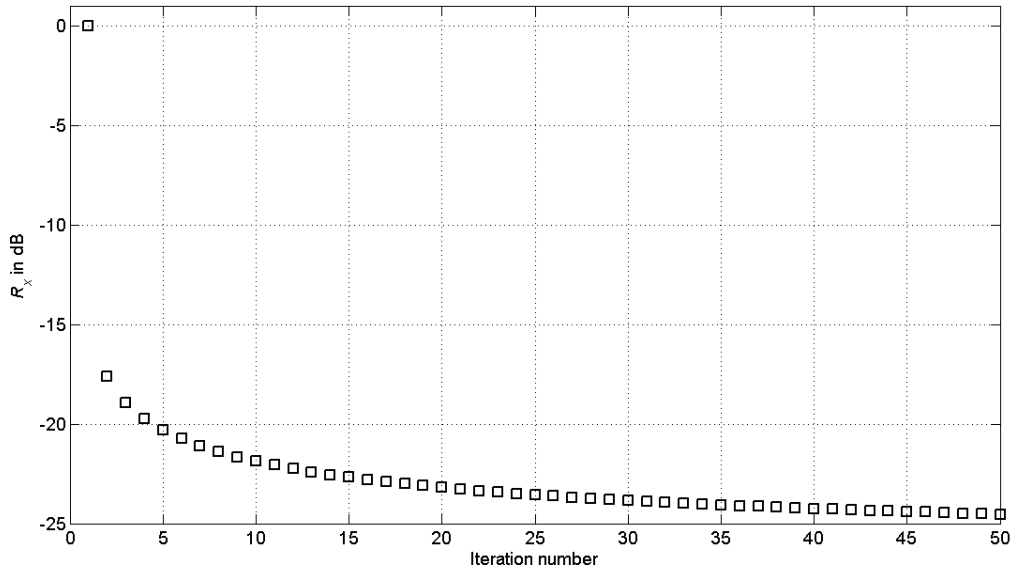

Figure 69.The convergence of the rejection ratio through the iterations of the alternate projections starting from an arbitrary initial phase.

Now if we apply the alternate projection technique on both waveforms for the same number of iterations, the evolution of the clutter performance indicator K_x depends on the initial phase vector. Figure 68 shows the mean$\pm$standard deviation ($M \pm \sigma$) boundaries for 1000 different initial phase vectors of size $N = T_p.F_s = 17250$, and whose elements are uniformly distributed in $[0,2\pi[$. As the projection technique succeeded in shaping the signal's spectrum up to 20 dB of pass to stop band ratio on average after just 5 iterations as it could be seen in Figure 69, we see that for this value the optimised waveform spanned 0.4 dB into the $M \pm \sigma$ interval against 1.8 dB for the conventional one and with a 4 dB lower mean value of the contrast ratio loss.

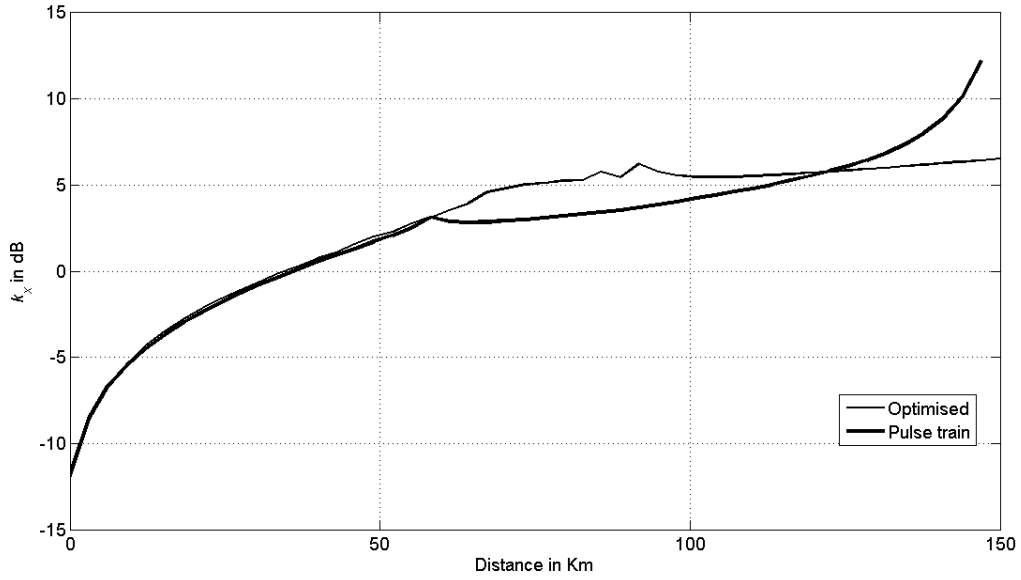

Figure 70.The achieved loss of contrast ratio vs. distance for two cases of optimised and conventional waveform showing how the gain is achieved at the end of the radar range extent beyond 120 km.

As an example of the performances achieved after the spectrum fitting, Figure 70 shows the evolution of the contrast ratio loss for samples of both waveforms in question over the operating range of radar. We could see that the gain of contrast ratio starts to build up beyond 120 km.

3.11 Conclusion

After presenting the different sparse coding techniques, the alternate projection technique seemed to combine calculation efficiency and good results whether on the rejection ratio side or the sidelobe suppression level. Used as a very fast spectrum fitting technique with a complexity of only $\mathcal{O}(\mathrm{N}\log\mathrm{N})$, the alternate projections could be applied to design real time waveform for the HFSWR. The use of optimised envelope guarantees better and more deterministic performance in terms of minimal contrast ratio compared to the simple train of pulses when using this technique. This solution could be used to rapidly change the transmitted waveform in order to enhance the low probability of intercept or to adapt to a rapidly changing spectral environment. The other advantage is that even when designing ideal like codes the obtained solution doesn't fall into any previously known category like the frequency based codes (P1, P4 …) commonly used in continuous LPI radars, therefore presenting a severe difficulty for the classification and hence the exploitation.

Next, we will practically test the performance of this new coding technique along with optimised envelopes in an aircraft detection scenario.

Technique	*AP*	*Gradient*	*GA*	*Stationary phase*
Implementation	Simple	Hard	Medium	Very Simple
Complexity	Quasi-linear	Quasi-linear	?	Quasi-linear
Spectral constraints	Yes	Yes	Yes	Yes (No)
Sidelobes level control	Yes	Yes	Yes	No(Yes)
Ideal codes generation	Yes	?	?	?

Chapter 4

Experimental Validation

4.1 Introduction

In this chapter the test of optimised envelope and coding technique previously developed is described. The ability of the high duty cycle waveform to operate at near and far ranges despite the shelter effect is examined. The combinations of optimised and conventional envelopes with linear frequency or alternate projections phase coding are considered for comparison.

4.2 Geometrical considerations

Experimentation was carried out at Onera-Palaiseau which is located only 10 km away from Paris-Orly Airport. Therefore aircrafts taking off or landing in this airport make perfect targets for radar experiments at this center.

Figure 71 shows an aerial view of the region surrounding Orly's Airport and the Onera's center of Palaiseau as well as the trajectory here considered of a taking off aircraft. We notice that the trajectory begins with a first part where the aircraft is approaching and then a second part where it's going away. Hence the radar target returns should exhibit positive then negative Doppler shifts corresponding to these two flight phases respectively.

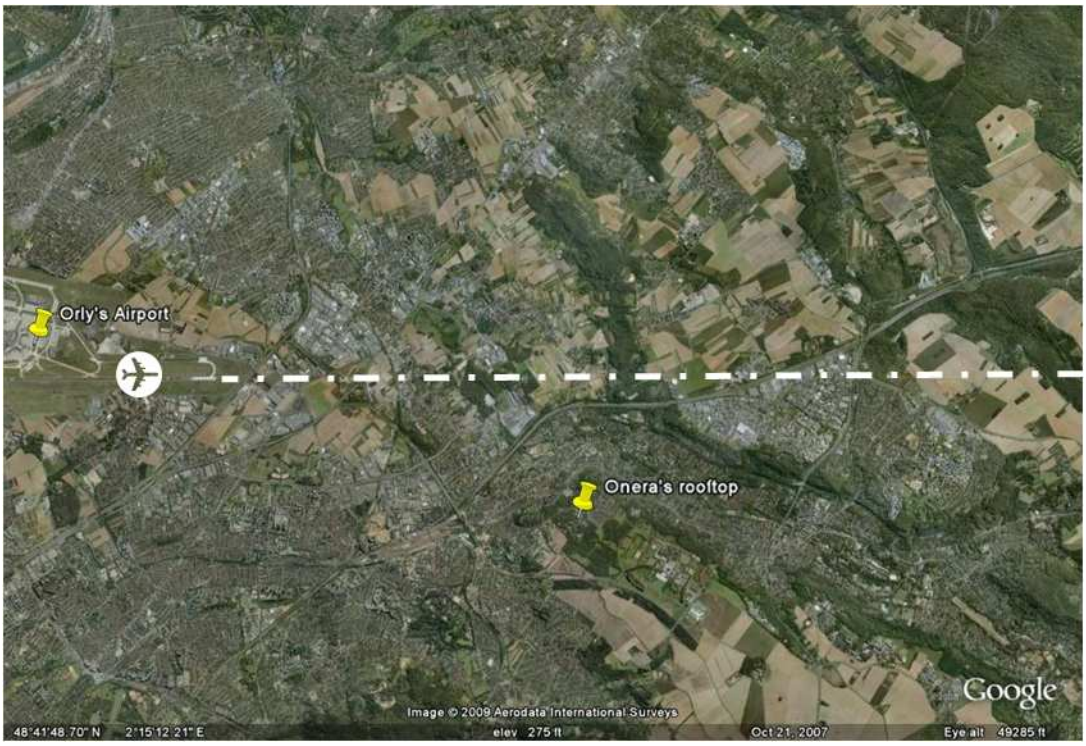

Figure 71. An aerial view of the experimental area with the indication of the airliner route.

For example if the aircraft is flying at a constant velocity v_0 along a rectilinear trajectory and the radar is separated from the trajectory line by distance d_0 then the relation between the Doppler shifts of the radar returns f_D and the measured distance to the radar d is as follows:

$$f_D = \pm \frac{2v_0}{c} f_0 \sqrt{1 - \left(\frac{d_0}{d}\right)^2}$$

where f_0 is the central frequency of the radar emissions and c the velocity of propagation.

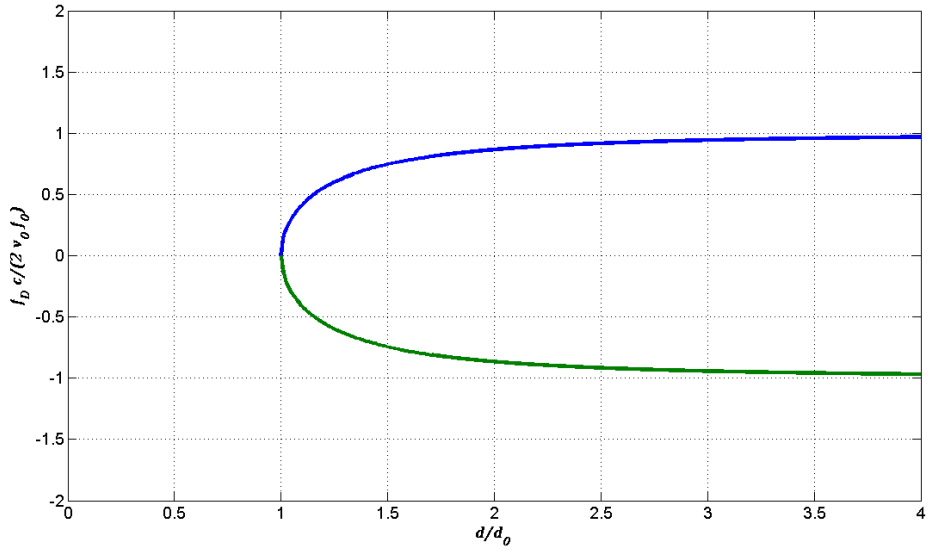

Figure 72. Normalised range-Doppler map showing the evolution of a target having a constant velocity and rectilinear trajectory relatively to a monostatic radar.

The evolution of the target in the range-Doppler map should therefore exhibit a typical plot as shown in Figure 72.

4.3 The radar equipment

Positioned at the rooftop of one building in the Onera's center, the measurement system consisted of the following:

- A transmit and a receive (passive) omnidirectional antenna placed 20 m away from each other, on one side and on another of the rooftop separated by the shelter chamber hosting the rest of the equipments.
- An industrial PC hosting two ICS cards 554 and 564, serving as ADC and DAC respectively with 14 bits resolution.
- Amplifiers and RF generators

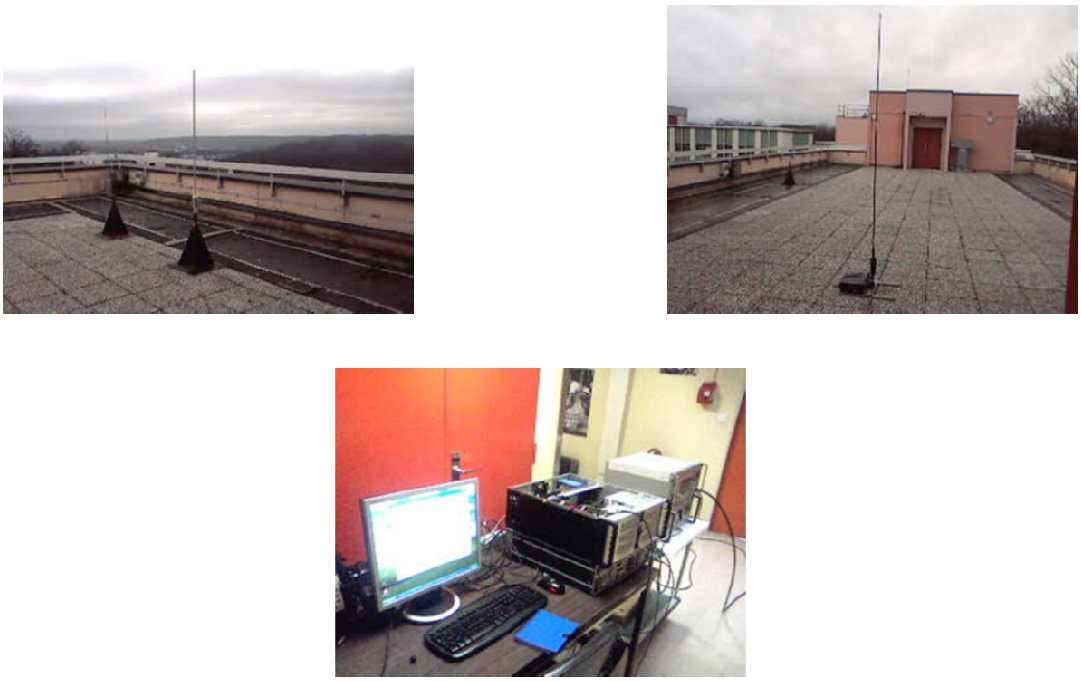

Figure 73. The experimentation equipment consisted of the transmit and receive antennas (from right to left) and a processing unit with ADC and DAC cards.

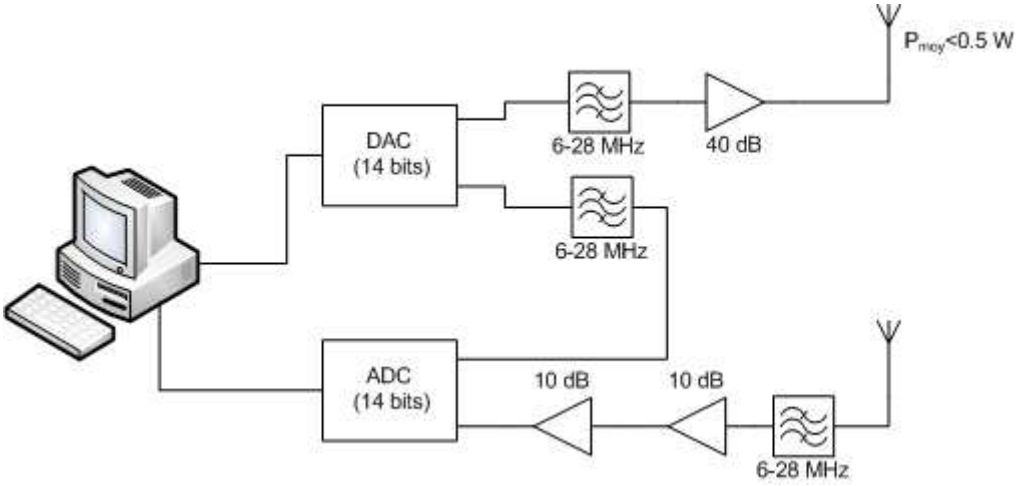

Figure 74. The block diagram of the radar that has been assembled to conduct the experimentations.

The block diagram of the system is presented in Figure 74.

One transmit channel of the DAC card was looped back into one receiving channel and served as a reference for the processing. Since a direct strong path exists between the transmit and the receive antenna, blanking the receive channel is necessary during the transmit time. As the available equipment didn't allow such an isolation between the transmit and the receive channel, we managed to accomplish this numerically by transmitting power low enough that the direct path level don't exceed the maximal safe input of the ADC card and then we eliminated the direct path after acquisition during the signal processing phase.

4.4 System validation trial

The first objective was to perform a detection of an aircraft in order to verify the power budget, check and solve any technical issue and then validate the signal processing part behind before proceeding with the comparison of the waveforms performances.

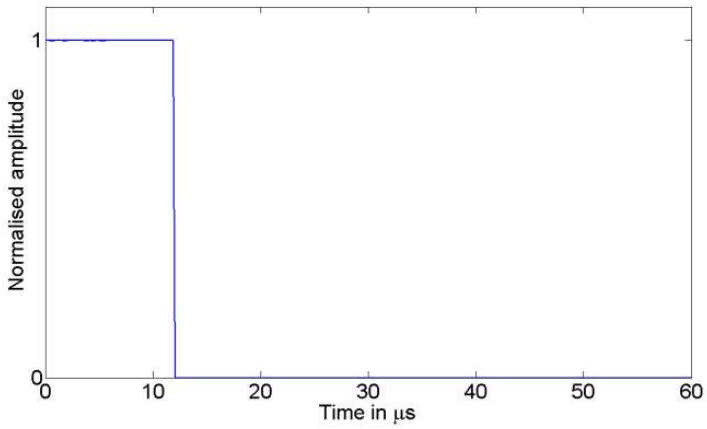

Figure 75. A basic chirp coded pulsed waveform used for a first test of verification.

Therefore, we started by transmitting a basic pulsed waveform (Figure 75) with a duty cycle of 20 % and having a linear frequency modulation covering a channel of 300 kHz around a central frequency of 24 MHz, with a repetition period of 60 µs.

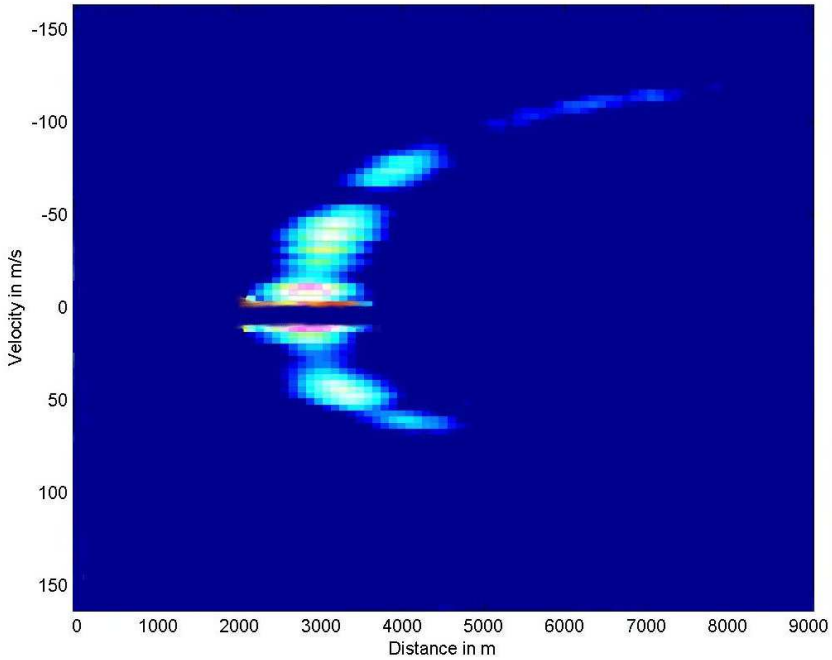

Figure 76.The track of an aircraft in the range-Doppler map.

After many trials in which we adjusted the power budget and synchronized the ADC and DAC cards we were able to detect and track the aircrafts on the range-Doppler map. The evolution of the target in this map was as expected theoretically. Figure 76 shows the track of the aircraft collected over a duration of 120 seconds. The different range Doppler-maps calculated every 2 seconds were merged together in order to obtain the track of the target.

4.5 Waveforms performance test

In Chapter 2 we presented new waveform envelopes that combine different pulse widths in order to overcome the eclipse consequences especially on the radar resolution greatly affected inside the blind zone of the conventional pulsed waveform.

Hence, in this part we will practically assess the performances of these waveforms in terms of resolution and SNR. We will use either a linear frequency coding or the alternate projection technique in order to occupy an available channel of 300 kHz with either the optimised or the conventional pulsed envelope. This leads us to four waveforms denoted W1 W2, W3 and W4.

Table 4. The characteristics of the different tested waveforms.

Waveform	*Envelope*	*Pulse width*	*Repetition Period*	*Duty Cycle*	*Bandwidth*	*Code Type*
W1	Pulse	56.4 μs	120 μs	0.47	300 kHz	Chirp
W2	Pulse	56.4 μs	120 μs	0.47	300 kHz	AP
W3	Optimised	-	120 μs	0.47	300 kHz	Chirp
W4	Optimised	-	120 μs	0.47	300 kHz	AP

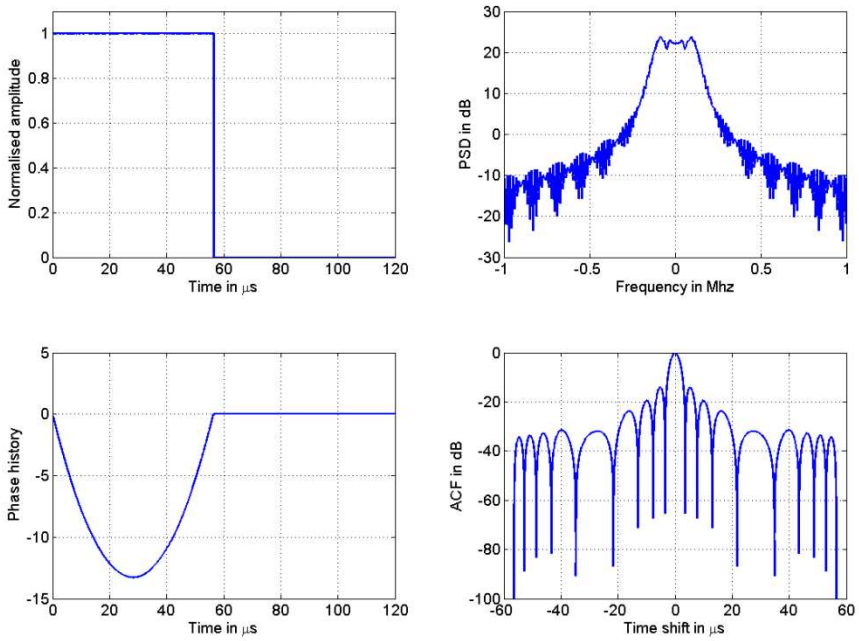

Figure 77. Characteristics of a chirp modulated conventional pulse occupying a channel of 300 kHz (W1).

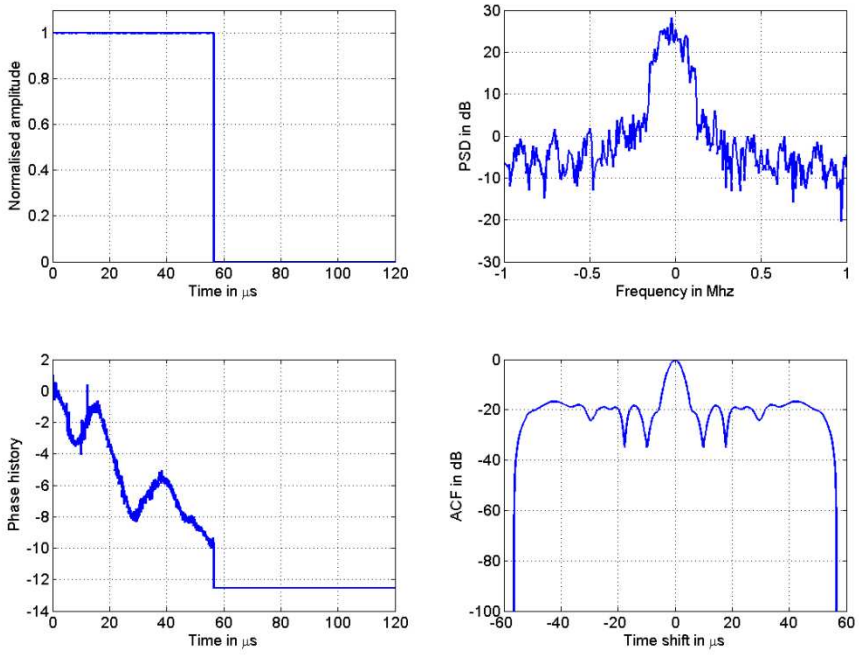

Figure 78. Characteristics of a conventional pulse coded with alternate projections occupying a channel of 300 kHz (W2).

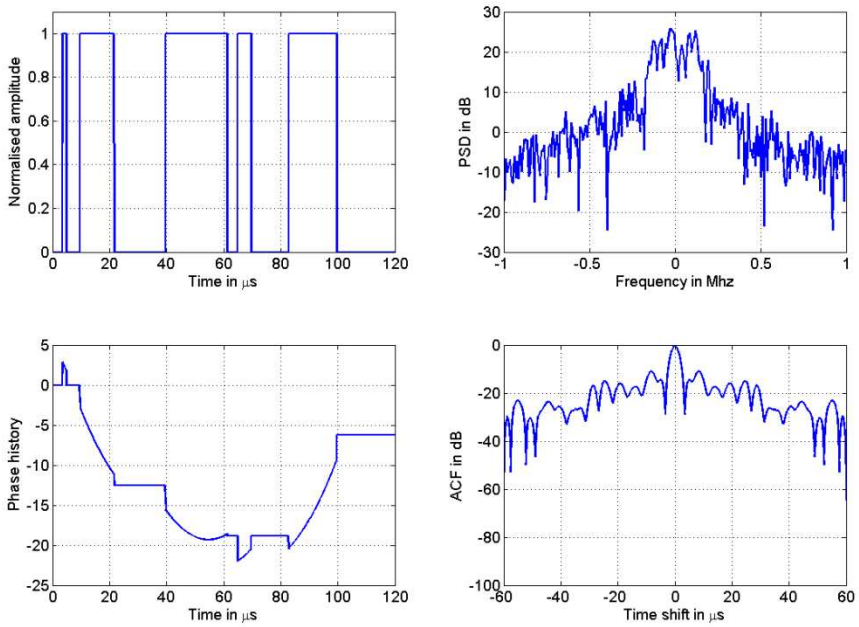

Figure 79. Characteristics of an optimised envelope coded with a linear chirp of 300 kHz (W3).

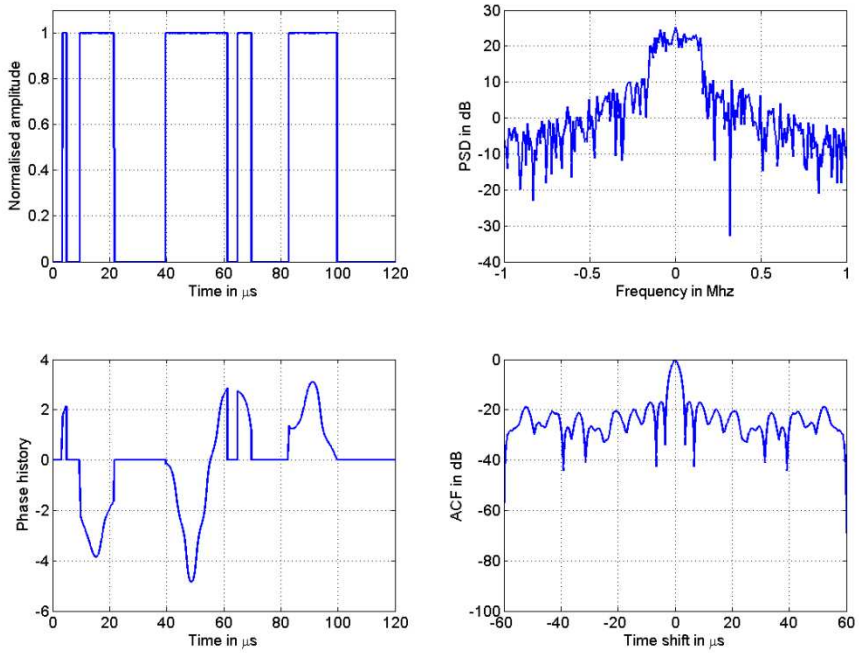

Figure 80. Characteristics of an optimised envelope coded with alternate projections and occupying a channel of 300 kHz (W4).

The characteristics of these waveforms are given in the Figures 75 to 78. For waveforms W3 and W4 we used an optimised envelope obtained as described in

Chapter 2 for $\alpha = 0.03$ and with a duty cycle of 47%. We notice that for waveform W3 the chirp coding becomes inadequate increasing the sidelobes of the ACF. However we managed to lower back these sidelobes by using the alternate projections technique as it could be seen for W4.

These waveforms were then transmitted separately. Each waveform is transmitted with a repetition period of 120 μs. The maximal desired range considered in the optimisation of the envelope corresponds to a shift of half the repetition period therefore 9 km.

The central frequency was chosen in a relatively clear channel at 24 MHz in the HF band which was checked before transmitting using a spectrum analyser. Although we transmitted less than half a watt of average power, we only transmitted during a short periods of 120 s for each trial, which was long enough to track the aircrafts, in order to reduce the risk of any potential undesired interference with other applications that may operate in this band.

The received signal was sampled at a rate of 1.6 MHz. The samples were processed using a two ways fast Fourier transforms in order to create the range Doppler map, each corresponding to 2 s of coherent integration time. Therefore the corresponding velocity resolution at 24 MHz is:

$$\Delta v = \frac{c}{2Tf_0} = 3.125\ m/s$$

The expected range resolution corresponding to the 300 kHz bandwidth is:

$$\Delta r = \frac{c}{2B} = 500\ m$$

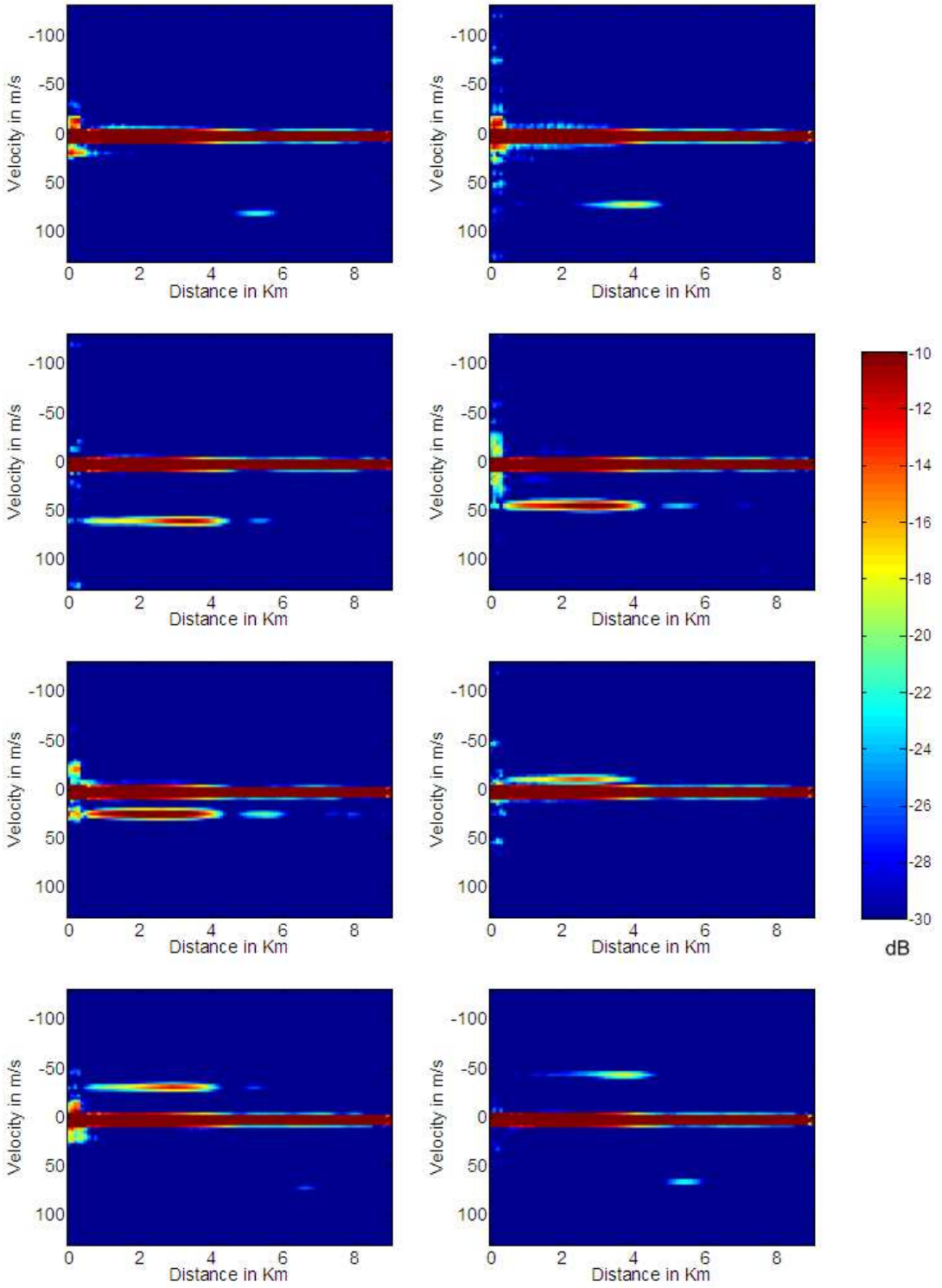

Figure 81. From left to right up to down, snapshots of the range-Doppler map through time for the waveform W1.

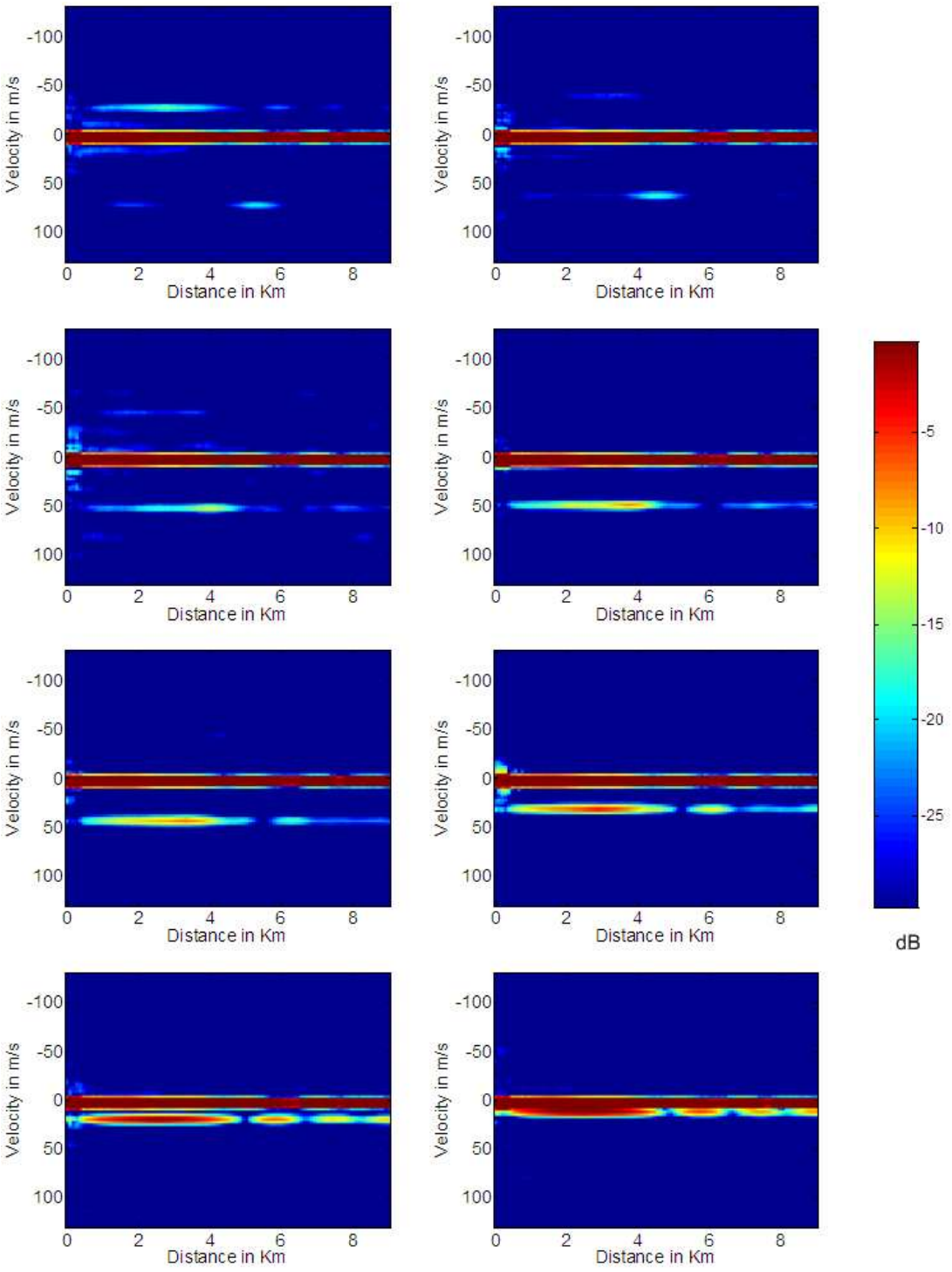

Figure 82. From left to right up to down, snapshots of the range-Doppler map through time for the waveform W2.

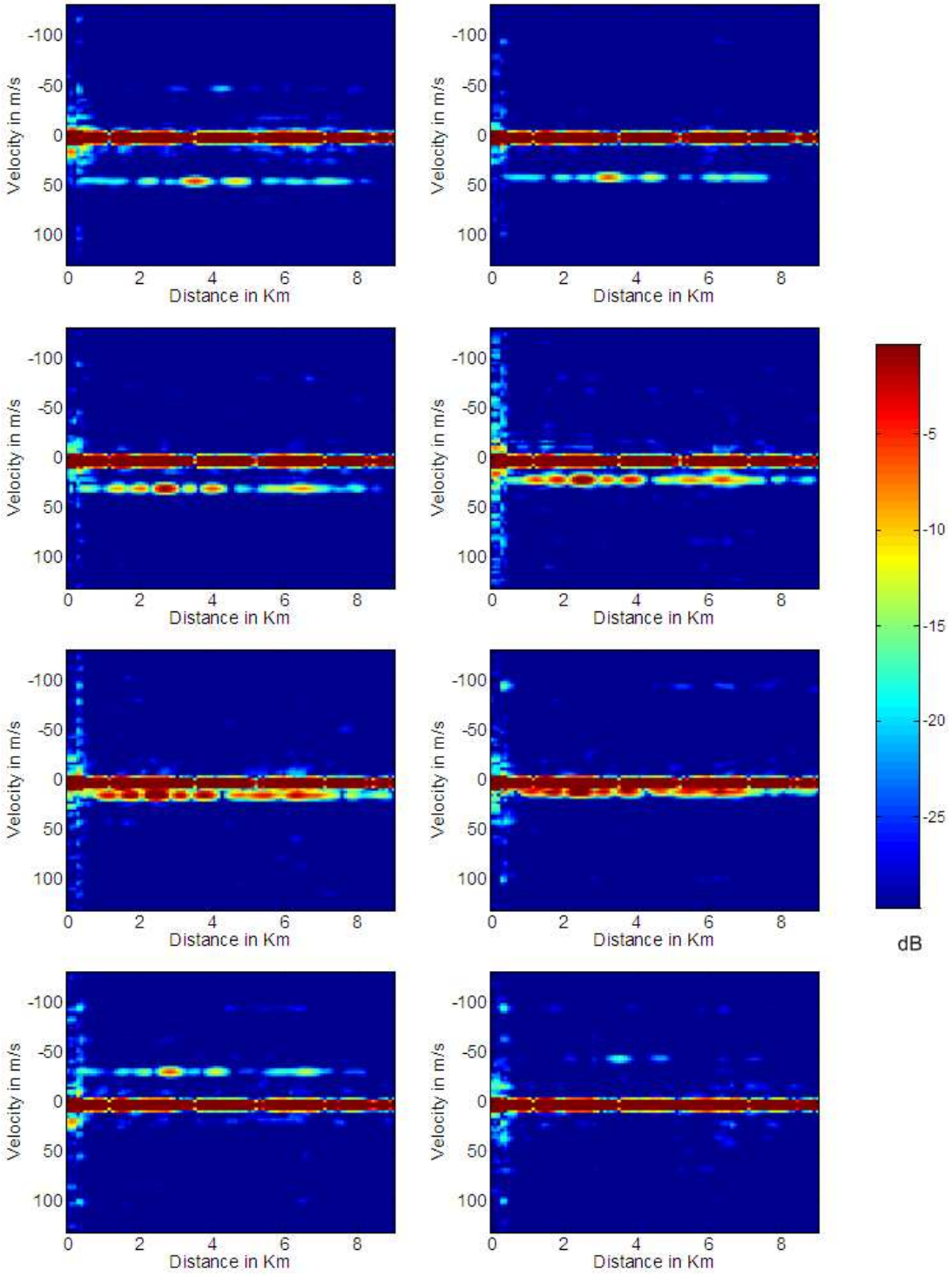

Figure 83. From left to right up to down, snapshots of the range-Doppler map through time for the waveform W3.

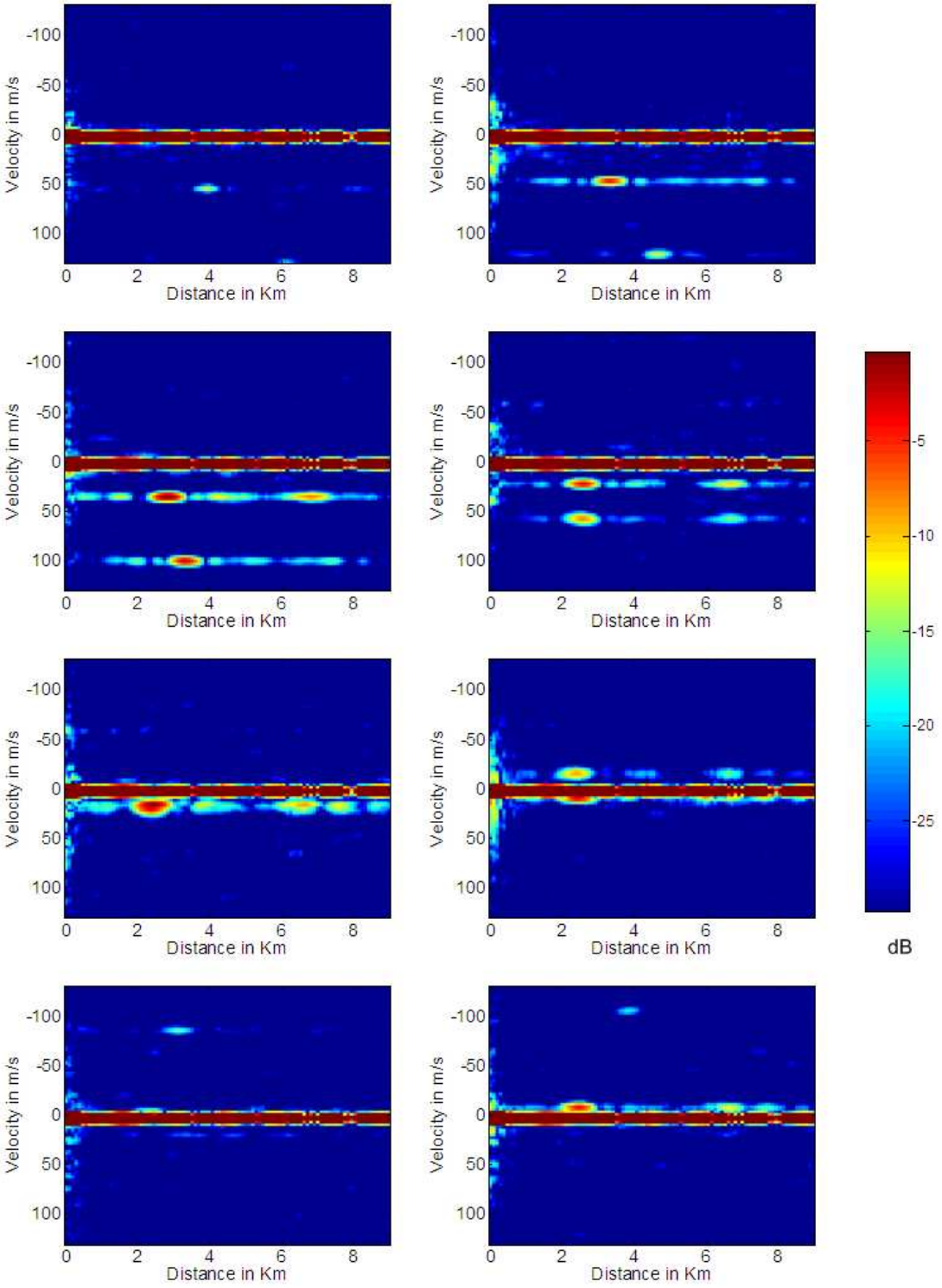

Figure 84. From left to right up to down, snapshots of the range-Doppler map through time for the waveform W4.

Figures 79 to 82 show snapshots of the range Doppler maps obtained during the 120s acquisition time for the different transmitted waveforms. These figures put in evidence the deterioration of resolution that occurs for the monopulse case

and this whether the transmitted code is a conventional chirp or an arbitrary phase code obtained by the alternate projections technique.

In Figures 81 and 82 we start to identify the AF mainlobe that seems to maintain its width along the track of the target. We notice the strong sidelobe levels as predicted in the case of the chirp coding of the optimised envelope and how they have been lowered by the alternate projections coding that was able to find a more suitable code to occupy the 300 kHz channel.

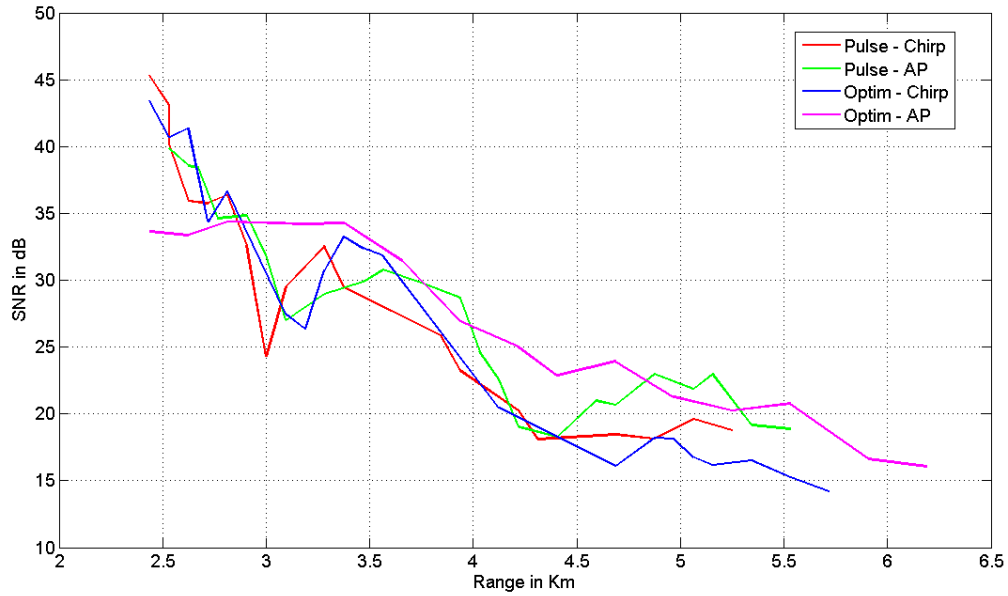

Figure 85.The measured SNR vs. distance for the different waveforms.

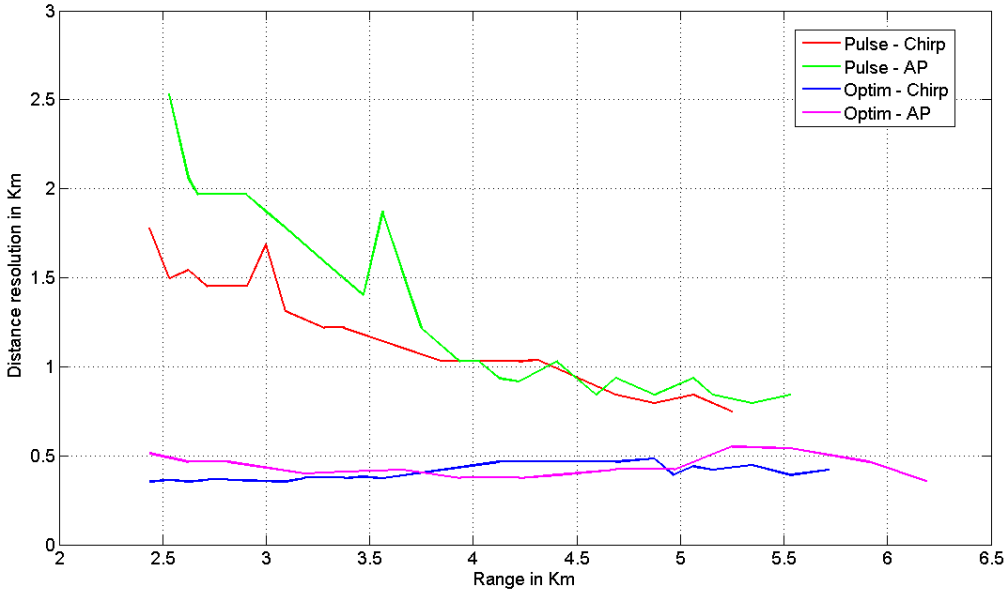

Figure 86.The measured distance resolution vs. distance for the different waveforms.

In order to better quantify the performances of these waveforms, the evolution of the SNR and the distance resolution was determined for each case from one position to another of the target on his track in the range-Doppler map.

The SNR plots in Figure 85 show that the waveforms have almost the same behaviour from the dynamics point of view although we were able to track the aircraft for longer distances in the case of the optimised waveform. Direct comparison of the levels could not be done since we are dealing with different targets and therefore different RCS.

Now if we look to the distance resolution measurements we notice that the optimised waveform succeeded in maintaining a steady good resolution of 500 m across the range extent of the radar while this resolution deteriorates as expected due to the eclipsing effect the more we go closer to the radar. At 2.5 km the monopulse waveform has as 3 to 5 times worse distance resolution than the optimised envelope waveform. The reason for which the monopulse waveform with chirp coding has better resolution than the monopulse with alternate projections coding could be interpreted by the higher suppression ratio attained in the spectrum domain by the alternate projections technique i.e. occupying less spectrum outside the authorised 300 kHz window (see Figure 77 and Figure 78).

4.6 Conclusion

A digital radar was successfully mounted around two ADC and DAC cards (ICS564 and 554) and has proven the ability to detect aircrafts flying around the Onera's research centre in the HF band. The optimised waveforms have been transmitted and tested and their performances compared to the conventional ones. The results showed the ability of the optimised waveforms to maintain their optimal resolution within the blind zone without degradation as predicted in theory. The predictions were also true for the conventional waveforms for which we witnessed the expected deterioration of resolution. In addition the phase codes obtained through the alternate projections techniques worked well as predicted by occupying the desired frequency channel and controlling the sidelobe level as it was the case for the last waveform.

Chapter 5

Conclusion

Spreading the radar transmissions in time and in frequency as required by the LPI strategy isn't always as straightforward as it may seem to be. In monostatic configuration using the time isolation between the transmit and receive channels, spreading the transmission in time increases the shelter loss which deteriorates the performances of the radar for the affected ranges.

On the other hand, as the spectrum available for radar use is subject to restriction and shall be shared with other applications, the radar should be able to adapt its transmissions to cope with a congested and sometimes rapidly changing spectral environment.

In an attempt to overcome the shelter loss limitations, Chapter 2 presented the design of a transmit/receive strategy. In the first case, the shelter loss was managed from a SNR point view in a way that it was less tolerated for long distances than for shorter ones which are less affected by the propagation losses. As a result the dynamic range of the matched filter was reduced and the end of the range extent benefited from very low and sometimes no shelter loss. Furthermore, the range resolution was improved up to 4 times compared with the conventional pulsed waveform and was kept almost unaltered, inside what was known as blind zone of the conventional waveform. This result was practically verified by experimentation in chapter 4 where the exact trend of performances was observed.

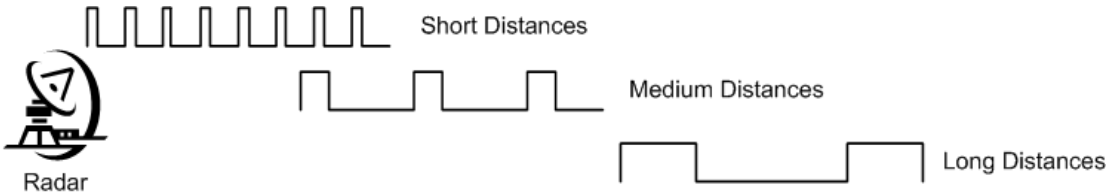

Figure 87. An example of three radar operating modes and their corresponding waveforms.

The resulting waveform combining variable length pulses is capable of operating at short, medium and long ranges therefore replacing what is conventionally achieved by different radars using either short pulses for close target detection or larger pulses with lower PRF to cover long distances as illustrated in Figure 87.

The specific case of the HFSWR was then studied taking into consideration the sea clutter power density function in order to suppress it and guarantee the best

contrast ratio encountered across the range extent of the radar. In fact, by spreading the radar transmission in time so does the extent of the ambiguity function therefore integrating more sea echoes to the target's response. An approximation of the Pareto front linking this ratio to the duty cycle was therefore calculated. It has been shown that a better performance could be achieved especially at the end of the radar range extent compared to the conventional waveforms. The result is a set of waveforms solutions corresponding to the Pareto front and if implemented, the radar could easily shift from one waveform to another, adjusting its duty cycle and transmitted power depending on the sea condition. These waveforms were planned to be tested at Onera's HFSWR at the Bay of Biscay but the trials were then cancelled due to the "Klaus" storm that affected mainly the south-west of France between the 23rd and the 25th of January 2009. These tests therefore remain in the category of the prospects for this study. It must be emphasized however, that the study done for the HFSWR could be applied to other radar applications by replacing the sea clutter density function to meet the corresponding type of clutter.

Once the time profile has been optimised comes the choice of the internal code either frequency or phase code. In this context, chapter 3 presented different existing solutions for the radar phase code design that try to fit the transmissions into a defined set of authorised bands. In fact, despite the great importance of all the well-known radar codes, any practical realisation is often faced with spectral allocation problems or the presence of strong interference in some channels of the band in which the radar wishes to operate. This is where the general codes become inconvenient to the problem and other specific solutions are needed in order to match the spectrum constraints.

To this end, a new technique was introduced based on successive corrections and transforms between the time, frequency and autocorrelation domains. Based primarily on Fourier transforms, it is efficient (quasi-linear complexity) and easy to implement and gave even better results than the previously presented sparse waveform design techniques for the same considered study-cases. Some new ideal –like codes were even calculated using the proposed technique. These codes have the advantage of not belonging to any existing library which makes their classification a difficult, if not an impossible task. This would eventually prevent the possibility of designing a special purpose intercept receiver in order to detect the radar in question, similarly to the case for the receivers built to detect the police speed radars for example. Moreover, rapidly changing the radar transmissions could be useful to mitigate fast change of environment or even to prevent exploitation by receivers of opportunity. This last point gets significant importance given the surge in bistatic radars development for military applications.

The coding technique was evaluated in chapter 4, where it was used to fit the different waveforms into the available frequency channel and to reduce the range sidelobes successfully. These were the results of practical aircrafts radio localisation experiments undertaken at the rooftop of the Onera's centre at Palaiseau.

Finally, due to the noise-like properties of the different solutions achieved when applying the proposed coding technique, the cross- correlation between these solutions is expected to be low. When used by different radars in proximity, this may reduce their mutual interference. These codes also may serve as quasi-orthogonal codes to be transmitted by the multiple transmitters of a MIMO radar system.

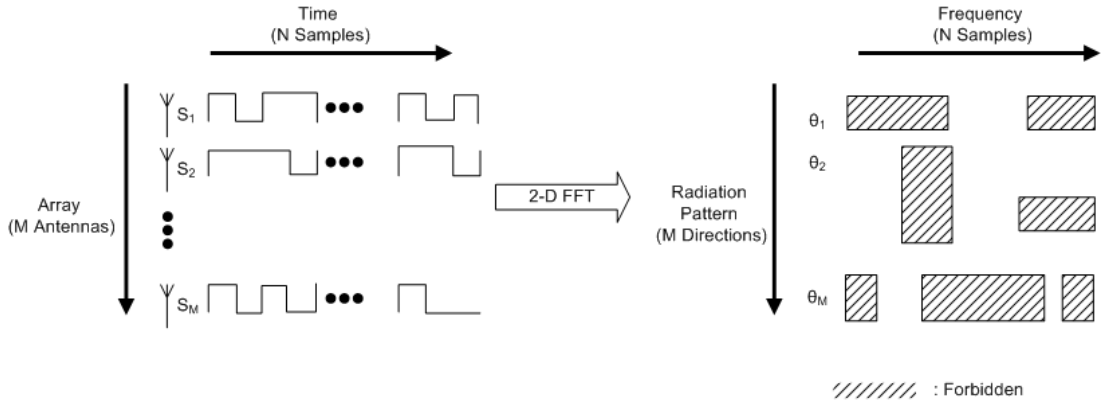

Figure 88. A possible extension of the alternate projection technique to the space-frequency for a regular array of transmitters.

In this context, the technique could be easily extended for an array of transmitters in the frame of a joint angular-spectrum constraint. In that way, the radar could privilege to transmit using some frequency bands in particular directions and avoid some other frequency bands in directions where the presence of strong interferences or other critical applications are suspected. This extension is best explained by Figure 88 showing its application for a regular array of M transmitters. A 2D-FFT is required in this case rather than the previous 1D-FFT in order to move to the radiation pattern- frequency space. The following steps include similar corrections in the corresponding planes.

Although the alternate projections technique is a powerful and simple technique for finding sets' intersection and seemed to achieve satisfactory results, a thorough study should be carried on in order to study the nature of the non-convex sets that have been used during the process. Some alternating minimization and projection methods for non-convex problems already exist and have been used in crystallography and inverse scattering problems. The aim would be to find the most convenient method for the radar waveform design problem.

Moreover, an interesting area of study is on the generation of a set of orthogonal codes that meet the available spectrum condition. To achieve this, one should be able to introduce corrections to reduce the cross-correlation between the different codes in addition to the needed corrections of spectrum and autocorrelation. The initial step would be to find a way to generate a set of codes having good autocorrelation and minimal cross correlation. Concerning the interruption strategy optimization that has been proposed, research should be carried for even longer codes and create a database of ready to use envelopes depending on the required application.

Finally, there's no doubt that the use of evolutionary algorithms especially for cognitive radar applications is a promising research topic especially with the increase of complexity and the amount of information the future radar should be able to provide and process in real time. In this context comes the importance of the research work introducing advancements in the domain of evolutionary algorithms [50] and optimisation and having the radar as a main application.

Publications

Kassab, R. and Lesturgie, M. and Fiorina, J**.**, *Dynamic Range Reduction by Quasi-Continuous Waveform Optimisation*, 2007, December, *1st Franco-Singaporean Signal Processing Workshop*, Singapore

Kassab, R. and Lesturgie, M. and Fiorina, J., *Quasi-Continuous Waveform Design for Dynamic Range Reduction*, 2008, 8 May, *IET Electronics Letters*, vol. 44, Issue 10, pp. 646-648

Kassab, R. and Lesturgie, M. and Fiorina, J., *The Duty Cycle and Contrast Ratio Trade-off in the Design of Interrupted HFSWR Waveform,* 2008, October, *European Radar Conference (Eurad08),* Amsterdam, Netherlands

Kassab, R. and Lesturgie, M. and Fiorina, J., *Performance Analysis of Interrupted Sparse HFSWR Waveform Coded with Successive Fast Fourier Transforms*, 2009, 7 May, *IET Electronics Letters*, vol. 45, Issue 10, pp. 527-528

Kassab, R. and Lesturgie, M. and Fiorina, J., *Alternate Projections Technique for Radar Waveform Design, Accepted for Radar 2009*

Bibliography

[1] *Applications of operational calculus to ground-wave propagation, particularly for long waves.* **Bremmer, H.** 1958, IRE Transactions on Antennas and Propagation, Vol. 6, pp. 267-272.

[2] *The surface-wave concept in connection with propagation trajectories associated with Sommerfeld problem.* **Bremmer, H.** 1959, IRE Transactions on Antennas and Propagation, Vol. 7, pp. 175-182.

[3] *The interaction of HF/VHF radio waves with the sea surface and its implications on electromagnetics of the sea.* **Barrick, D. E.** 1970. Proc. AGARD Symp.

[4] *Sparse frequency transmit-and-receive waveform design.* **Lindenfeld, M. J.** 2004, #IEEE_J_AES#, Vol. 40, pp. 851-861.

[5] *Optimal sparse waveform design for HFSWR system.* **Liu, W. X., Lu, Y. L. and Lesturgie, M.** 2007. Proc. International Waveform Diversity and Design Conference. pp. 127-130.

[6] **SAAB BOFOR DYNAMICS.** *PILOT The LPI Radar for All Applications.* 2006.

[7] *A digital leakage cancellation scheme for monostatic FMCW radar.* **Lin, K., Messerian, R. H. and Wang, Yuanxun.** 2004. Proc. IEEE MTT-S International Microwave Symposium Digest. Vol. 2, pp. 747-750.

[8] *Real-time DSP for reflected power cancellation in FMCW radars.* **Lin, K. and Wang, Y. E.** 2004. Proc. VTC2004-Fall Vehicular Technology Conference 2004 IEEE 60th. Vol. 6, pp. 3905-3907.

[9] *Transmitter Noise Cancellation in Monostatic FMCW Radar.* **Lin, Kaihui and Wang, Yuanxun Ethan.** 2006. Proc. IEEE MTT-S International Microwave Symposium Digest. pp. 1406-1409.

[10] *Study on the Design Method of Quasi-CW Radar Waveform.* **Weiming, Yuan.** 2006. Proc. International Conference on Radar CIE '06. pp. 1-4.

[11] *RFI suppression for ultra wideband radar.* **Miller, T., Potter, L. and McCorkle, J.** 1997, #IEEE_J_AES#, Vol. 33, pp. 1142-1156.

[12] *Range sidelobe suppression technique for coherent ultra wide-band random noise radar imaging.* **Xu, Xiaojian and Narayanan, R. M.** 2001, #IEEE_J_AP#, Vol. 49, pp. 1836-1842.

[13] *Optimum transmit-receiver design in the presence of signal-dependent interference and channel noise.* **Pillai, S. U., et al.** 1999. Conference Record of the Thirty-Third Asilomar Conference on Signals, Systems, and Computers. Vol. 2, pp. 870-875.

[14] **Levanon, Nadav and Mozeson, Eli.** *Radar Signals.* s.l. : Wiley-Interscience, 2004.

[15] *Dynamic Range Reduction by Quasi-Continuous Waveform Optimisation.* **Kassab, R., Lesturgie, M. and Fiorina, J.** 2007. Proc. 1st Franco-Singaporean Signal Processing Workshop.

[16] *Quasi-continuous waveform design for dynamic range reduction.* **Kassab, R., Lesturgie, M. and Fiorina, J.** 2008, Electronics Letters, Vol. 44, pp. 646-647.

[17] *The duty cycle and contrast ratio trade-off in the design of interrupted HFSWR waveform.* **Kassab, R., Lesturgie, M. and Fiorina, J.** 2008. Proc. European Radar Conference

EuRAD 2008. pp. 60-63.

[18] *Performance analysis of interrupted sparse HFSWR waveform coded with successive fast Fourier transforms.* **Kassab, R., Lesturgie, M. and Fiorina, J.** 2009, Electronics Letters, Vol. 45, pp. 525-527.

[19] *Alternate Projections Technique for Radar Waveform Design.* **Kassab, R., Lesturgie, M. and Fiorina, J.** 2009. Proc. International Radar Conference RADAR 2009.

[20] *Synchronisation of bistatic radar systems.* **Weib, M.** 2004. Proc. IEEE International Geoscience and Remote Sensing Symposium IGARSS '04. Vol. 3, pp. 1750-1753.

[21] *Low probability of intercept radar strategies.* **Stove, A. G., Hume, A. L. and Baker, C. J.** 2004, IEE Proceedings -Radar, Sonar and Navigation, Vol. 151, pp. 249-260.

[22] *Low probability of intercept radar.* **Schleher, D. C.** 1985. Proc. Record of the IEEE 1985 International Radar Conference. pp. 346-349.

[23] *LPI radar: fact or fiction.* **Schleher, D. C.** 2006, IEEE Aerospace and Electronic Systems Magazine, Vol. 21, pp. 3-6.

[24] *Eclipsing effects with high-duty-factor waveforms in long-range radar.* **Billam, E. R.** 1985, IEE Proceedings F Communications, Radar and Signal Processing, Vol. 132, pp. 598-603.

[25] *Etude d'une forme d'onde quasi continue à codage de phase avec contrôle des lobes secondaires pour un radar LPI.* **Lesturgie, Marc and Dugrosprez, Bruno.** 2005. SEE.

[26] *Properties and application of a randomly interrupted, random radar waveform.* **Porter, N. J., A., R. J. and Ward, K. D.** 1992. Proc. Radar 92. International Conference. pp. 5-8.

[27] **Chevalier, F.Le.** *Principles of Radar and Sonar Signal Processing.* s.l. : Artech House, 2003.

[28] *Pareto-, Aggregation-, and Indicator-based Methods in Many-objective Optimization.* **Wagner, Tobias, et al.** s.l. : Springer, 2007. pp. 742-756.

[29] *Full digital High Frequency Surface Wave Radar: French trials in the biscay bay.* **Menelle, M., Auffray, G. and Jangal, F.** 2008. Proc. International Conference on Radar. pp. 224-229.

[30] *Airborne clutter performance of randomized radar waveforms.* **Maier, M. W. and Weber, C. L.** 1995, #IEEE_J_AES#, Vol. 31, pp. 951-959.

[31] *On the design of optimum radar waveforms for clutter rejection.* **DeLong, D. and Hofstetter, E.** 1967, #IEEE_J_IT#, Vol. 13, pp. 454-463.

[32] *The design of clutter-resistant radar waveforms with limited dynamic range.* **DeLong, D. and Hofstetter, E.** 1969, #IEEE_J_IT#, Vol. 15, pp. 376-385.

[33] *A fast and elitist multiobjective genetic algorithm: NSGA-II.* **Deb, K., et al.** 2002, #IEEE_J_EVC#, Vol. 6, pp. 182-197.

[34] *How well do multi-objective evolutionary algorithms scale to large problems.* **Praditwong, K. and Yao, Xin.** 2007. Proc. IEEE Congress on Evolutionary Computation CEC 2007. pp. 3959-3966.

[35] *Evolutionary many-objective optimisation: many once or one many?* **Hughes, E. J.** 2005. Proc. IEEE Congress on Evolutionary Computation. Vol. 1, pp. 222-227.

[36] **Camacho, Joseph P.** *Federal Radar Spectrum Requirements.* NTIA. 2000.

[37] **Hurt, Gerald, Cerezo, Ernesto and Slye, Russell.** *NTIA Special Publication 01-44.* NTIA. 2001.

[38] *Waveform Diversity: Past, Present and Future.* **A., De Maio and A., Farina.** s.l. : RTA, 2008.

[39] *Genetic algorithms in the design and optimization of antenna array patterns.* **Ares-Pena, F. J., et al.** 1999, #IEEE_J_AP#, Vol. 47, pp. 506-510.

[40] *Particle swarm optimization versus genetic algorithms for phased array synthesis.* **Boeringer, D. W. and Werner, D. H.** 2004, #IEEE_J_AP#, Vol. 52, pp. 771-779.

[41] **Leong, Hank W.H. and Dawe, Barry.** *Channel Availability for East Coast High Frequency Surface Wave Radar Systems.* DEFENCE RESEARCH ESTABLISHMENT OTTAWA (ONTARIO). 2001.

[42] **Darrigol, Olivier.** *Worlds of flow.* s.l. : Oxford University Press, 2005.

[43] *Determination of phase functions for a desired one-dimensional pattern.* **Chakraborty, A., Das, B. and Sanyal, G.** 1981, #IEEE_J_AP#, Vol. 29, pp. 502-506.

[44] *The design of FM pulse compression signals.* **Fowle, E.** 1964, #IEEE_J_IT#, Vol. 10, pp. 61-67.

[45] *Nonlinear frequency modulation chirps for active sonar.* **Collins, T. and Atkins, P.** 1999, IEE Proceedings -Radar, Sonar and Navigation, Vol. 146, pp. 312-316.

[46] *The foundations of set theoretic estimation.* **Combettes, P. L.** 1993, #IEEE_J_PROC#, Vol. 81, pp. 182-208.

[47] *Intersection approach to array pattern synthesis.* **Bucci, O. M., et al.** 1990, IEE Proceedings H Microwaves, Antennas and Propagation, Vol. 137, pp. 349-357.

[48] *Fast Low-Sidelobe Synthesis for Large Planar Array Antennas Utilizing Successive Fast Fourier Transforms of the Array Factor.* **Keizer, W. P. M. N.** 2007, #IEEE_J_AP#, Vol. 55, pp. 715-722.

[49] *Polyphase sequences with low autocorrelation.* **Borwein, P. and Ferguson, R.** 2005, #IEEE_J_IT#, Vol. 51, pp. 1564-1567.

[50] *Radar Waveform Optimisation as a Many-Objective Application Benchmark.* **Hughes, Evan J.** 2007. EMO. pp. 700-714.

Abstract

The low probability of intercept is an important feature for the radar to survive modern warfare. In order to achieve this feature, studies show that the radar's transmitted energy should be well spread in time and frequency. However for monostatic configuration where the received echoes are blanked during the transmission, the spread in time increases the eclipsing loss, therefore declining the radar performances for the ranges in question. On another hand, the spectrum available for radar use is subject to restrictions and often shared with other applications. Hence, in this study, the transmit receive/strategy was first optimised in order to manage the eclipsing loss while achieving high duty cycle waveforms. Then, a new, simple and yet efficient coding technique was proposed for the radar to adapt its transmissions to a congested and rapidly changing spectral environment. Finally, the resulting waveform and coding technique were practically tested during trials of aircraft detection and localisation in HF band.

Keywords: radar, waveform design, optimisation, eclipsing loss, sparse frequency coding, experimental validation

Résumé

L'un des traits les plus importants du radar moderne est la faible probabilité d'interception. Afin de garantir cette propriété, le radar doit étaler le plus possible son énergie en temps et en fréquence. Cependant, pour une configuration monostatique où la voie de réception est coupée pendant l'émission, l'étalement de l'énergie dans le temps entraîne une augmentation des pertes d'éclipses dégradant les performances radar pour les distances en question. D'autre part, la bande disponible est limitée, contrainte par des restrictions et parfois partagée avec d'autres applications. Ainsi, dans cette étude, la stratégie de transmission-réception est dans un premier temps optimisée afin de gérer les pertes d'éclipse et atteindre un bon rapport cyclique. Ensuite, une nouvelle technique simple et efficace est proposée permettant au radar d'adapter rapidement ses transmissions à un environnement spectral congestionné. Finalement, les formes d'onde résultantes ainsi que la technique de codage ont été testées en pratique dans le cadre de détection et de localisation d'avions en bande HF.

Mots clefs: radar, conception de forme d'onde, optimisation, perte d'éclipse, codage lacunaire en fréquence, validation expérimentale